SERIES 100
ISSUE 19

STRUCTURES AND MATERIALS RESEARCH
DEPARTMENT OF CIVIL ENGINEERING

THE STRESS DISTRIBUTION OF NORFORK DAM

BY
RAY W. CLOUGH

FINAL REPORT TO
U. S. ENGINEER DISTRICT, LITTLE ROCK
CORPS OF ENGINEERS

MARCH 1962
REVISED AUGUST 1962

INSTITUTE OF ENGINEERING RESEARCH
UNIVERSITY OF CALIFORNIA
BERKELEY CALIFORNIA

STRUCTURES AND MATERIALS RESEARCH
DEPARTMENT OF CIVIL ENGINEERING

SERIES 100 ISSUE 19

THE STRESS DISTRIBUTION OF NORFORK DAM

A Report of an Investigation

by

Ray W. Clough

Professor of Civil Engineering

to

U. S. ARMY ENGINEER DISTRICT, LITTLE ROCK

CORPS OF ENGINEERS

Under Contract DA-03-050-Civeng-62-511

Institute of Engineering Research
University of California
Berkeley, California

March, 1962

Revised August 1962

TABLE OF CONTENTS

LIST OF ILLUSTRATIONS

LIST OF ILLUSTRATIONS (Cont'd)

LIST OF TABLES

NOTATION

All symbols are defined in the text where first introduced. In addition, the most important symbols are assembled here for convenient reference.

σ_x	Normal Stress acting on vertical sections, positive in tension
σ_y	Normal stress acting on horizontal sections, positive in tension
τ_{xy}	Shearing stress acting on vertical and horizontal sections
$[k]$	Triangular element stiffness matrix
$[a]$	Displacement transformation matrix
$[K]$	Stiffness of the assembled triangular element system
$[\ ]^T$	Transposition of a matrix
$\{Q\}$	Elastic nodal point forces in assembled system
$\{R\}$	Applied nodal point forces
$\{r\}$	Nodal point displacement components
$[F]$	Flexibility of assembled system
$\{v\}$	Deformation of individual triangular elements
$\{S\}$	Nodal forces in individual triangular elements
$\{\sigma\}$	Stresses in individual triangular elements
$[M]$	Stress matrix, relating element stresses to element deformations
a_j, b_j, a_k, b_k	Dimensions of triangular element (see Fig. 2)
E	Modulus of elasticity
ν	Poisson's ratio
ξ	$\frac{1-\nu}{2}$
t	Thickness of finite element (one foot in this study)
r	Proportion of soft material in layered orthotropic material (see Fig. 3)

G	Shear Modulus
μ	Ratio of horizontal to vertical modulus in orthotropic material
$[\bar{k}]$	Triangular element stiffness matrix, orthotropic material
σ_1, σ_2	Major and minor principal stresses
θ	Direction of principal stress from horizontal
γ	Unit weight
Φ	Slope of face of dam (from horizontal)
$\tilde{\sigma}$	Constrained thermal stress
α	Thermal coefficient of expansion
ΔT	Temperature increase
β	Over-relaxation factor
X, Y	Nodal point constraints (eliminated by relaxation)

SUMMARY

In this report is described an investigation of the stress distribution within the cross-section of a gravity dam. The analysis was performed by an automatic digital computer, using the finite element method. The principal purpose of the study was to determine the effect on the stress distribution, of a vertical crack extending from the center of the base through most of the height of the section. The dam was subjected to dead load, live load, and thermal stress conditions; a total of 17 different loading and crack configurations were considered, including cases in which the foundation material was assumed to be orthotropically elastic.

Results of the studies are presented graphically in the form of stress contours and boundary displacement diagrams for each case. In addition, figures are presented depicting the amount of opening or closing of the crack resulting from the various load conditions. Although the results show that definite stress concentrations result from the presence of the crack, the maximum stresses that develop are not severe, being less than about 500 psi in all cases.

Subsequent to the completion of the original report, a supplementary investigation was carried out in which additional conditions of loading and of crack configuration were considered. Included among these were cases in which the crack was assumed to extend through the upper surface of the dam, effectively separating it into two blocks. Because the

filling of the reservoir behind such a section causes the crack to close gradually from the top downwards, it was necessary to develop an incremental analysis procedure for the full crack height cases. The results of this supplementary investigation are presented here as a supplement to the original report (see p. 85). They show that, although the presence of a crack extending through the full height of the section leads to a moderate increase of stress concentration at the base, the stresses still are not severe--only about 600 psi maximum.

THE STRESS DISTRIBUTION OF NORFORK DAM

INTRODUCTION

Origin of the Problem

The distribution of stress which actually exists in massive concrete gravity dams has long been the subject of conjecture. A number of experimental studies have been carried out[1,2,3]* both in the laboratory and in the field, in an attempt to establish the order of magnitude of the errors inherent in the simplified assumptions which form the basis for design. The results of these investigations have shed considerable light on the problem and bear out the adequacy of the design assumptions in normal cases. However, little is known about the distribution of stress in dams in which conditions differ radically from the normal.

One condition which is known to exist in a number of structures, but the effect of which has not been studied previously, is the presence of a vertical crack or system of cracks, extending in planes parallel to the longitudinal axis of the dam. Such a crack, if it extended through a major portion of the height of the dam, obviously could have a significant effect on its structural action in resisting water loads, and conceivably could reduce materially its overall factor of safety.

The purpose of the investigation described in this report was to determine the influence of such a vertical crack on the stress distribution and deformations of an actual concrete gravity dam. The subject of the study was the Norfork Dam, a 230 foot high structure built on the North Fork River in Arkansas by the United States Army Corps of Engineers. Extensive cracking was noticed in this structure during its construction,

*Numbers in parentheses refer to similarly numbered References listed at the end of this report.

and a rather extensive survey of the distribution and size of the principal cracks has been carried out during the 18 years since its completion. On the basis of this study it was apparent that Monolith 16 was one of the most severely cracked portions of the structure and it was selected as a subject for mathematical analysis.

Within this monolith was one principal crack, located approximately in mid-width and extending vertically over most of its height. The specific objective of this study was to determine how such a single crack in an otherwise solid section would affect the distribution of stress within the section. The vertical extent of the crack could not be established with great reliability, thus this factor was selected as one of the principal variables of the study.

Analytical Procedure

A second, and also very valuable, purpose of the investigation was the evaluation of a recently developed method of plane stress analysis[4]. This method, which is known as the "finite element method", takes advantage of the tremendous computational capacity of modern high-speed digital computers. It had been tested previously in relatively minor academic problems, but its effectiveness in solving a full scale practical problem had not yet been demonstrated.

The fundamental concept of the finite element method was developed originally[5] in an attempt to extend and generalize the "lattice analogy" which had been proposed as a method of plane stress analysis by Hrennikoff[6] and McHenry[7] over twenty years ago. An interesting side issue of this investigation was the offer of Mr. McHenry*, now working with the Portland Cement Association, to make a similar analysis by the

* Director of Development, Portland Cement Association Research and Development Laboratories, Skokie, Illinois.

lattice analogy procedure (which had not previously been programmed for the digital computer). This analysis provided an independent check on the results obtained by the finite element method, and also made possible a comparison of the relative merits of the two procedures.

Scope of the Investigation

The geometry of the cross-section considered in the investigation and the properties of the concrete and foundation rock were specified by the Contracting Office. Loadings which were considered included dead load, live load (hydrostatic pressure), and the effects of temperature changes. Stress distributions and deformations were calculated due to these load conditions applied in various combinations, as agreed upon by the investigators and the Contracting Office. The initial width of crack opening was defined under a combined temperature change and dead load condition. The additional influence of the live load in closing the crack and stressing the structure was then evaluated. Because the foundation rock appeared to have a considerable amount of jointing in horizontal planes, it seemed probable that its effective modulus of elasticity in the vertical direction was considerably less than in the horizontal direction. Therefore, the effects of an orthotropic foundation was studied in two cases.

All of the analyses were performed on the IBM 704 electronic digital computer operated by the University of California Computer Center. The principal computer program used in the analyses was developed by the investigators, prior to the initiation of this contract, on a research grant from the National Science Foundation. However, a few minor program modifications and extensions were made during the course of this study. Stress distribution and displacement results were printed by the computer in tabular form, but were subsequently portrayed graphically for easier comprehension.

METHOD OF ANALYSIS

The basic problem to be solved in this investigation was the determination of the stresses and displacements in a plane-stress system of arbitrary dimensions and properties, due to the application of temperature changes, external loads, and its own dead weight. The finite element method which was employed in the analysis has been described previously[4] so the basic principles of the procedure will be reviewed here only briefly. However, several aspects of the present problem required the development of new concepts and techniques which will be described in full.

The Finite Element Approximation

The basic approximation introduced in this method of analysis is the representation of the actual plane-stress system as an assemblage of triangular plate elements, interconnected only at the corners or nodal points, and each subjected to a state of plane stress. This idealization replaces the actual elasticity problem by a structural analysis problem. The advantage of the substitution is that the conditions of compatibility and equilibrium, which must be represented by partial differential equations in the elasticity problem, may be expressed by a set of simultaneous algebraic equations in the structural problem. This problem may then be solved by standard methods of structural analysis.

A very coarse mesh (and therefore quite crude) idealization of a dam cross-section is shown in Fig. 1. The triangular elements are joined only at their corners and the loads are also applied only at these nodal points. Deformations of the assemblage depend, of course, not only on the stiffnesses of the individual elements, but also on the manner in which they are coupled. Thus it would appear that the idealization would be excessively flexible, due to the fact that continuity between

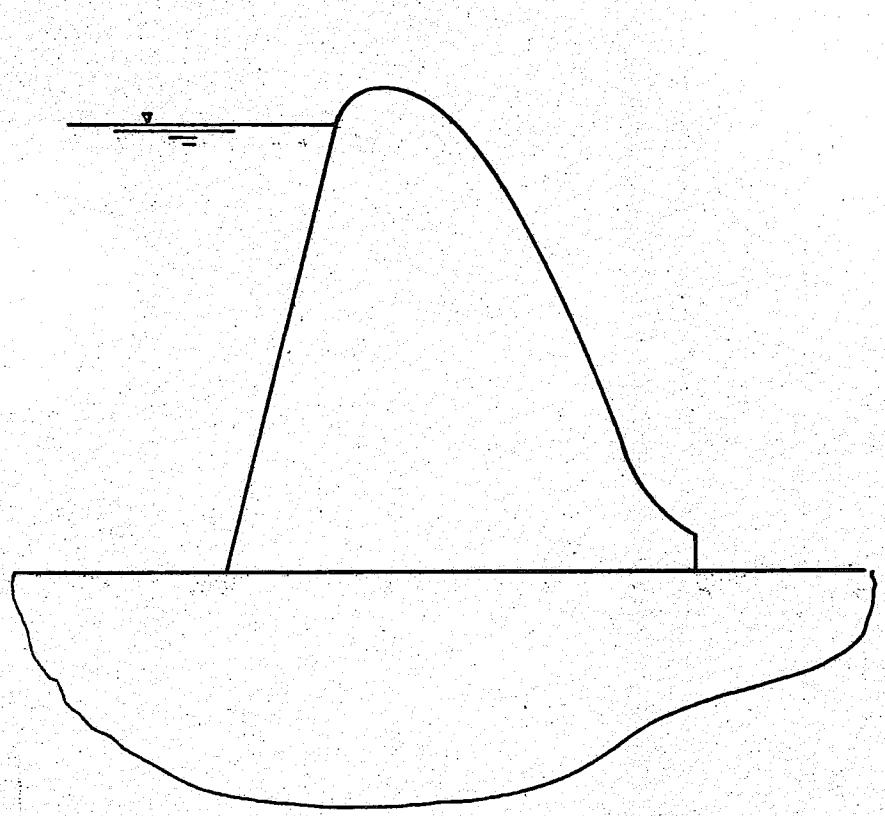

a. ACTUAL DAM SECTION

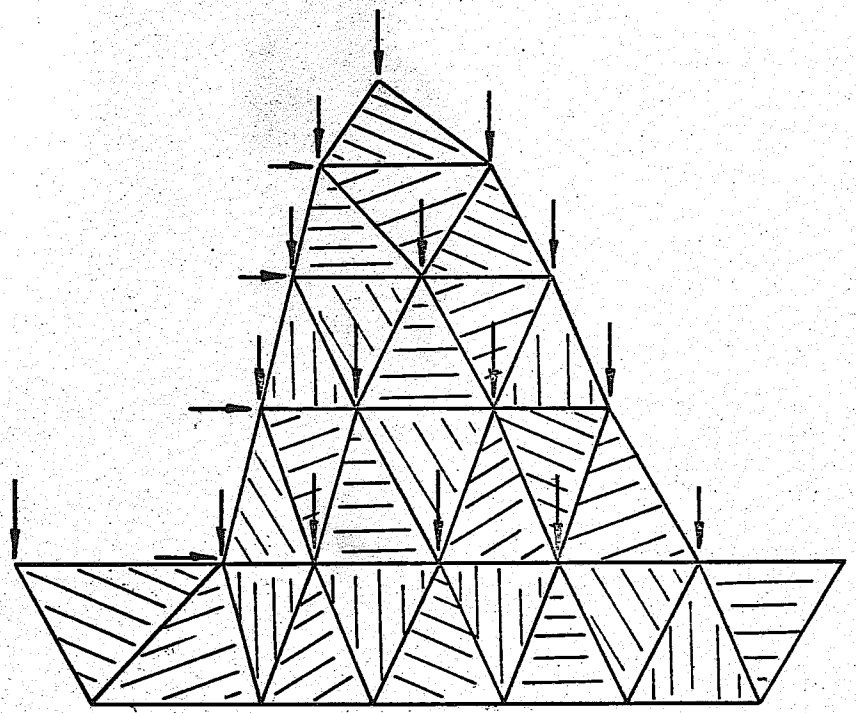

b. ELEMENT AND LOAD APPROXIMATION

FIG. 1 THE TRIANGULAR FINITE ELEMENT IDEALIZATION

the elements is imposed at so few points. However, this incomplete continuity condition is compensated by the assumption that the stresses within each element must be uniform; i.e., the normal stresses in the horizontal (σ_x) and vertical (σ_y) directions, and shearing stress (τ) are constant within each element. As a result of this assumption, the edges of each element remain straight under load, and therefore continuity is achieved not only at the nodal points but also along the element boundaries as well.

It should be noted that one of the major advantages of the finite element approximation is that the properties of each element may be selected independently. Thus different moduli of elasticity, Poisson's ratios, unit weights, thermal changes, etc., can be imposed in each element without increasing the complexity of the analysis. This characteristic of the method is particularly advantageous in the analysis of dams where a definite discontinuity of properties is likely to exist between the foundation rock and the concrete of the structure.

The Matrix Analysis Procedure

The finite element idealization of a plane stress problem constitutes a highly interconnected structural system. For such systems, the displacement method of structural analysis has proven to be most effective; and for large systems, the use of matrix algebra leads to the most efficient computational processes. A general description of the displacement method formulated as a sequence of matrix operations has been published previously[8], but the principles will be reviewed here for the convenience of the reader.

The analysis begins with a description of the structure and its loading expressed in matrix form. The properties of the structure are

defined in two matrices; one, called the element stiffness matrix, expresses the elastic properties of each of the triangular elements making up the structure; the second, called the displacement transformation matrix, defines the geometry of the assemblage. In addition, the listing of the vertical and horizontal load components applied to each nodal point comprises the load matrix. These three matrices, which will be designated $[k]$, $[a]$, and $\{R\}$ respectively, are discussed further in the following sections of this chapter.

When the properties of the structure have been expressed in matrix form, the analysis proceeds as follows. First, the stiffness of the assembled structural system $[K]$ is obtained by multiplying together the element stiffness and displacement transformation matrices:

$$[K] = [a]^T [k][a] \tag{1}$$

in which $[a]^T$ is the transpose of $[a]$. The structural stiffness matrix $[K]$ defines the nodal force components in the assembled structure which result from unit displacements of the nodal points. Representing these elastic force components and nodal displacements by the column matrices $\{Q\}$ and $\{r\}$, respectively, this force-displacement relationship may be expressed:

$$\{Q\} = [K]\{r\} \tag{2}$$

However, equilibrium considerations require that the elastic forces $\{Q\}$ developed at the nodal points must equal the externally applied loads $\{R\}$. Thus Eq. 2 may be rewritten in terms of the external load matrix:

$$\{R\} = [K]\{r\} \tag{3}$$

In a typical problem the loads $\{R\}$ are given, while the displacements $\{r\}$ are to be determined, thus the next step in the analysis is the inversion of the stiffness matrix $[K]$ to obtain the flexibility of the structure $[F]$:

$$[F] = [K]^{-1} \tag{4}$$

Multiplying both sides of Eq. 3 by the flexibility matrix then yields an expression for the displacements in terms of the loads,

$$\{r\} = [F]\{R\} \tag{5}$$

Eq. 5 thus provides one part of the final analytical results which were required: the deformations of the structure.

After the nodal displacements have been determined, the deformations of the individual plate elements: denoted by the column matrix $\{v\}$ can be determined by applying the displacement transformation matrix,

$$\{v\} = [a]\{r\} \tag{6}$$

Multiplying these element deformations by the element stiffness matrix then yields the nodal point forces $\{S\}$ in each element,

$$\{S\} = [k]\{v\} = [k][a]\{r\} \tag{7}$$

(It may be noted that Eqs. 6 and 7 essentially constitute definitions of the matrixes $[a]$ and $[k]$).

In the analysis of a structural system which is composed of bar type elements, the nodal point forces would represent the final results. However, in the plane stress problem considered here, the distributed stresses

within the elements, $\{\sigma\}$, rather than the resultant nodal forces, are of primary interest. Thus one final step is needed, the transformation from nodal forces to element stresses. Designating the stress transformation matrix by the symbol $[m]$, this operation is performed as follows,

$$\{\sigma\} = [m]\{S\} = [m][k]\{\sigma\} \tag{8}$$

Finally, representing the above matrix product by a single symbol

$$[M] \equiv [m][k] \tag{9}$$

Eq. 8 may be written

$$\{\sigma\} = [M][a]\{r\} \tag{10}$$

in which $[M]$ performs the function of transforming from element deformations to element stresses. The entire analytic procedure is now contained in Eqs. 1, 4, 5, and 10.

Although the procedure described above is straight-forward, and provides a convenient method for the analysis of small to moderate-size systems, the inversion of the stiffness matrix (Eq. 4) is a tremendous task when large systems (involving over perhaps 100 nodal points) are to be analyzed. In order to avoid this problem, an iterative solution of Eq. 3 for the nodal point displacements was substituted for the inversion process. Using this approach the procedure is capable of treating systems having as many as 600 nodal points.

Element Stiffnesses

Isotropic Elasticity - The method used in deriving expressions for the stiffnesses of triangular plate elements composed of isotropic elastic material has been described previously[4] so only the results will be presented here. The geometry of a typical element is defined in Fig. 2.

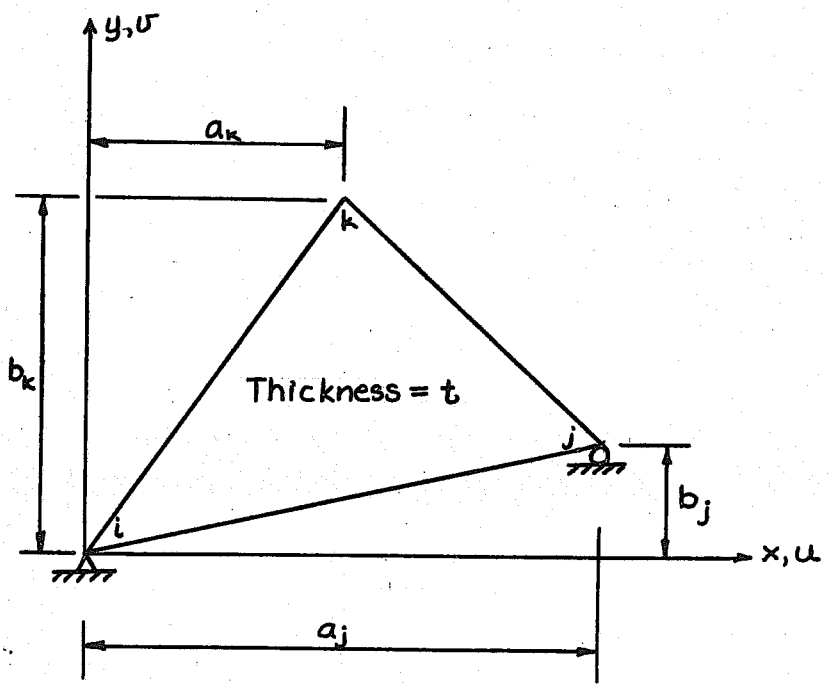

FIG. 2 TRIANGULAR PLATE ELEMENT DIMENSIONS

Its stiffness matrix is presented in Eq. 11, below:

$$[k] = \frac{Et}{2(1-\nu^2)(a_j b_k - b_j a_k)} \begin{bmatrix} b_k^2 + \xi a_k^2 & (\text{Symmetrical}) & \\ -b_k b_j - \xi a_j a_k & b_j^2 + \xi a_j^2 & \\ \nu a_j b_k + \xi a_k b_j & -\left(\frac{1+\nu}{2}\right) a_j b_j & a_j^2 + \xi b_j^2 \end{bmatrix} \qquad (11)$$

in which

E = Modulus of Elasticity

ν = Poisson's ratios

$\xi = \frac{1-\nu}{2}$

In the preceding discussion of the finite element method, it has been assumed that the system to be solved is subjected to a condition of plane <u>stress</u>, and Eq. 11 applies to this condition. On the other hand, there may be some justification for assuming that a gravity dam is in a state of plane <u>strain</u>. The plane stress stiffness matrix of Eq. 11 can be applied in a plane strain analysis if modified elastic properties are introduced in the equations as follows:

$$E^* = \frac{E}{1-\nu^2}$$
$$\nu^* = \frac{\nu}{1-\nu} \qquad (12)$$

In these equations, the "starred" values are the modified properties to be used in applying Eq. 11 to a plane strain analysis, while the unstarred values are the actual properties.

In the present investigation, the plane stress equations were used

exclusively, because it was assumed that the method of construction (in large monoliths) would lead more closely to such conditions. However, it may also be noted that for the values of Poisson's ratio used in this study ($\nu = 0.17$), the difference between the modified and actual properties ($E^* = 1.03E$; $\nu^* = 1.20\nu$) is well within the limits of accuracy with which these values can be estimated. Thus the question as to whether a condition of plane stress or plane strain exists is only of academic interest.

Orthotropic Elasticity - In order to establish the influence of an orthotropic foundation material on the stress distribution in the dam, it was necessary to develop the stiffness matrix for an orthotropic triangular element. The derivation of the orthotropic stiffness matrix followed exactly the same procedure used in deriving the isotropic stiffness matrix except that the stress-strain relationship for the orthotropic material was substituted for the isotropic stress-strain relationship used in Reference 4. Thus, the first requirement was the derivation of the orthotropic stress-strain relationship.

For this purpose, it was assumed that the orthotropic material was actually a layered system consisting of two isotropic materials of different stiffnesses, E_1 and E_2, as shown in Figure 3.

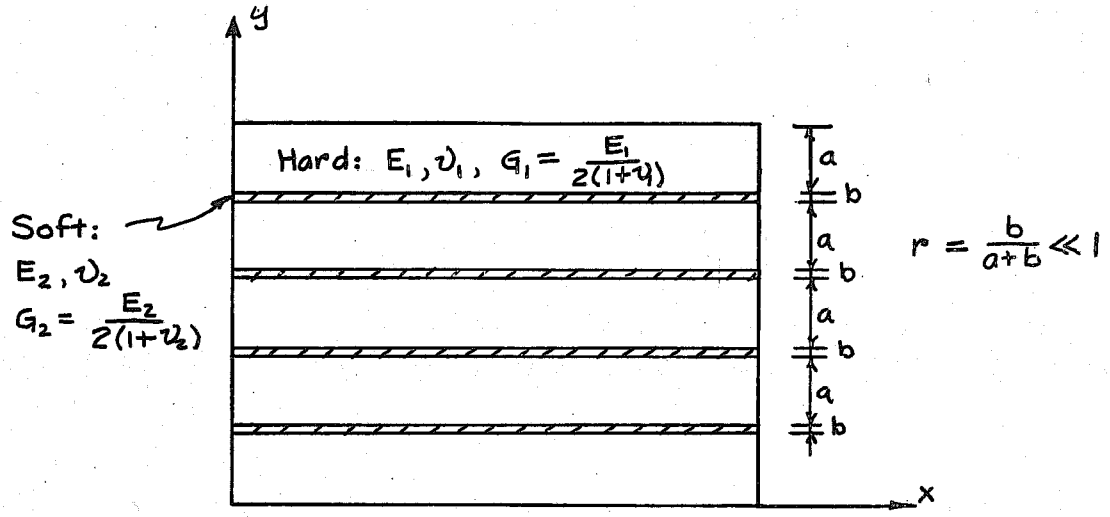

FIG. 3 ASSUMED ORTHOTROPIC MATERIAL

The softer material (E_2) was assumed to occupy only a small proportion, r, of the total thickness, and it was further assumed that the ratios of the elastic moduli of the two materials was the same as the ratios of their Poisson's ratios:

$$\frac{\nu_1}{\nu_2} = \frac{E_1}{E_2} \tag{13}$$

The effective elastic properties of this layered material were determined by applying successively stresses σ_x, σ_y, and τ_{xy}, and computing the resulting strains ε_x, ε_y, and γ_{xy}.

Applying the horizontal stress, σ_x, the effective horizontal modulus is found to be

$$E_x \equiv \frac{\sigma_x}{\varepsilon_x} = E_1 (1 - r^*)$$

$$\text{where} \quad r^* = r\left(1 - \frac{E_2}{E_1}\right) \tag{14}$$

while the effective Poisson's ratio is given by

$$\upsilon_x \equiv -\frac{\varepsilon_y}{\varepsilon_x} = \upsilon_1 (1 - r^*) \tag{15}$$

Similarly, applying the vertical stress, σ_y, the effective vertical modulus is

$$E_y \equiv \frac{\sigma_y}{\varepsilon_y} = \frac{E_2}{\frac{E_2}{E_1} + r^*} \tag{16}$$

and the corresponding Poisson's ratio is

$$\upsilon_y \equiv -\frac{\varepsilon_x}{\varepsilon_y} = \upsilon_x \frac{E_y}{E_x} = \upsilon_x \frac{1}{\mu} \tag{17}$$

$$\text{where} \quad \mu = \frac{E_x}{E_y}$$

Finally, applying the shear stress, τ_{xy}, the effective shear modulus is found to be

$$G = \frac{E_x}{2(\mu + \upsilon_x)} \tag{18}$$

These elastic properties may be summarized by the orthotropic stress-strain relationship, which follows:

$$\begin{bmatrix} \varepsilon_x \\ \varepsilon_y \\ \gamma_{xy} \end{bmatrix} = \frac{1}{E_x} \begin{bmatrix} 1 & -\nu_x & 0 \\ -\nu_x & \mu & 0 \\ 0 & 0 & 2(\mu+\nu_x) \end{bmatrix} \begin{bmatrix} \sigma_x \\ \sigma_y \\ \tau_{xy} \end{bmatrix} \quad (19)$$

In the derivation of the element stiffness, the inverse form of this stress-strain relationship is required, as follows;

$$\begin{bmatrix} \sigma_x \\ \sigma_y \\ \tau_{xy} \end{bmatrix} = \frac{E_x}{\mu - \nu_x^2} \begin{bmatrix} \mu & \nu_x & 0 \\ \nu_x & 1 & 0 \\ 0 & 0 & \frac{\mu-\nu_x^2}{2(\mu+\nu_x)} \end{bmatrix} \begin{bmatrix} \varepsilon_x \\ \varepsilon_y \\ \gamma_{xy} \end{bmatrix} \quad (20)$$

Employing this orthotropic stress-strain relationship in the procedure described in Reference 4 for the derivation of the triangular element stiffness leads to the following final result for the orthotropic plate element stiffness matrix, $[\bar{k}]$:

$$[\bar{k}] = \frac{E t}{2(\mu-\nu_x^2)(a_j b_k - b_j a_k)} \begin{bmatrix} \mu b_k^2 + \eta a_k^2 & (\text{Symmetrical}) & \\ -\mu b_j b_k - \eta a_j a_k & \mu b_j^2 + \eta a_j^2 & \\ \nu_x a_j b_k + \eta a_k b_j & -(\eta+\nu_x) a_j b_j & a_j^2 + \eta b_j^2 \end{bmatrix} \quad (21)$$

where

$$\eta = \frac{\mu - \nu_x^2}{2(\mu+\nu_x)}$$

Complete Element Stiffness Matrix - The complete element stiffness matrix is formed merely by arranging the individual element stiffnesses as submatrices on the diagonal of the complete matrix. Thus, if the individual element stiffness matrices of elements a, b, c, . . . n are designated k_a, k_b, k_c, . . . k_n the complete matrix may be written

$$[k] = \begin{bmatrix} k_a & & & & \\ & k_b & & & \\ & & k_c & & \\ & & & \ddots & \\ & & & & k_n \end{bmatrix} \tag{22}$$

Element Stress Matrix - It was noted above that the stresses in an element are of greater interest than the nodal forces, and that the matrix $[M]$ would serve to transform from the element deformations to the stresses. This stress transformation matrix, which was not presented in the previous publication, is given below for any arbitrary element "i",

$$[M_i] = \frac{E}{(1-\nu^2)(a_j b_k - b_j a_k)} \begin{bmatrix} b_k & -b_j & \nu a_j \\ \nu b_k & -\nu b_j & a_j \\ -\xi a_k & \xi a_j & -\xi b_j \end{bmatrix} \tag{23}$$

where $\xi = \frac{1-\nu}{2}$

The transformation of stress for all elements in the structure thus may

be accomplished by means of a diagonal matrix made up of the individual element stress transformations,

$$[M] = \begin{bmatrix} M_a & & & & \\ & M_b & & & \\ & & M_c & & \\ & & & \ddots & \\ & & & & M_n \end{bmatrix} \qquad (24)$$

Although the normal and shear stresses (σ_x, σ_y, & τ_{xy}) completely define the state of stress in the elements, it frequently is of interest to know the principal stresses σ_1 and σ_2 and their directions θ. In this investigation these principal stress values were determined from the stress values related to the x, y coordinate axes by the standard transformation formulas of elementary mechanics.

Displacement Transformation Matrix

The displacement transformation matrix serves to relate the deformations of the finite elements to the displacements of the nodal points, as is shown by Eq. 6. The derivation of this matrix will be discussed with reference to Fig. 4, which shows a portion of a triangular element system. The form of the displacement transformation can be demonstrated by establishing the rationship between the displacements of nodal points I, J, and K, and the resulting deformations of element "n". Similar relationships could be established between any nodal displacements and the deformations of the elements connected thereto.

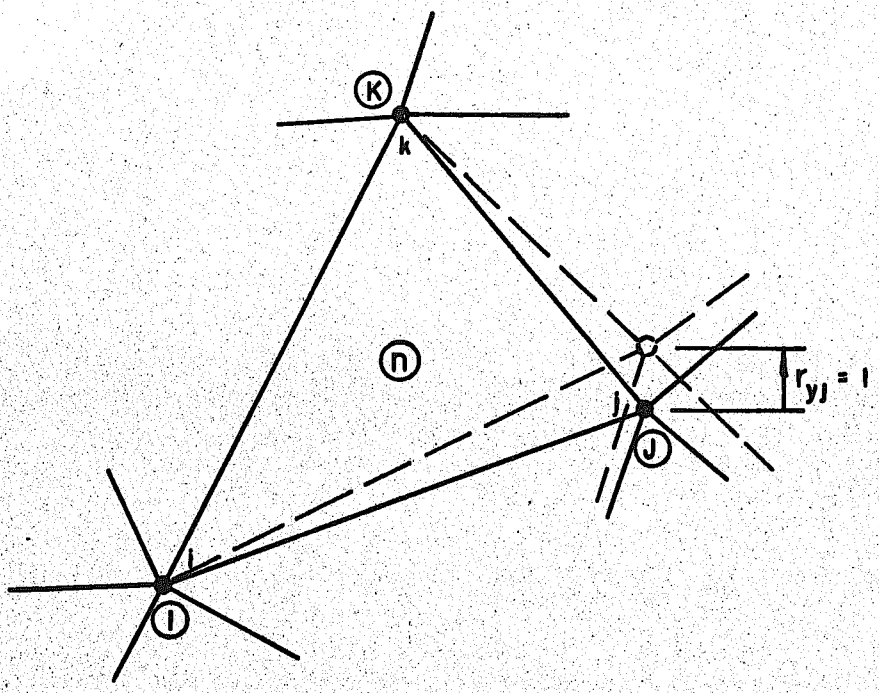

a. VERTICAL DISPLACEMENT OF JOINT J

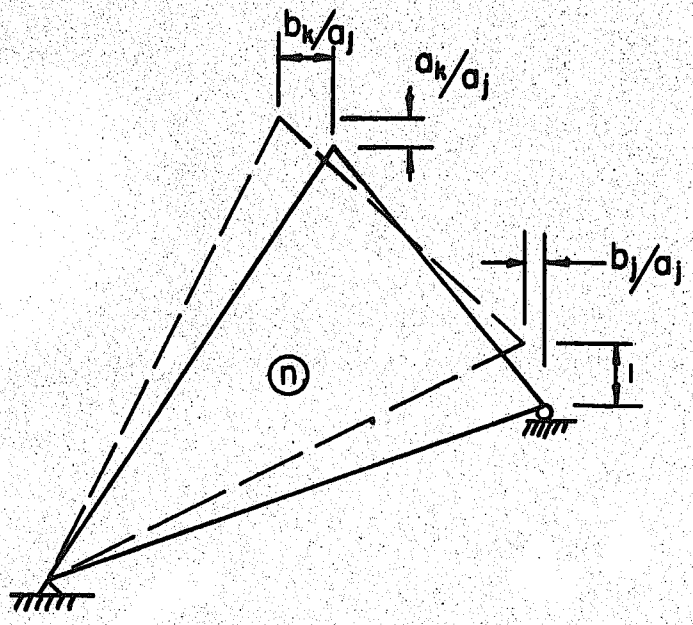

b. NODAL DISPLACEMENTS DUE TO RIGID BODY ROTATION

FIG. 4 TYPICAL DISPLACEMENT TRANSFORMATION ANALYSIS

As an example, a unit vertical displacement at joint J is indicated in Fig. 4a, and the resulting distorted configuration of element "n" is shown by the dashed lines. This distortion pattern violates the support conditions which were assumed for the element in deriving its stiffness (see Fig. 2). To return the element to the required support conditions, a rigid body rotation is applied, as shown in Fig. 4b. The actual distortion shown in Fig. 4a, can now be expressed in terms of the required support conditions as is indicated in the second column of the matrix below

$$\begin{bmatrix} u_j \\ u_k \\ v_k \end{bmatrix}_n = \begin{bmatrix} 1 & b_j/a_j \\ 0 & b_k/a_j \\ 0 & -a_k/a_j \end{bmatrix}_n \begin{bmatrix} r_x \\ r_y \end{bmatrix}_J \tag{25a}$$

The first column of this matrix represents the relationship between the horizontal displacements of joint J and the element deformations. Since this displacement does not violate the required support conditions for the element, it is clear that $u_{j_n} = r_{x_J}$ directly.

Eq. 25a may be written symbolically as follows

$$\{v_n\} = [a_{nJ}]\{r_J\}$$

Similar relationships can be developed for the displacements of nodal points I and K as follows

$$\begin{bmatrix} u_j \\ v_j \\ v_k \end{bmatrix}_n = \begin{bmatrix} 0 & 0 \\ 1 & 0 \\ 0 & 1 \end{bmatrix}_n \begin{bmatrix} r_x \\ r_y \end{bmatrix}_{ij} \quad ; \quad \begin{bmatrix} u_j \\ u_k \\ v_k \end{bmatrix}_n = \begin{bmatrix} -1 & -b_j/a_j \\ -1 & -b_k/a_j \\ 0 & \frac{a_k - a_j}{a_j} \end{bmatrix}_n \begin{bmatrix} r_x \\ r_y \end{bmatrix}_k \tag{25b}$$

or in symbolic form

$$\{v_n\} = [a_{nI}]\{r_I\} \; ; \quad \{v_n\} = [a_{nK}]\{r_K\}$$

Eqs. 25a and 25b may also be combined into a single relationship, expressed symbolically as follows

$$\{v_n\} = [a_{nI} \; a_{nJ} \; a_{nK}] \begin{Bmatrix} r_I \\ r_J \\ r_K \end{Bmatrix} \tag{26}$$

Relationships similar to Eq. 26 can be established between all nodal point displacements and element deformations. For example, for the simple system shown in Fig. 5, the complete displacement transformation would be of the form

$$\begin{bmatrix} v_a \\ v_b \\ v_c \\ v_d \end{bmatrix} = \begin{bmatrix} a_{aK} & a_{aI} & a_{aJ} \\ 0 & a_{bK} & 0 \\ 0 & a_{cI} & a_{cK} \\ 0 & 0 & a_{dK} \end{bmatrix} \begin{bmatrix} r_1 \\ r_2 \\ r_3 \end{bmatrix} \tag{27}$$

in which each of the symbols is as defined in Eqs. 25a and 25b, with dimensions selected as appropriate to the particular element.

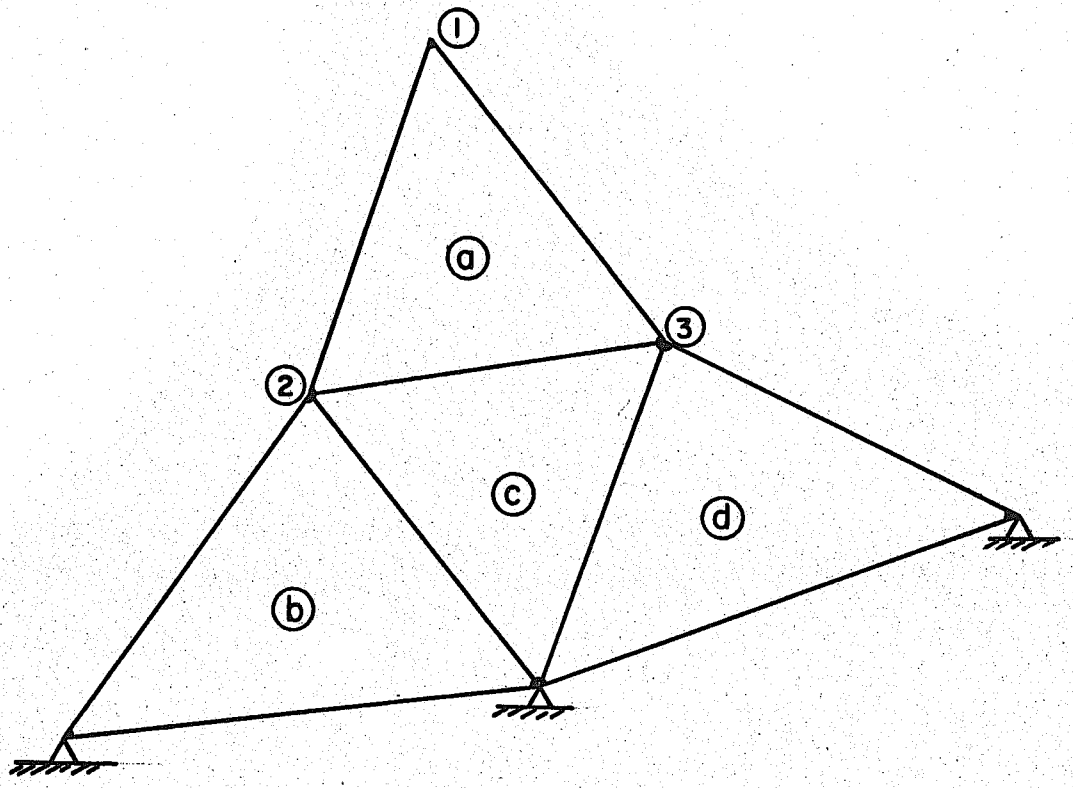

FIG. 5 SIMPLE TRIANGULAR ELEMENT SYSTEM

Load Matrix

The load matrix is merely a listing $\{R\}$ of the load components applied to the nodal points of the plate element assemblage, presented in the same sequence as were the displacement components $\{r\}$ in the development of the displacement transformation matrix. Three types of loadings were considered in this investigation, dead loads, live loads, and thermal loads, each of which will be discussed separately below.

Dead Loads - The dead weight of each plate element is given, of course, by the product of its area, its thickness (which was taken as one foot) and its unit weight, γ_c . One third of the total element weight was applied at each of the three nodal points to which it was attached. Thus the total dead load at any nodal point was taken as one-third of the weights of all elements attached at that point, applied in a downward, or negative "y" direction.

Live Loads - In calculating the hydrostatic water load acting at each nodal point, it was assumed that the pressure was distributed against an auxiliary stringer system, as shown in Fig. 6b. The reactions at the ends of the stringers, resolved into vertical and horizontal components as shown in Fig. 6c, then constituted the live loads. For any given nodal point, the live load depends not only on the depth of water at that level, but also upon the depths at the points above and below. Where the slopes of successive element faces are the same, as is the case in Fig. 6, the live load components at an arbitrary nodal point N are given by

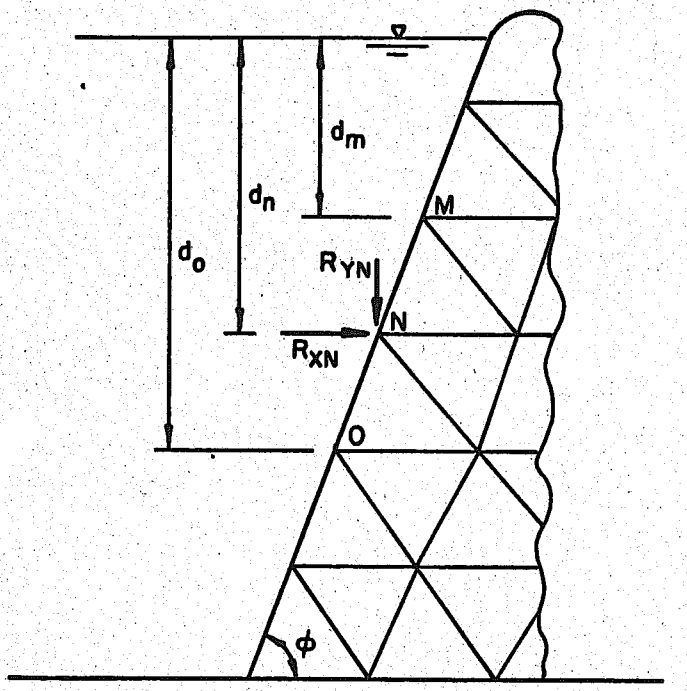

a. TYPICAL DAM SYSTEM

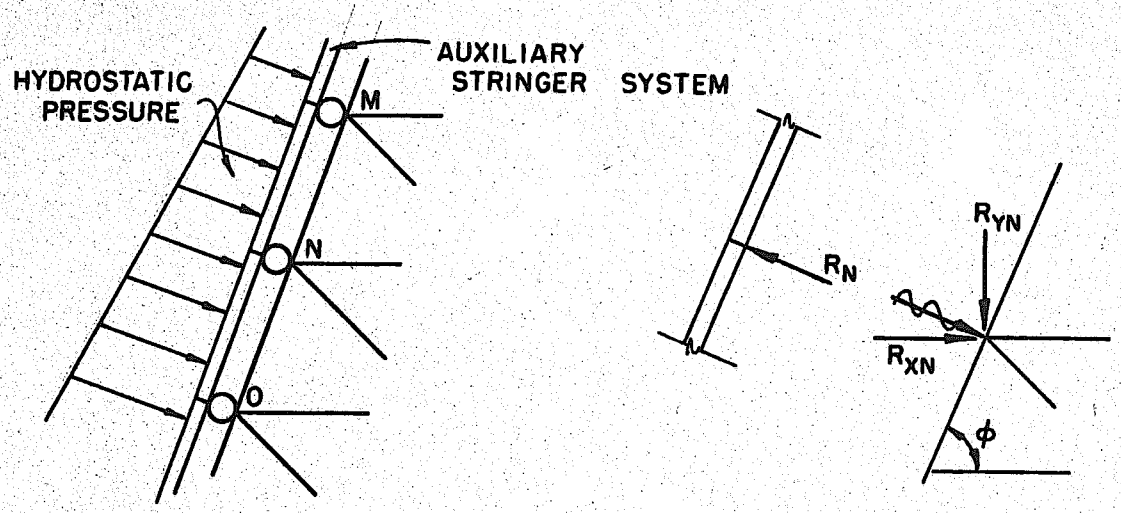

b. ASSUMED STRINGER SYSTEM

c. APPLIED NODAL FORCES

FIG. 6 REPRESENTATION OF HYDROSTATIC PRESSURES BY NODAL FORCES

$$R_{xN} = \frac{\gamma_w}{6}(d_o + d_n + d_m)(d_o - d_m)$$
$$R_{yN} = R_{xN} \cot \phi \qquad (28)$$

in which γ_w is the unit weight of water and the other symbols are defined in Fig. 6a.

Thermal Loads - The thermal loads may be calculated by first calculating the stresses which would exist in the elements if strains due to temperature changes were fully constrained. In a plane stress system* these stresses are given by

$$\sigma_x = \sigma_y = \sigma = -\frac{E\alpha}{1-\nu}\Delta T \qquad (29)$$

in which α = thermal coefficient of expansion

ΔT = change of temperature

The nodal forces required to maintain these internal stresses in each element may then be found by simple statics. While these constraining forces are applied, no displacements or deformations of the structure may occur, and the stresses are given directly by Eq. 29. However, the constraints are not really present, so their effect must be eliminated by applying equal and opposite nodal forces. These reversed constraining forces are the thermal loads for which the structure is analyzed.

---

*In a plane strain system, the corresponding expression is

$$\sigma = -\frac{E\alpha}{(1+\nu)(1-2\nu)}\Delta T$$

but for the relatively low Poisson's ratio assumed in this investigation, the difference between this and Eq. 29 is less than 5 per cent. As was mentioned previously, the plane stress condition was assumed throughout this investigation.

For the element shown in Fig. 2, they would be expressed by

$$\begin{bmatrix} R_{xi} \\ R_{yi} \\ R_{xj} \\ R_{yj} \\ R_{xk} \\ R_{yk} \end{bmatrix} = \frac{1}{2} \begin{bmatrix} b_k - b_j \\ a_j - a_k \\ -b_k \\ a_k \\ b_j \\ -a_j \end{bmatrix} \tilde{\sigma} \qquad (30)$$

in which $\tilde{\sigma}$ is given by Eq. 29.

The displacements resulting from these thermal loads are the true thermal displacements in the system. However, the stresses resulting from these loads are only the part of the thermal stress associated with the nodal displacements. The total thermal stress is the sum of the deformation stress resulting from the thermal loads, plus the constrained stress given by Eq. 29.

Boundary Displacements

In the preceding discussion of the general matrix analysis procedure, it was indicated that the typical analysis requires the determination of nodal displacements resulting from a given set of applied loads. In some cases, however, a "mixed" problem may exist in which forces are specified at only part of the nodal points and certain specific displacements are imposed at other points. Such mixed problems may be solved with no greater difficulty than cases in which nodal point loads are the only stress producing effects.

The analysis is formulated by partitioning the nodal point forces $\{R\}$ into two submatrices: the specified loads $\{R_s\}$ and the unknown force components $\{X\}$ (which correspond with specified nodal displacements). At the same time, the nodal point displacements $\{r\}$ are

partitioned into submatrices representing the specified displacements $\{r_s\}$ and the unknown displacements $\{U\}$ (which correspond with the specified nodal forces). In this partitioned form, Eq. 3 may be written

$$\left\{\begin{array}{c} R_s \\ \hline X \end{array}\right\} = \left[\begin{array}{c|c} K_{00} & K_{01} \\ \hline K_{10} & K_{11} \end{array}\right] \left\{\begin{array}{c} U \\ \hline r_s \end{array}\right\} \tag{31}$$

in which the stiffness matrix $[K]$ has been partitioned to correspond with the partitioning of the load and displacement matrices. Then a formal solution for the unknown displacements $\{U\}$ is obtained from the first of these submatrix equations:

$$\{R\} = [K_{00}]\{U\} + [K_{01}]\{r_s\} \tag{31a}$$

i.e.
$$\{U\} = [K_{00}]^{-1}\{R_s\} - [K_{00}]^{-1}[K_{01}]\{r_s\} \tag{32}$$

Finally the unknown forces $\{X\}$ may be determined from the remaining submatrix equation

$$\{X\} = [K_{10}]\{U\} + [K_{11}]\{r_s\} \tag{31b}$$

or introducing the value of $\{U\}$ from Eq. 32,

$$\{X\} = [K_{10}][K_{00}]^{-1}\{R_s\} + \left[[K_{11}] - [K_{10}][K_{00}]^{-1}[K_{01}]\right]\{r_s\} \tag{33}$$

Because the matrix inversions required in the formal solution of a large structural system, (the calculation of $[K_{00}]^{-1}$ in Eq. 33) is a formidable problem, an iterative solution for the displacements was employed in this investigation, as has been mentioned earlier. The

solution of a mixed problem in which certain displacements $\{r_s\}$ are specified, does not require any modification of the iterative process. No iteration is required at these points because a reaction is available to support any unbalanced forces which develop.

COMPUTER PROGRAM

The digital computer program performs three major tasks in the complete analysis of a plane stress system. First the stiffness, displacement transformation, and load matrices are formed from a basic numerical description of the system. Second, Equation 3 is solved for the displacements of the nodal points by an iteration procedure. Third, the internal element stresses are determined from these displacements. The general features of the program which carries out these operations will be described in this chapter.

Numerical Procedure

Before presenting the sequence of operations that is performed by the computer program, it is necessary to discuss in some detail the actual numerical method that was employed. This method is a modification of the well-known Gauss-Seidel iteration procedure which, when applied to Equation 3, involves the repeated calculation of new displacements from the equation

$$r_n^{(s+1)} = k_{nn}^{-1}\left[R_n - \sum_{i=1,n-1} k_{ni}\, r_i^{(s+1)} - \sum_{i=n+1,N} k_{ni}\, r_i^{(s)}\right] \qquad (34)$$

where n is the number of the unknown and s is the cycle of iteration.

The only modification of the procedure introduced in this analysis is the application of Eq. 34 simultaneously to both components of displacement at each nodal point. Therefore, r_n and R_n become vectors with x and y components, and the stiffness coefficients may be expressed

in the form

$$k_{\ell m} = \begin{bmatrix} k_{xx} & k_{xy} \\ k_{yx} & k_{yy} \end{bmatrix}_{\ell m} \tag{35}$$

in which 1 and m are nodal point numbers.

Over-Relaxation Factor - The rate of convergence of the Gauss-Seidel procedure can be greatly increased by the use of an over-relaxation factor[9]. However, in order to apply this factor it is first necessary to calculate the change in the displacement of nodal point n between cycles of iteration:

$$\Delta r_n^{(s)} = r_n^{(s+1)} - r_n^{(s)} \tag{36}$$

The substitution of Equation 34 into Equation 36 yields for the change in displacement

$$\Delta r_n^{(s)} = k_{nn}^{-1}\left[R_n - \sum_{i=1,n-1} k_{ni}\, r_i^{(s+1)} - \sum_{i=n,N} k_{ni}\, r_i^{(s)}\right] \tag{37}$$

The new displacement of nodal point n is then determined from the following equation:

$$r_n^{(s+1)} = r_n^{(s)} + \beta\, \Delta r_n^{(s)} \tag{38}$$

where β is the over-relaxation factor. For the structure considered in this report it was found that a value of β equal to 1.86 gave the most rapid convergence.

Physical Interpretation of Method - There is important physical significance in the terms of Eq. 37. The term $(k_m)^{-1}$ is the flexibility of nodal point n. This represents the nodal point displacements resulting from unit nodal point forces, and can be written in the form of a sub-matrix.

$$k_{nn}^{-1} = \begin{bmatrix} f_{xx} & f_{xy} \\ f_{yx} & f_{yy} \end{bmatrix} \tag{39}$$

The summation terms in Eq. 37 represent the elastic forces acting at nodal point n due to the deformations of the plate elements:

$$Q_n^{(s+1)} = \sum_{i=1,n} k_{ni} r_i^{(s+1)} + \sum_{i=n+1,N} k_{ni} r_i^{(s)} \tag{40}$$

The difference between these elastic forces and the applied loads is the total unbalanced force which in sub-matrix form may be written:

$$\begin{Bmatrix} X \\ Y \end{Bmatrix}_n^{(s+1)} = \begin{Bmatrix} R_x \\ R_y \end{Bmatrix}_n - \begin{Bmatrix} Q_x \\ Q_y \end{Bmatrix}^{(s+1)} \tag{41}$$

Eq. 38, which gives the new displacement of nodal point n, may now be rewritten in the following sub-matrix form:

$$\begin{Bmatrix} r_x \\ r_y \end{Bmatrix}_n^{(s+1)} = \begin{Bmatrix} r_x \\ r_y \end{Bmatrix}_n^{(s)} + \beta \begin{bmatrix} f_{xx} & f_{xy} \\ f_{yx} & f_{yy} \end{bmatrix}_n \begin{Bmatrix} X \\ Y \end{Bmatrix}^{(s+1)} \tag{42}$$

It is important to note that any desired nodal point displacement $r_n^{(o)}$ may be assumed for the first cycle of iteration. A good choice of these displacements will greatly speed the convergence of the solution. In fact, if all displacements were assumed correctly, the unbalanced forces given by Eq. 41 would be zero and no iteration would be necessary. However, in a practical case there always will be unbalanced forces in the system at first, and the iteration process continually reduces them toward zero.

Boundary Condition - Eq. 42 is valid for all nodal points within the structure; however, in order for it to be applied to boundary nodal points the flexibility coefficients must be modified to account for the specific types of restraint which may exist. Since these flexibility coefficients are independent of the cycle of iteration, this modification is performed before the start of iteration. There are three possible types of boundary nodal points whose flexibility coefficients must be modified as follows:

(1) For points fixed in both x and y directions, $\Delta r_x = \Delta r_y = 0$:

$$f_{xx}^* = f_{xy}^* = f_{yx}^* = f_{yy}^* = 0 \tag{43a}$$

(2) For points fixed in the x direction only, $\Delta r_x = 0$:

$$\left.\begin{aligned} f_{xx}^* &= f_{xy}^* = f_{yx}^* = 0 \\ f_{yy}^* &= f_{yy} - \frac{f_{yx}\, f_{xy}}{f_{xx}} \end{aligned}\right\} \tag{43b}$$

(3) For points fixed in y direction only, $\Delta r_y = 0$:

$$\left.\begin{aligned} f^*_{xy} &= f^*_{yx} = f^*_{yy} = 0 \\ f^*_{xx} &= f_{xx} - \frac{f_{yx} f_{xy}}{f_{yy}} \end{aligned}\right\} \qquad (43c)$$

For the structure considered in this report all boundary nodal points were fully fixed, and Eq. 43a was applied.

Sequence of Operations

Only the main operations of the computer program will be described; the details of coding will be omitted. The program was written for an IBM 704 computer with 32768 storage locations. The operation of the program is flexible in that both input and output can be "on-line" or may be effected "off-line" through the use of magnetic tapes and peripheral equipment.

Input Data - For the purpose of numerically defining a structure, all nodal points and elements are numbered as illustrated in Fig. 7. The numerical description is read into the machine in the form of punched cards, by the following four arrays:

A. Parameter Array (6 numbers)

1. Numbered elements
2. Number of nodal points
3. Number of boundary points
4. Over-relaxation factor
5. Convergence limit
6. Coefficient of thermal expansion

B. Element Array (9 numbers per element)

1. Element number
2. Number of nodal point i
3. Number of nodal point j
4. Number of nodal point k
5. Modulus of elasticity E
6. Poisson's ratio ν

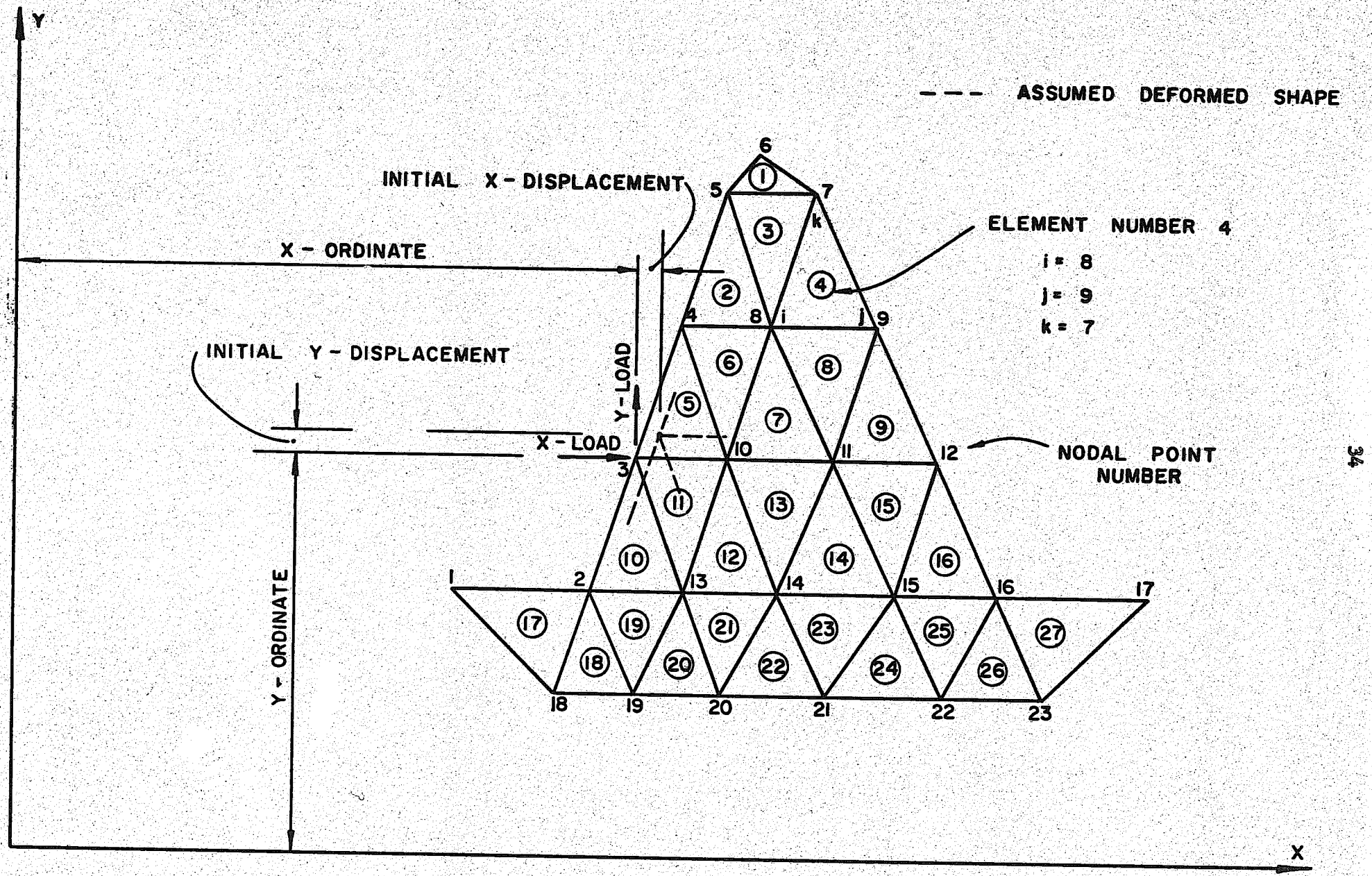

FIG. 7 NUMBERING SYSTEM FOR NODAL POINTS AND PLATE ELEMENTS

7. Unit weight of element γ_c
8. Temperature change within element ΔT
9. Orthotropic factor $\mu = \frac{E_x}{E_y}$

C. Nodal Point Array (7 numbers per nodal point)

1. Nodal point number
2. x-ordinate
3. y-ordinate
4. X-load
5. Y-load
6. Initial x-displacement
7. Initial y-displacement

D. Boundary Condition Array (2 numbers per boundary point)

1. Nodal point number
2. This number indicates the type of restraint; "0" for fixed in both directions; "1" for fixed in x-direction; and "2" for fixed in y-direction.

It should be noted that for a fixed boundary point, the initial displacement is the final displacement of the point, since it is not altered by the iteration procedure.

Formation of Element Stiffness Matrices - The stiffness matrix for each element is determined from Eq. 11 or Eq. 21. The basic element dimensions are calculated from the coordinates of the connecting nodal points:

$$a_j = x_j - x_i$$
$$b_j = y_j - y_i$$
$$a_k = x_k - x_i$$
$$b_k = y_k - y_i$$

where i, j, and k are the nodal point numbers of the three connecting points and are given in the element array.

Formation of Complete Stiffness of System - Because of the large matrices that are developed in a plane stress system, the formal matrix procedure represented by Eq. 1 is not used directly. Since the complete stiffness matrix contains many zero elements, only the non-zero elements are developed

and retained by the program; thus, it is possible to treat large plane stress systems without exceeding the storage capacity of the computer.

Formation of Load Matrix - The load matrix $\{R\}$ is composed of live loads, dead loads, and temperature loads. The equations which are used to determine these loads have been presented in the previous section of this report.

Formation of Nodal Flexibilities - The nodal point flexibilities are determined from the previously developed stiffness coefficients. The flexibilities associated with the boundary nodal points are modified by the application of Eqs. 43, as required.

Iterative Solution - The repeated application of Eq. 42 at all nodal points constitutes the iterative procedure. The sum of the absolute magnitude of the unbalanced forces at all nodal points (given by Eq. 41) is also computed for each cycle; this sum, when compared to the convergence limit, serves as a check on the convergence of the procedure. In all analyses presented in this report, this sum was reduced to less than 1/1000 of the value obtained in the first cycle of iteration.

Calculation of Element Stresses - From the nodal point displacements, with the aid of Eq. 23, the element stresses σ_x, σ_y, & τ_{xy} are calculated. As added information the principal stresses σ_1 and σ_2 and directions θ are also calculated.

Output Information - At desired points in the iteration procedure, nodal displacements and element stresses are printed. Fig. 8 illustrates the form of the computer output, in a typical case.

Timing

The computational time required by the program is approximately equal to 0.07 n•m seconds, where n equals the number of nodal points and

ELEMENT	(PSI) X-STRESS	(PSI) Y-STRESS	(PSI) XY-STRESS	(PSI) MAX-STRESS	(PSI) MIN-STRESS	(DEGREES) DIRECTION
1	-21.637024	-40.614304	33.432649	3.6	-65.9	-37.1
2	15.095711	3.577621	21.158474	31.3	-12.6	-37.4
3	-42.514305	-38.270859	2.591661	-37.0	-43.7	-64.7
4	-31.742538	-16.989304	14.911327	-7.7	-41.0	-58.2
5	-5.087471	9.535896	-4.226090	10.7	-6.2	75.0
6	-60.592682	-21.883614	5.673300	-21.1	-61.4	-81.8
7	3.596840	-6.501434	8.060141	8.1	-11.0	-29.0
8	-41.907402	8.325272	22.115488	16.7	-50.3	-69.3
9	-29.894760	-14.201363	2.760811	-13.7	-30.4	-80.3
10	-19.019836	-113.042328	41.108610	-3.6	-128.5	-20.6
11	-9.670067	-3.545715	1.172920	-3.3	-9.9	-79.5
12	-19.362946	24.689590	0.280712	24.7	-19.4	-89.6
13	-42.158066	2.489532	-3.621626	2.8	-42.4	85.4
14	-13.876846	9.762047	-1.376879	9.8	-14.0	86.7
15	-55.332329	12.838753	11.194128	14.6	-57.1	-80.9
16	-11.221085	21.112564	13.384552	25.9	-16.0	-70.2
17	-61.941177	-16.112938	31.179846	-0.3	-77.7	-63.2
18	14.900993	-10.251991	33.216614	37.8	-33.2	-34.6
19	-77.299423	-18.673866	45.481194	6.1	-102.1	-61.4
20	-68.392212	-25.644630	21.986590	-16.4	-77.7	-67.1
21	-34.477783	-10.517090	11.790384	-5.7	-39.3	-67.7
22	-7.344345	8.977432	-4.832099	10.3	-8.7	74.7
23	-34.220215	23.321732	-8.167995	24.5	-35.4	82.1
24	-11.582161	32.631912	-2.718958	32.8	-11.7	86.5
25	-46.657974	19.291512	3.835845	19.5	-46.9	-86.7
26	-13.946526	43.675842	18.032915	48.9	-19.1	-74.0
27	-83.458755	-12.719467	45.440448	9.5	-105.7	-63.9
28	-4.890427	13.208176	37.164865	42.4	-34.1	-51.8
29	1.348351	-10.524033	30.664423	26.6	-35.8	-39.5
30	-102.706940	-89.829132	46.319461	-49.5	-143.0	-49.0
31	-36.349174	-70.508469	66.600939	15.3	-122.2	-37.8
32	-1.370247	-44.906326	25.714500	10.6	-56.8	-24.9
33	-26.064774	-64.952545	59.050345	16.7	-107.7	-35.9
34	-20.962494	-16.453156	14.811054	-3.7	-33.7	-49.3
35	-32.728851	-5.217323	2.676623	-5.0	-33.0	-84.5
36	-45.844315	15.385841	-0.936499	15.4	-45.9	89.1
37	-22.696800	12.184837	-2.723261	12.4	-22.9	85.6
38	-9.309067	33.630989	-7.344516	34.9	-10.5	80.6
39	-16.388954	38.171394	-4.737985	38.6	-16.8	85.1
40	29.606812	46.513466	2.932751	47.0	29.1	-80.4
41	-6.309235	29.010864	-7.292584	30.5	-7.8	78.8
42	41.728279	65.571236	81.198050	135.7	-28.4	-49.2
43	-18.289627	-15.782555	19.939212	2.9	-37.0	-46.8
44	22.005043	-23.887611	62.266115	65.4	-67.3	-34.9
45	-9.252480	-55.976212	39.016029	12.9	-78.1	-29.5
46	-23.453789	-69.528412	51.371544	9.8	-102.8	-32.9
47	-57.654015	-19.821014	12.165121	-16.2	-61.2	-73.6
48	-16.010735	-1.447845	13.872331	6.9	-24.4	-58.8
49	-53.434456	6.212318	3.402412	6.4	-53.6	-86.7
50	-11.542534	29.182938	16.814773	35.2	-17.6	-70.2
51	-33.487152	19.204918	16.218376	23.8	-38.1	-74.2

NODAL POINT	(INCHES) X-DISPLACEMENT	(INCHES) Y-DISPLACEMENT
1	0.045173	-0.029458
2	0.058178	-0.013816
3	0.130151	-0.034537
4	0.166736	-0.067413
5	0.190258	-0.100647
6	0.209396	-0.136003
7	0.225354	-0.171480
8	0.238976	-0.207627
9	0.250559	-0.243729
10	0.261115	-0.279447
11	0.272950	-0.320961
12	0.289812	-0.371849
13	0.297384	-0.398693
14	0.238857	-0.416963
15	0.237644	-0.395673
16	0.191532	-0.400589
17	0.232356	-0.337109
18	0.190137	-0.351804
19	0.149180	-0.364911
20	0.141777	-0.380089
21	0.129665	-0.372276
22	0.238763	-0.288985
23	0.196613	-0.306839
24	0.154202	-0.323265
25	0.111614	-0.336806
26	0.087621	-0.344180
27	0.201616	-0.264921
28	0.159523	-0.282565
29	0.117430	-0.297379
30	0.096284	-0.302664
31	0.090143	-0.324456
32	0.068399	-0.327413
33	0.070444	-0.305661
34	0.046395	-0.305916
35	0.205631	-0.222702
36	0.163587	-0.241099
37	0.123230	-0.257917
38	0.084663	-0.269945
39	0.071567	-0.268477
40	0.048155	-0.267604
41	0.016155	-0.265461
42	0.207651	-0.180322
43	0.164601	-0.199870
44	0.122949	-0.217015
45	0.083207	-0.233610

FIG. 8 COMPUTER OUTPUT

m equals the number of cycles of iteration. The number of cycles required depends on the accuracy of the initially assumed displacements and on the desired degree of convergence. For the structure considered in this report, the computer time per solution was approximately 7 minutes for the coarse mesh and 17 minutes for the fine mesh idealization. Between 70 and 100 cycles of iteration were used in typical cases.

SCHEDULE OF ANALYSES

The Structural System

The dimensions and properties of the structural system considered in this investigation were supplied by the Contracting Office. Fig. 9 shows the basic geometry of the section of dam which was analyzed, Monolith 16. This was one of the most severely cracked portions of the structure. The extent of the cracking could not be defined exactly, but it appeared that there was one principal crack which extended from near the center of the base to roughly two-thirds of the height of the section, as shown in the figure. The physical properties assumed for the various materials in the system are listed in Table I, below.

Table I. ASSUMED PROPERTIES OF MATERIALS

Concrete:	Modulus of Elasticity	$E_c = 2.0 \times 10^6$ psi
	Poisson's Ratio	$\nu = 0.17$
	Unit Weight	$\gamma_c = 150$ pcf
	Thermal Coefficient	$\alpha = 7.0 \times 10^{-6}$ per ^oF
Foundation Rock:	Modulus of Elasticity	$E_f = 5.0 \times 10^6$ psi
	Poisson's Ratio	$\nu = 0.17$
	Thermal Coefficient	$\alpha = 7.0 \times 10^{-6}$ per ^oF
	Vertical Modulus (Orthotropic cases)	$\bar{E}_f = 1.0 \times 10^6$ psi
Water:	Unit Weight	$\gamma_w = 62.5$ pcf
Temperature change:	$\Delta T = -35^o$ in body of dam decreasing to 0^oF about 30 feet below the surface of the foundation rock (See Fig. 10)	

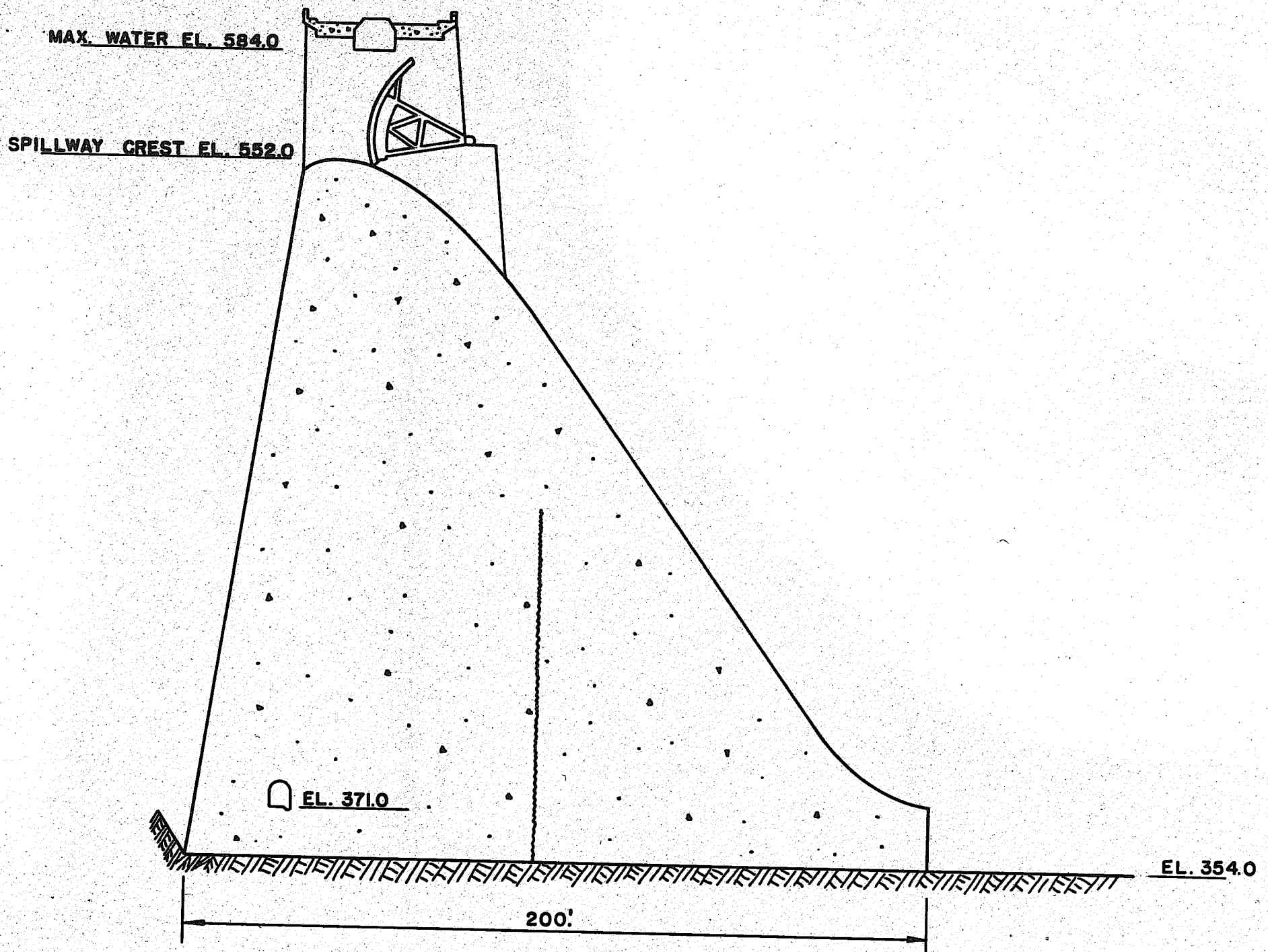

FIG. 9 BASIC GEOMETRY OF MONOLITH 16

The relatively low modulus of elasticity assumed for the concrete was chosen in order to account for the effects of creep which would be expected to have occurred in the twenty years since the dam was built. Dead weight of the foundation rock was not considered because the deformations and stresses resulting from this effect existed prior to the construction of the dam. Only conditions resulting from the construction of the dam were included in the investigation.

Cases Considered

The principal variables considered in these studies included the form of loading, the crack height, the type of foundation material (whether isotropic or orthotropic) and the possibility of uplift pressures at the upstream edge of the base. Several factors were considered in selecting the most significant combinations of these variables. For example, temperature changes are known to have played an important part in the behavior of the structure, and are assumed to have been the primary cause of cracking. Therefore, temperature effects were included with each of the basic configurations. However, because the computed thermal stresses were not considered to be representative of actual conditions, it was decided to use the thermal analysis primarily for determining the extent of the crack opening, and to calculate separately the stresses due to dead and live loads. Analyses of an uncracked section were included so that the specific influence of the crack on the stress distributions resulting from each of the loading conditions could be evaluated. The orthotropic foundation was considered only in those cases believed to be most representative of actual conditions in order to determine the importance of this factor. Similar considerations

dictated the choice of the case in which uplift pressures were included. The list of all cases studied is presented in Table II.

Table II. SCHEDULE OF ANALYSES

Case	Crack Height	Loading	Foundation	Uplift
A	None	Dead Load	Isotropic	No
B	"	Dead + Live	"	"
C	"	D + L + Temp.	"	"
D	Two-thirds	Dead Load	"	"
E	"	Dead + Live	"	"
F	"	Dead + Temp.	"	"
G	"	D + L + Temp.	"	"
H	"	Dead + Live	Orthotropic	"
I	Seven-Ninths	Dead Load	Isotropic	"
J	"	Dead + Live	"	"
K	"	Dead + Temp.	"	"
L-1	"	Dead + Live	"	3 nodal points
L-2	"	" "	"	3½ " "
M	"	" "	Orthotropic	No
N	2/9 to 7/9	" "	Isotropic	3 nodal points
*O-1	Two-thirds	Temperature	Isotropic	No
*O-2	"	Dead + Live	"	"

*These cases were included to provide a check on the analyses made by Mr. D. McHenry of the Portland Cement Association; material properties were those used in the PCA analyses rather than those cited above.

Analysis Procedure

Foundation Displacements - The finite element approximations used in the analysis of this dam are shown in Fig. 10. The coarse mesh approximation was employed first in order that a large foundation zone might be included in the analysis. With this idealization, the magnitude of the foundation deformations could be determined with good accuracy. Then the displacements calculated along the dashed line in the coarse mesh approximation were introduced as boundary displacements at the base of the fine mesh system. By this procedure it was possible to retain the effect of the complete foundation and still not devote a large number of elements to its treatment in the final analysis.

Separate coarse mesh analyses were carried out for each basic loading condition: dead load, dead plus live load, dead plus temperature, etc. Each set of calculated boundary displacements was then used in the analysis of the fine mesh case for the corresponding loading. It was assumed, however, that the extent of the crack would not affect the boundary displacements, thus the same displacements were introduced for a given load case regardless of the crack condition. It should be noted that water loads were applied to the appropriate foundation elements as well as to the dam structure in both coarse and fine mesh live load analyses.

Treatment of Crack - The presence of an open crack introduces no complication in the finite element analysis procedure; each side of the crack is treated just like any other external boundary. Nodal points are defined along both sides of the crack as shown in Fig. 11, and displacements of the two sets of points are assumed to take place independently.

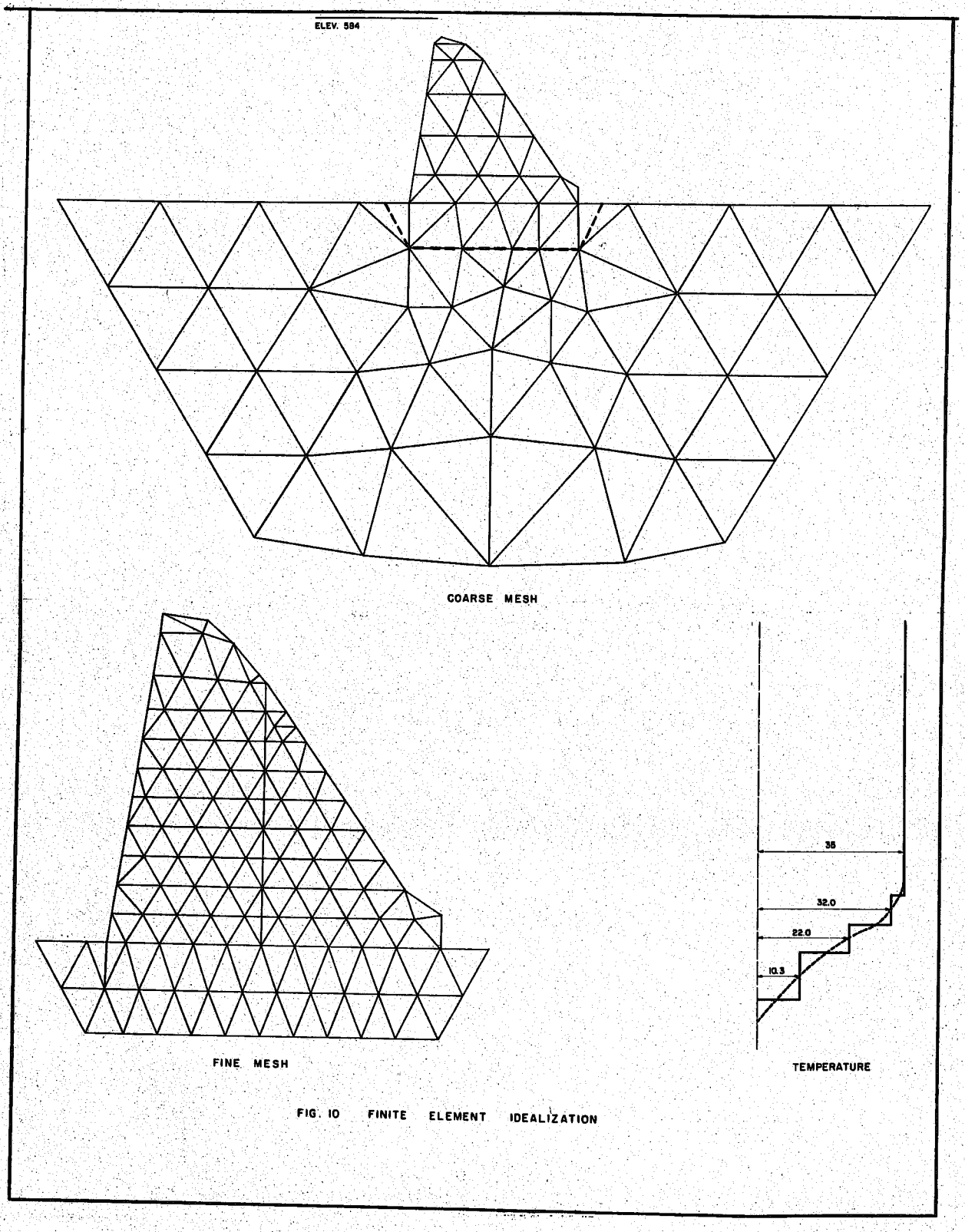

FIG. 10 FINITE ELEMENT IDEALIZATION

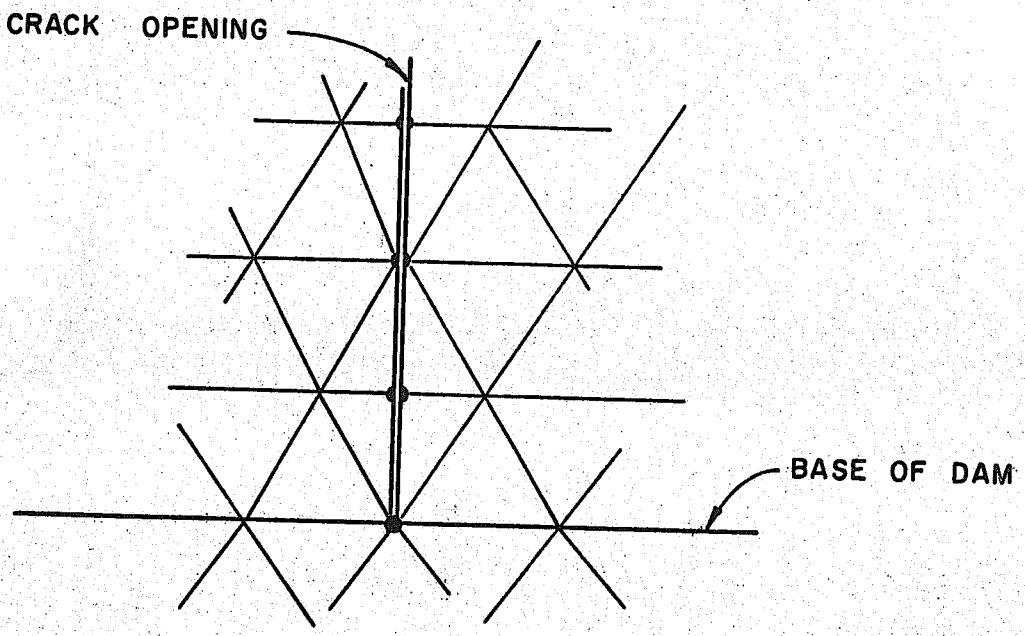

FIG. 11 REPRESENTATION OF CRACK USING PAIRS OF NODAL POINTS

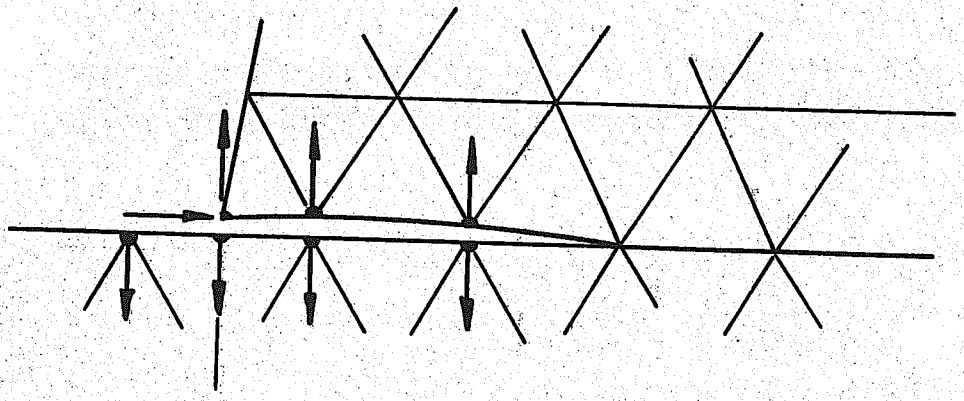

FIG. 12 HYDROSTATIC UPLIFT ACTING IN CRACK AT HEEL OF DAM

In order that this assumption be reasonable, it is necessary, of course, that each pair of points move apart rather than toward each other. Thus it was assumed that the dam was subjected first to the dead load plus temperature change conditions, which resulted in an opening of the crack. Then if the subsequent live loading did not completely eliminate the separation at any pair of nodal points it is clear that the two sides would continue to act independently as assumed.

Uplift Pressures - It was recognized at the outset of this investigation that there might be a tendency for tensile stresses to develop at the upstream edge of the base of the dam. Because the tensile strength at this point is essentially nil, it would be expected to crack open under any loading condition for which tensile stresses were indicated. Furthermore, since this crack would be exposed to the full hydrostatic pressure at the base of the dam (in live load conditions), uplift pressures would be developed over the full extent of the crack.

The uplift pressure analyses were treated in exactly the same manner as were the vertical crack analyses, with separate nodal points being located along the base of the dam and in the foundation rock, as shown in Fig. 12. The only difference was that hydrostatic live load forces were applied at the nodal points of this crack, acting normal to both the upper and lower surfaces, as shown. It was assumed that the crack extended downstream a distance of three nodal points (about 32 feet) because a grout curtain and relief drain system located in this vicinity would prevent the uplift pressure from extending further. (One analysis was made in which the uplift pressure was applied over a distance of about 42 feet, but this condition was not considered realistic).

RESULTS OF ANALYSES

The stress components in each element and the displacement components of each nodal point, which were calculated by the digital computer and printed in tabular form (see Fig. 8), constituted the direct results of the analysis procedure. However, the mass of numerical data was too bulky to be digested readily in this form, and a considerable effort was expended in representing the most significant of the data in graphical plots.

Stress data were presented in two different forms: stress vectors and stress contours. The stress vectors are merely direct graphical plots of the principal stresses in each element. They are plotted from the center of the element, and consist of arrows showing the sense and direction of the stresses, the length of the arrow representing the magnitude. Study of the stress vector diagrams, which are compiled in the Appendix, reveals a great deal of detailed information about the state of stress in the structure. However, a more easily interpreted representation is provided by the stress contours which are presented and discussed in the first section of this chapter.

Displacement data are also presented in two different sets of figures. The boundary displacements are merely figures depicting the deformed shape of the cross-section under load. These are of qualitative interest, but have no great significance with regard to the performance of the structure. The crack displacements are shown in these figures, but in order to provide a clearer impression of the extent of the crack opening, and of the effect on it of the various load combinations, separate figures have been constructed showing only the crack displacements. The displacement figures are presented and discussed in the latter part of this chapter.

Stress Contours

Lines connecting points of equal stress intensity in the cross-section are called iso-static lines or stress contours. Such contours were drawn in each case for the vertical normal stress σ_y, the shear stress τ_{xy}, and for the principal stresses σ_1 and σ_2. The major principal stress, σ_1 is defined as the maximum tensile (or minimum compressive) stress, while the minor principal stress, σ_2, is the maximum compressive component. In constructing the stress contours, it was assumed that the stress values computed for each element existed at the centroid of the element, and the contours were based on these controls. However, a certain amount of smoothing was required in converting the discontinuous finite element results into a representation of the actual continuous system.

Also presented for each case are plots of the σ_y and τ_{xy} stress distributions across the base section of the dam. These curves were defined by the intersections of the stress contours with the base line. The resultant forces represented by these base stress distributions were evaluated directly from the graphs by means of planimeters. Comparisons of the calculated force resultants with the applied loads for all cases are presented in Table III, at the end of this section.

Case A (Fig. 13)-- The base stress distribution computed in this uncracked section is very nearly of the simple trapezoidal form assumed by the elementary theory, although a slight tendency toward stress concentration is evident at the heel of the dam (the expected effect of foundation elasticity). The shear stress distribution across the base for this simple, dead load condition merely represents the resistance provided by the foundation rock to the Poisson's ratio expansion tendencies in the concrete. The principal stress plots show that no tensile stress is

developed at any point in the section, and that the maximum compressive stress is about 250 psi, only slightly more than would have been predicted by elementary theory.

Case B (Fig. 14)-- Comparison of this case with Case A shows the influence of the live load on the stresses. Some definite shifts in the distributions are evident, due to the change in location and direction of the resultant applied forces, but no significant change has occurred in the maximum stress values; actually the maximum stresses have been reduced slightly by the live load. The most notable change from Case A is the reversal of the base shear stress direction in the region of the heel. This is a direct result of the lateral hydrostatic force, which in this case must be balanced by the base shear stresses.

Case C (Fig. 15)-- In this figure it is seen that the addition of the thermal loads causes very substantial changes in the stress magnitudes and directions, especially near the base where the foundation resists the thermal strains. The primary thermal effect is a lateral contraction of the concrete together with the restraint to this contraction which is provided by the foundation rock. Although the assumed thermal gradient in the vertical direction tends to distribute this constraining effect over a fairly deep portion of the dam near the base, the stresses which result are quite large.

The direct consequence of the base restraint is a system of tensile stresses σ_x in the horizontal direction (near the base) accompanied by shear stresses (τ_{xy}) on horizontal planes. These shear stresses oppose those due to dead load, but when combined with live load effects they produce a maximum shear stress of nearly 400 psi near the heel. At the same time, the tensile normal stresses (σ_x) in the base zone tend to

cause a rounding of the base plane (convex downward), and this rounding tendency is resisted by vertical normal stresses (σ_y).

The resulting tensile stress of 400 psi (as well as the major principal stress of over 500 psi) in the vicinity of the heel demonstrates the severity of the loading produced by the temperature changes. Thus the fact that the structure cracked is not surprising.

On the other hand, it should be recognized that the assumed thermal stresses probably are considerably more severe than those which actually occurred, at least in the vicinity of the faces of the dam. These zones probably never achieved the high temperatures which developed in the mid-section, thus the σ_y thermal stresses near the faces would have been considerably less than the computed values. The assumed conditions probably are quite realistic in the mid-section, however, and the computed tendency for cracking in this area should be representative of actual conditions.

Case D (Fig. 16)-- The comparison of this case with Case A demonstrates the relatively minor influence which the crack had on the stresses due to dead load alone. The only notable effect is with respect to the stresses resulting from Poisson's ratio expansion. The lateral stresses due to this effect are greatly relieved by the vertical crack through the center of the section, thus the corresponding shear stresses at the base of the section are also reduced. Minor normal stress concentrations appear at both upper and lower ends of the crack, but the maximum stresses associated with these are negligible.

Case E (Fig. 17)-- The influence of the crack on the stress distribution due to live load is much greater than on that due to dead load, as is indicated by a comparison of Cases E and B. The cracked section tends to

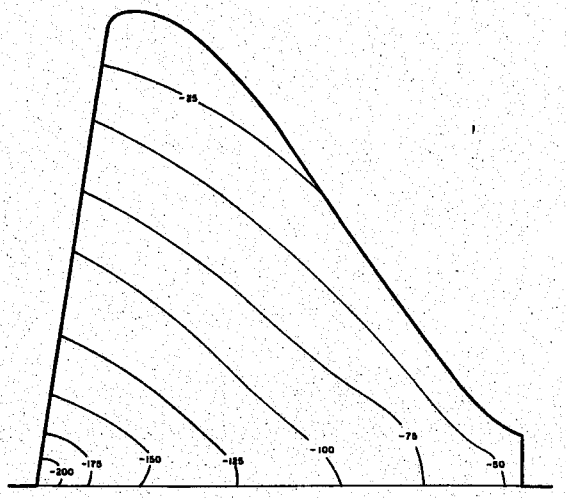

VERTICAL STRESSES - σ_y

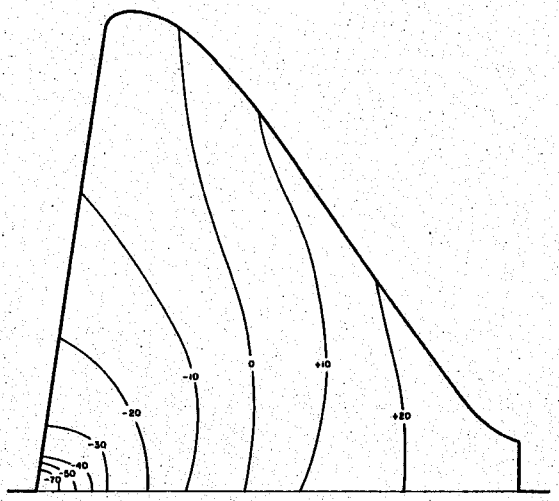

SHEAR STRESSES - σ_{xy}

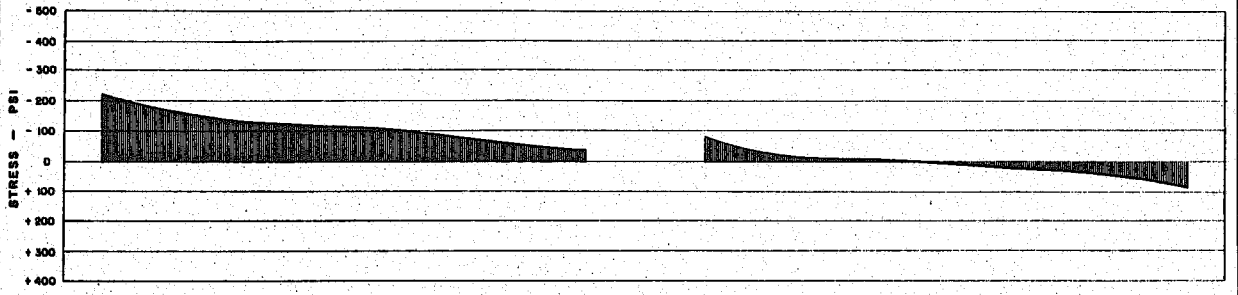

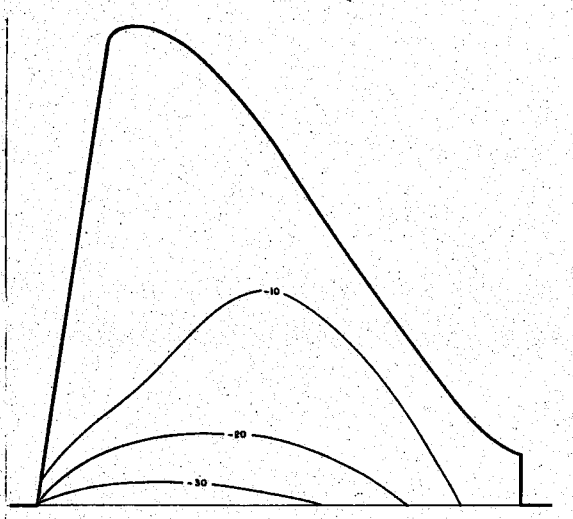

MAJOR STRESSES - σ_1

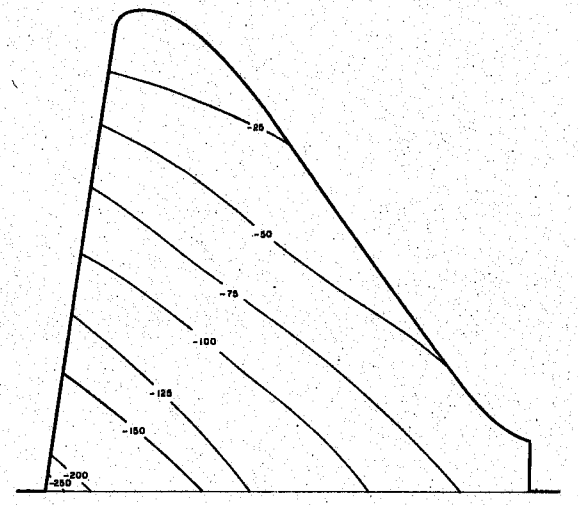

MINOR STRESSES - σ_2

UNIVERSITY OF CALIFORNIA - BERKELEY, CALIFORNIA
DIVISION OF STRUCTURAL ENGINEERING AND STRUCTURAL MECHANICS

STRESS DISTRIBUTION OF NORFORK DAM

STRESS CONTOURS

CASE *A*	LOADING *DL*	UPLIFT *NONE*
CRACK HEIGHT *NONE*	FOUNDATION *ISOTROPIC*	FIG. NO. *13*

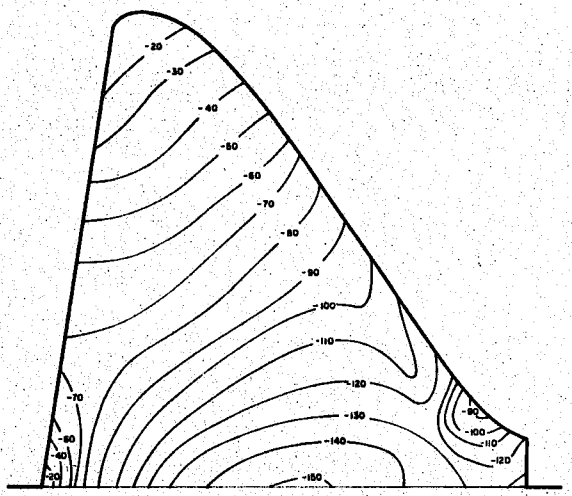

VERTICAL STRESSES – σ_y

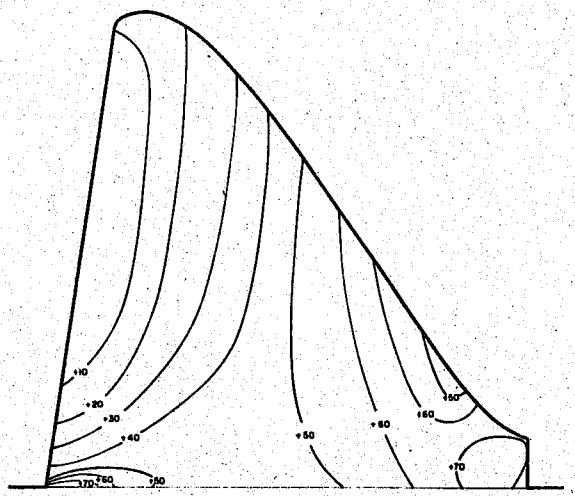

SHEAR STRESSES – σ_{xy}

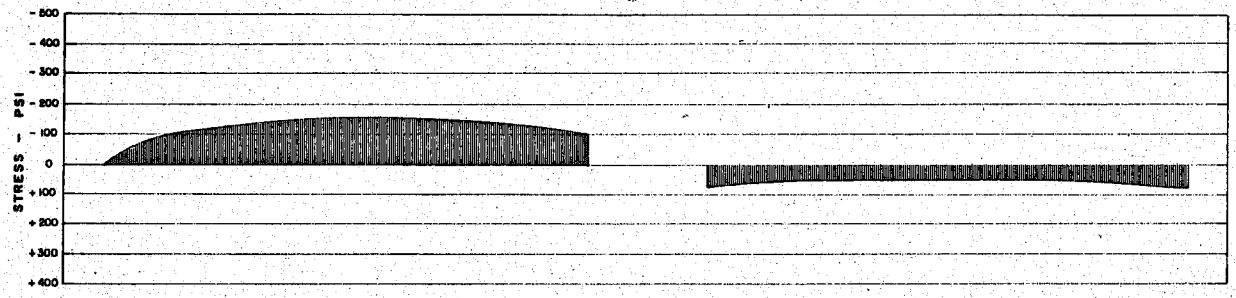

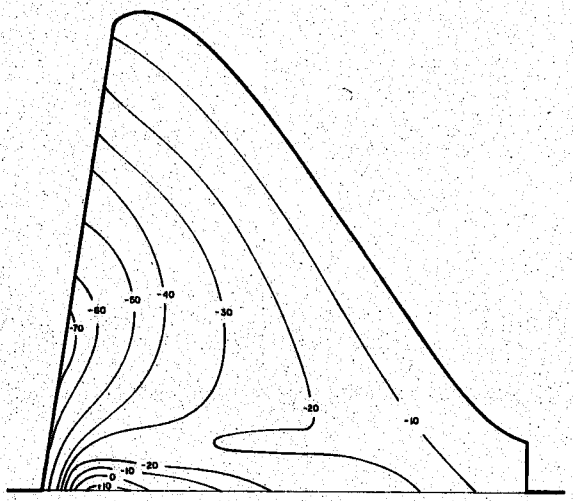

MAJOR STRESSES – σ_1

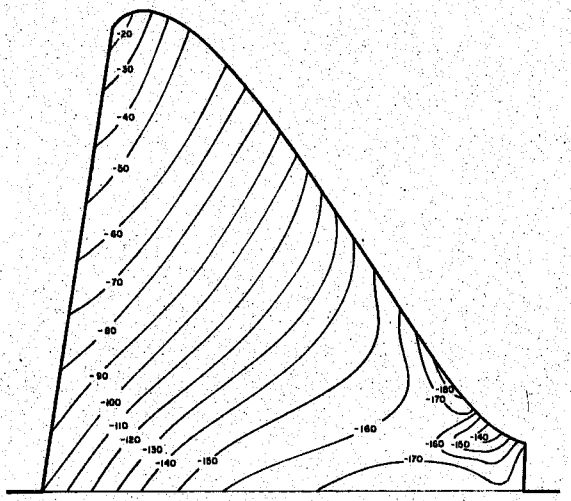

MINOR STRESSES – σ_2

UNIVERSITY OF CALIFORNIA – BERKELEY, CALIFORNIA
DIVISION OF STRUCTURAL ENGINEERING AND STRUCTURAL MECHANICS

STRESS DISTRIBUTION OF NORFORK DAM

STRESS CONTOURS

CASE	LOADING	UPLIFT
B	DL + LL	NONE
CRACK HEIGHT	FOUNDATION	FIG. NO.
NONE	ISOTROPIC	14

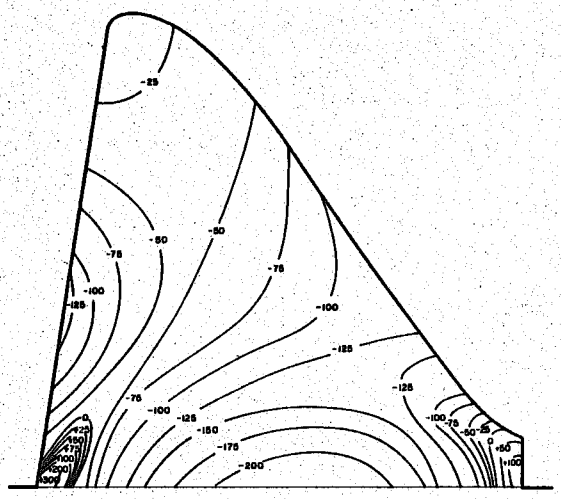

VERTICAL STRESSES - σ_y

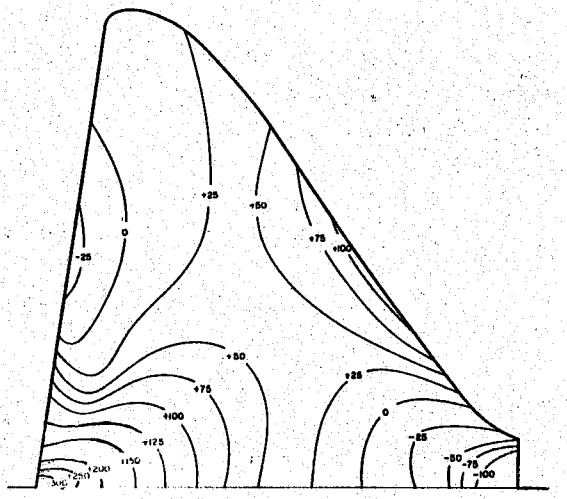

SHEAR STRESSES - σ_{xy}

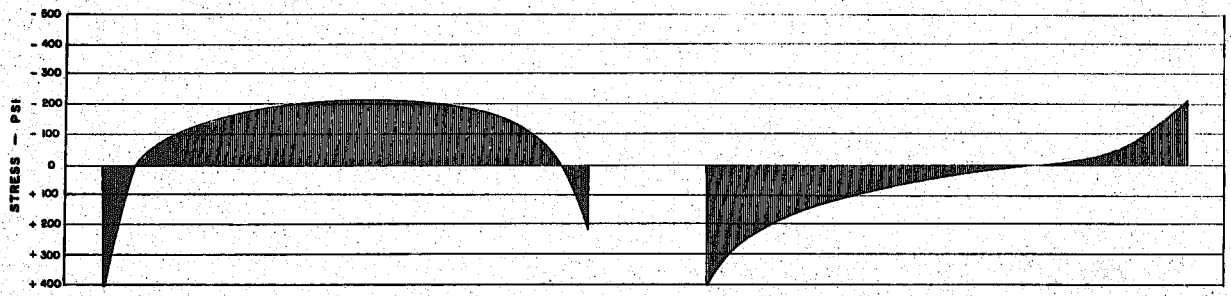

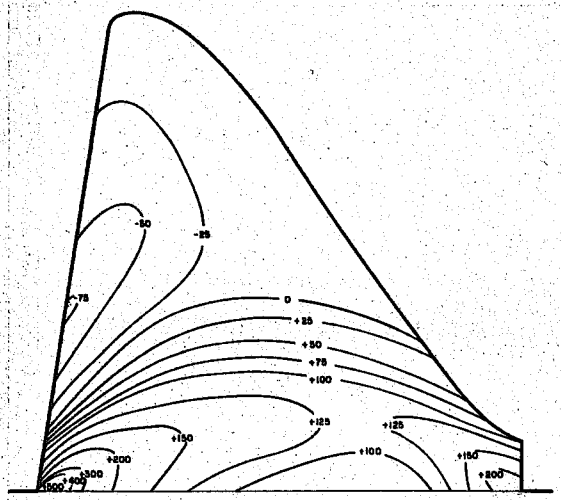

MAJOR STRESSES - σ_1

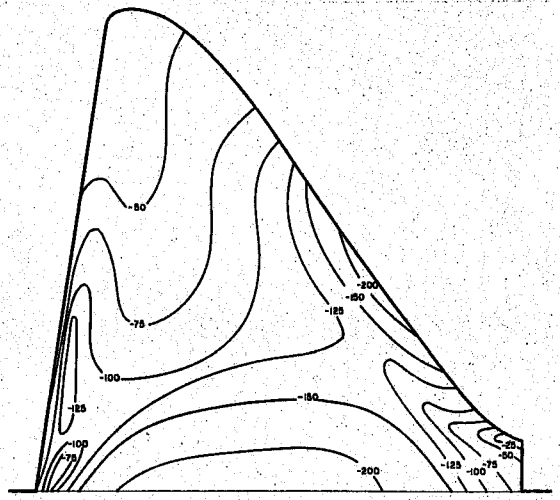

MINOR STRESSES - σ_2

UNIVERSITY OF CALIFORNIA – BERKELEY, CALIFORNIA DIVISION OF STRUCTURAL ENGINEERING AND STRUCTURAL MECHANICS		
STRESS DISTRIBUTION OF NORFORK DAM *STRESS CONTOURS*		
CASE *C*	LOADING *DL, LL & TH*	UPLIFT *None*
CRACK WEIGHT	FOUNDATION *ISOTROPIC*	FIG. NO. *15*

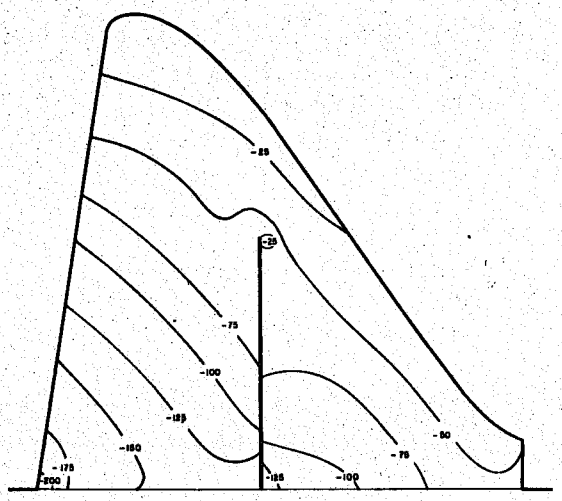

VERTICAL STRESSES - σ_y

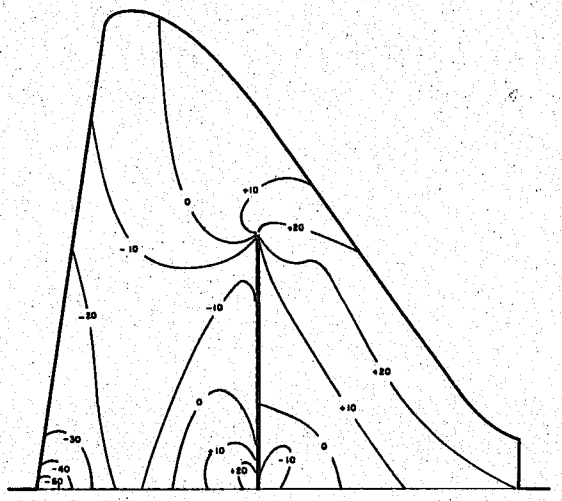

SHEAR STRESSES - σ_{xy}

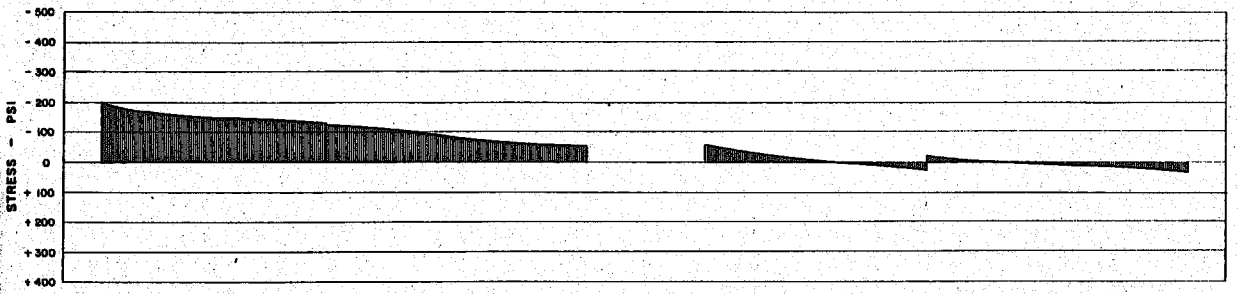

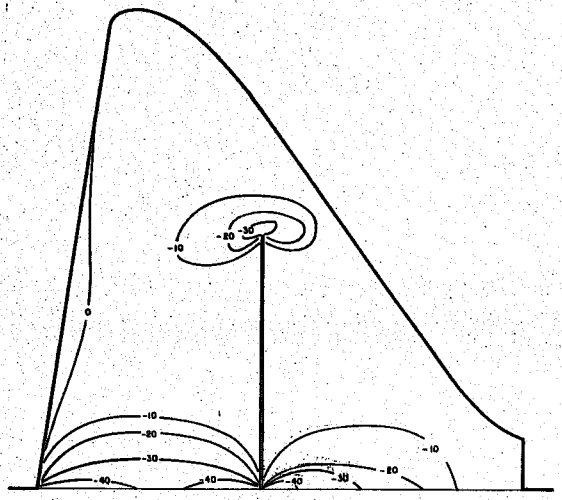

MAJOR STRESSES - σ_1

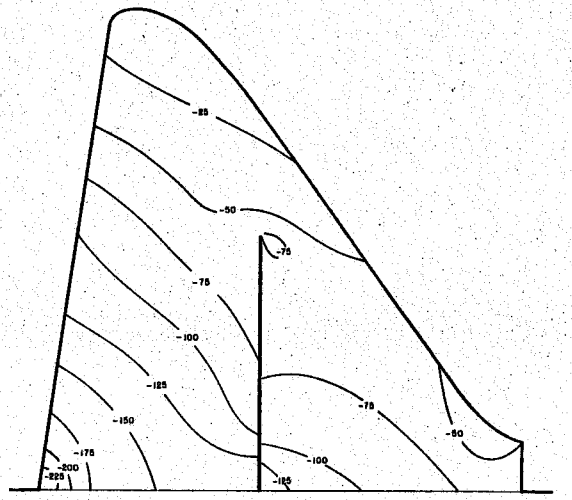

MINOR STRESSES - σ_2

UNIVERSITY OF CALIFORNIA - BERKELEY, CALIFORNIA
DIVISION OF STRUCTURAL ENGINEERING AND STRUCTURAL MECHANICS

STRESS DISTRIBUTION OF NORFORK DAM

STRESS CONTOURS

CASE D	LOADING DL	UPLIFT NONE
CRACK HEIGHT 4/3	FOUNDATION ISOTROPIC	FIG. NO. 16

resist the lateral load as two separate systems, connected only at the top. Thus the normal stresses (σ_y) associated with overturning are much greater in the upstream block than they were for the solid dam, reaching a value of about 400 psi. Similarly, the shear force is resisted only by the upstream block, causing a significant increase in shear stress as compared with the uncracked case.

Sizeable stress concentrations also were developed at the upper end of the crack in this case, due to the action of the zone above the crack in forcing continuity of displacement between the two blocks. Two distinct actions were involved in maintaining continuity. The lateral force acting on the upstream block pressed it against the restraint of the downstream block, causing horizontal compressive stresses (σ_x) to develop above the crack. At the same time, the bending of the two blocks tended to cause the contact surface of the left block to move downward while the corresponding surface of the right block tended to move up. The resulting shearing stresses in the zone above the crack put the upstream face of the crack in vertical tension (σ_y) and the downstream face in vertical compression. This σ_y tensile zone in the upstream block near the tip of the crack is of considerable interest, in that horizontal cracking was observed at this location in the prototype. The corresponding compressive stress in the downstream block is considerable larger in magnitude, of course, because the dead weight stress in this case is an additive rather than a reducing influence. The maximum compressive stress in this zone is no larger than the maximum base stress, however, and thus is not of particular interest.

Case F (Fig. 18)-- Comparison of this case with Case D shows the relative importance of the thermal loads on the cracked section. The thermal

effects everywhere are similar to those observed for the uncracked section (see the comparison between Cases B and C) when due allowance has been made for the fact that the crack has converted the system into two practically independent structures. As was noted in the discussion of Case C, however, the assumed thermal conditions are not entirely realistic, and a better impression of the importance of the crack is provided by the comparison of Cases E and B, in which only live and dead loads are considered.

Case G (Fig. 19)-- The differences observed between Cases G and E are equivalent to the differences between Cases F and D, in that in each case the differences represent the effect of the thermal load on the cracked section. On the other hand, the comparison of Cases G and C demonstrates the influence of the crack on the stress distributions due to identical load conditions. However, because the stresses resulting from the temperature changes are quite large, and because the assumed thermal conditions are a rather crude approximation of the actual conditions, this comparison is considered to be less significant than that discussed above for live and dead loads only (Cases E and B).

Case H (Fig. 20)-- The influence of the orthotropic foundation is indicated by a comparison of Cases H and E, since otherwise these two cases were identical. It is apparent from the similarity of the stress contours for the two cases that the vertical foundation flexibility has very little effect on the distribution of stress in the upper regions of the structure. The only noticeable effect is observed near the base, and is most evident in the σ_y and τ_{xy} values plotted for that section. The reduced vertical foundation modulus considered in this case makes the dam behave relatively

more like a rigid body. Thus the computed stress distribution is more like that associated with a rigid dam on a flexible base, in which stress concentrations tend to develop at toe and heel. However, it will be noted that these increased stress concentration tendencies in Case H as compared with Case E are not great; in fact they are almost within the range of accuracy of the method of analysis.

Case I (Fig. 21)-- This case corresponds exactly with Case D, the only difference being that the crack has been extended upward for one more nodal point to 7/9 height. Comparison of these cases demonstrates that the additional crack height has a negligible influence on all aspects of the stress distribution due to dead load alone.

Case J (Fig. 22)-- The relationship between Cases I and D, which was discussed above, applies also to Cases J and E, except that in these latter cases the live load also is acting. Although the effect is not large, it is apparent that the increased crack height does result in a definite increase in certain critical live load stress values. Over most of the cross-section, the similarities between the two cases are quite remarkable; but the maximum tensile and compressive stresses at the base show a significant increase in the 7/9 crack case, as does the maximum tensile stress at the upstream face of the crack. This finding is not surprising, of course; since these critical stress values are a direct consequence of the crack, it is to be expected that extending the crack would result in an increase in their magnitude.

Case K (Fig. 23)-- Another indication of the effect of extending the crack height is shown by the comparison of cases K and F. As would be expected in the absence of live load, the difference shown by this comparison (for dead and thermal loads) is negligible.

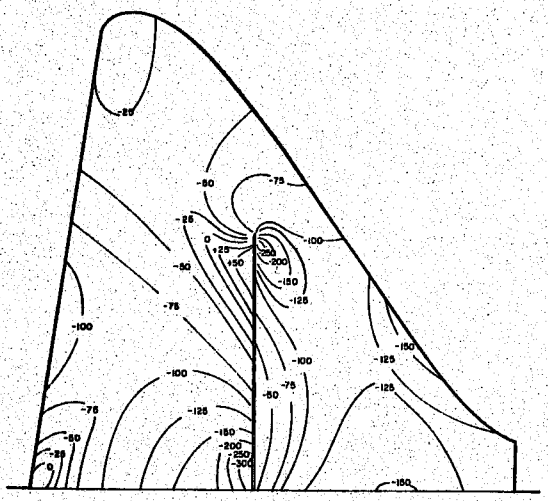

VERTICAL STRESSES - σ_y

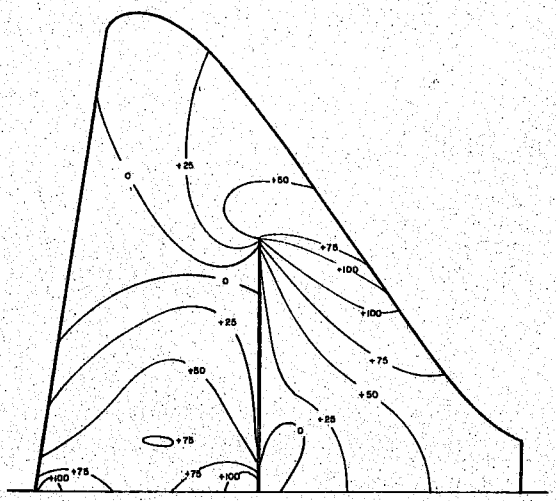

SHEAR STRESSES - σ_{xy}

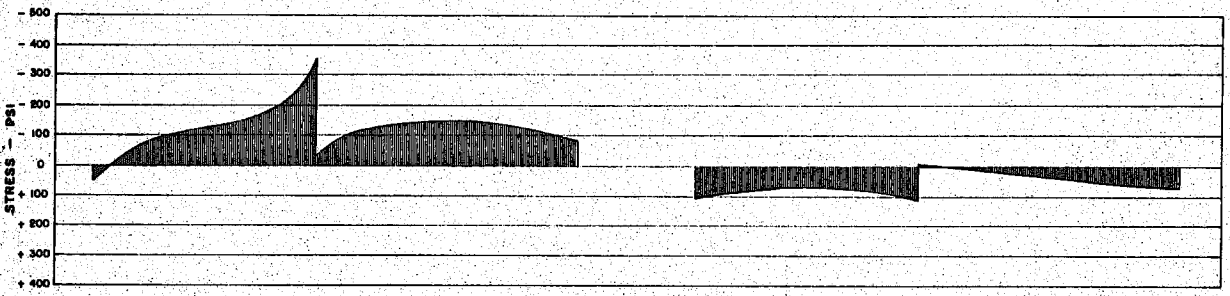

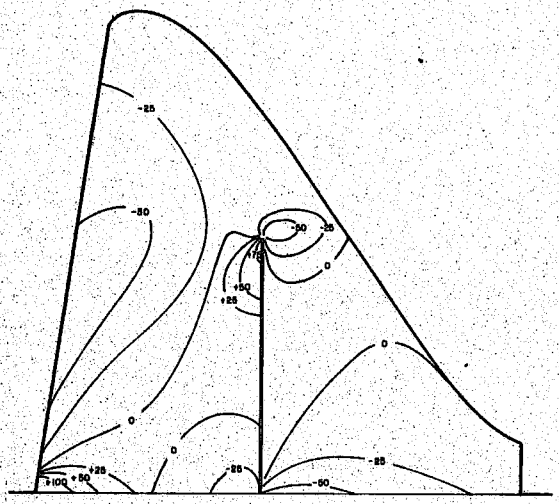

MAJOR STRESSES - σ_1

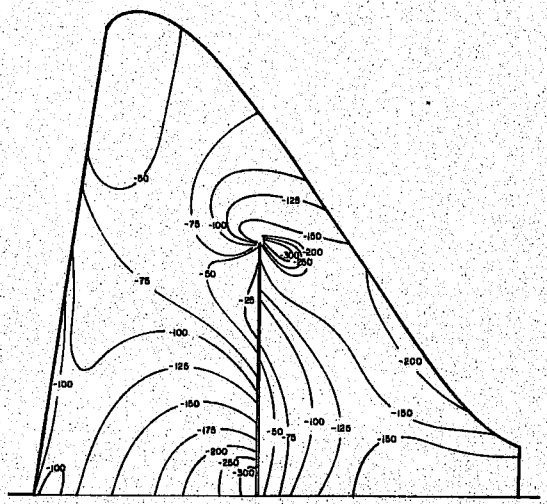

MINOR STRESSES - σ_2

UNIVERSITY OF CALIFORNIA - BERKELEY, CALIFORNIA DIVISION OF STRUCTURAL ENGINEERING AND STRUCTURAL MECHANICS		
STRESS DISTRIBUTION OF NORFORK DAM *STRESS CONTOURS*		
CASE *E*	LOADING *DL & LL*	UPLIFT *NONE*
CRACK HEIGHT *1/3*	FOUNDATION *ISOTROPIC*	FIG. NO. *17*

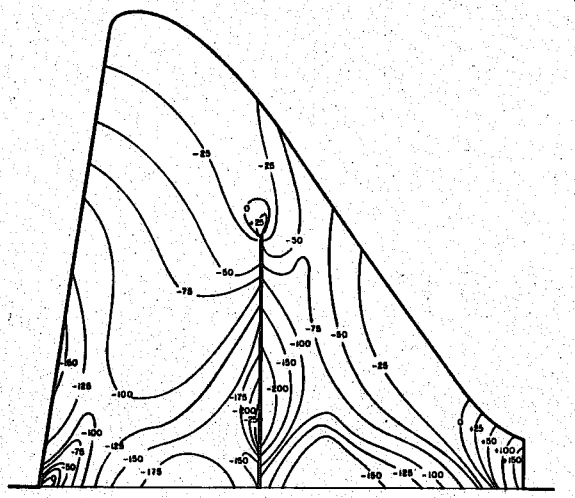

VERTICAL STRESSES - σ_y

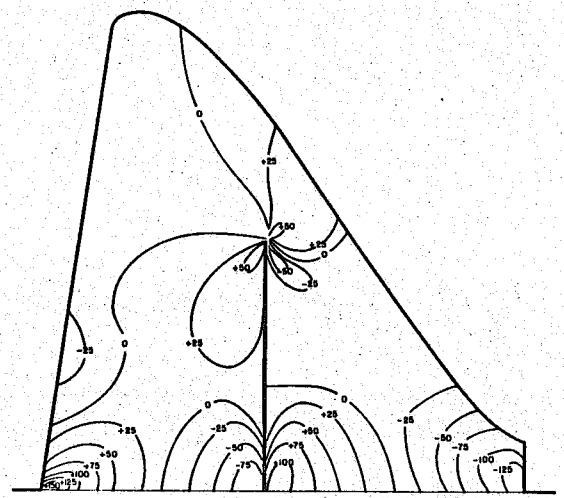

SHEAR STRESSES - σ_{xy}

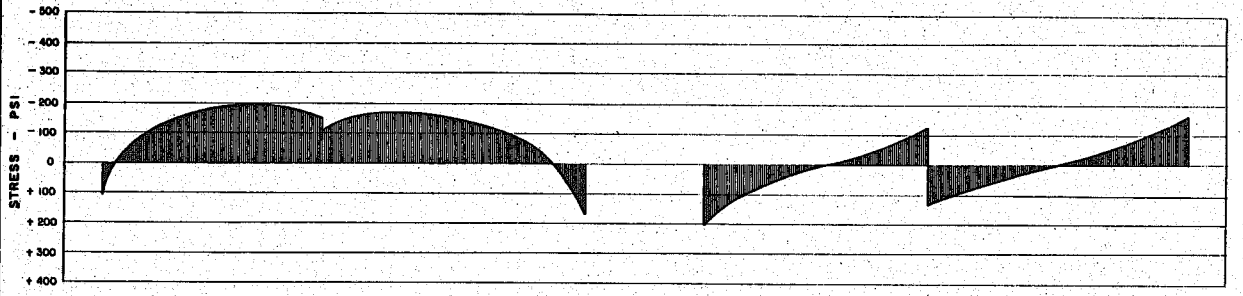

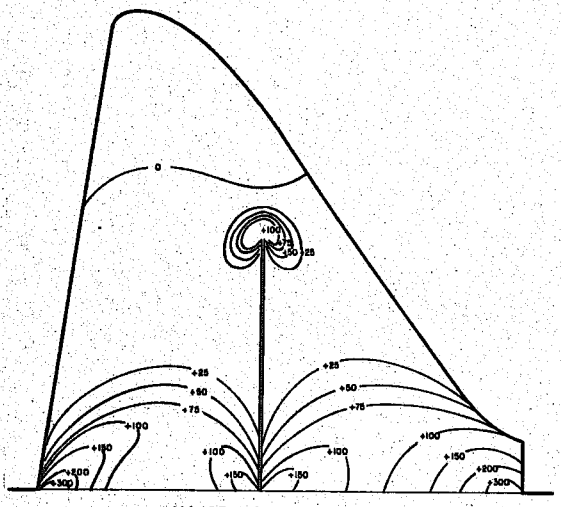

MAJOR STRESSES - σ_1

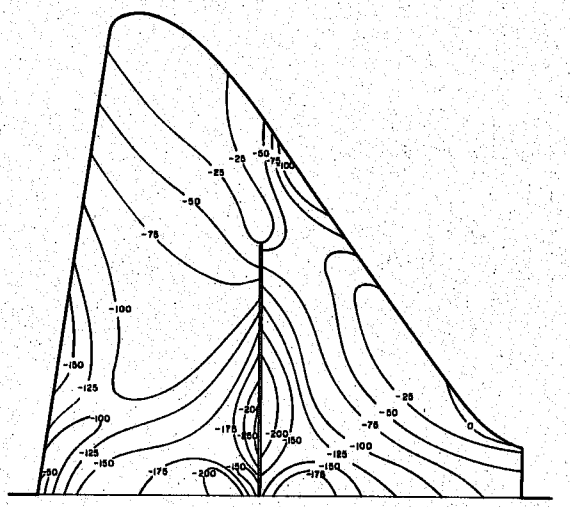

MINOR STRESSES - σ_2

UNIVERSITY OF CALIFORNIA - BERKELEY, CALIFORNIA DIVISION OF STRUCTURAL ENGINEERING AND STRUCTURAL MECHANICS		
STRESS DISTRIBUTION OF NORFORK DAM *STRESS CONTOURS*		
CASE *F*	LOADING *DL & TH*	UPLIFT *NONE*
CRACK HEIGHT *2/3*	FOUNDATION *ISOTROPIC*	FIG. NO. *18*

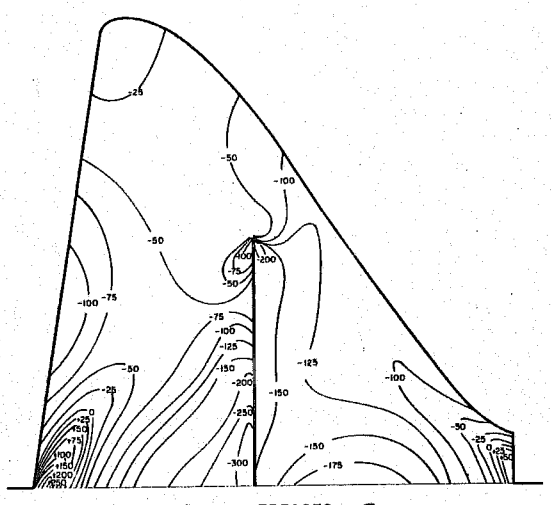

VERTICAL STRESSES - σ_y

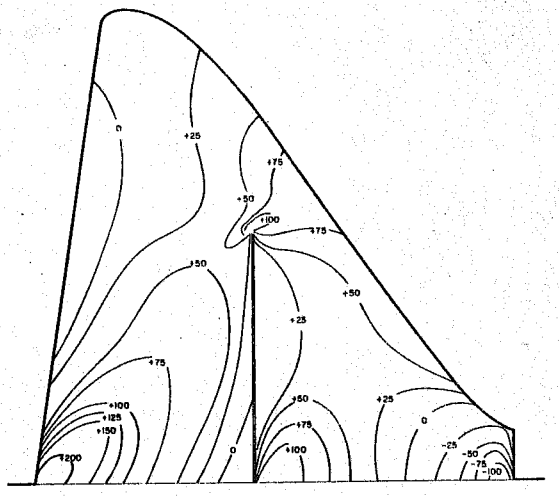

SHEAR STRESSES - σ_{xy}

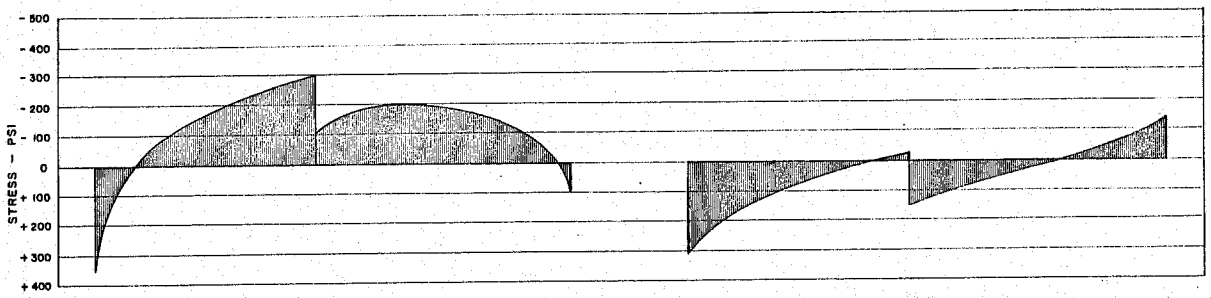

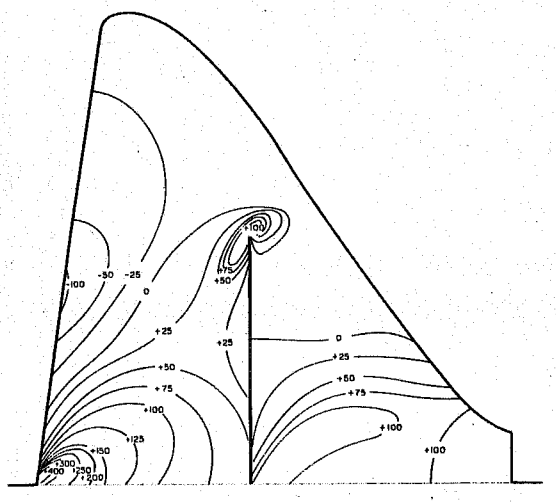

MAJOR STRESSES - σ_1

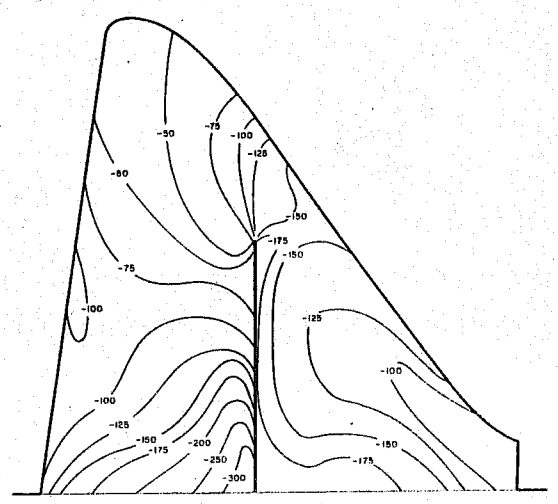

MINOR STRESSES - σ_2

UNIVERSITY OF CALIFORNIA - BERKELEY, CALIFORNIA DIVISION OF STRUCTURAL ENGINEERING AND STRUCTURAL MECHANICS		
STRESS DISTRIBUTION OF NORFORK DAM STRESS CONTOURS		
CASE G	LOADING DL, LL & TH	UPLIFT NONE
CRACK HEIGHT 2/3	FOUNDATION ISOTROPIC	FIG NO. 13

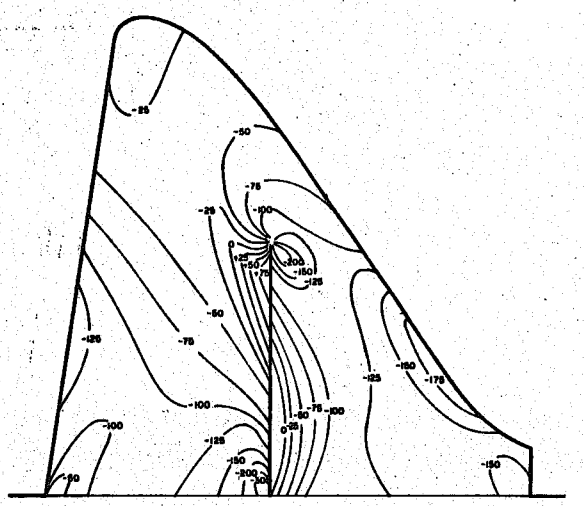

VERTICAL STRESSES - σ_y

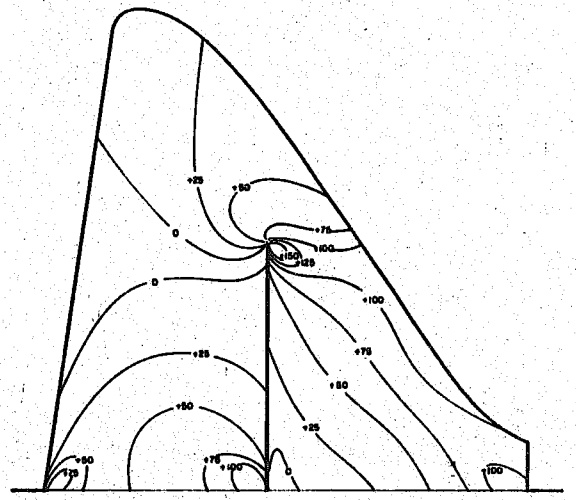

SHEAR STRESSES - σ_{xy}

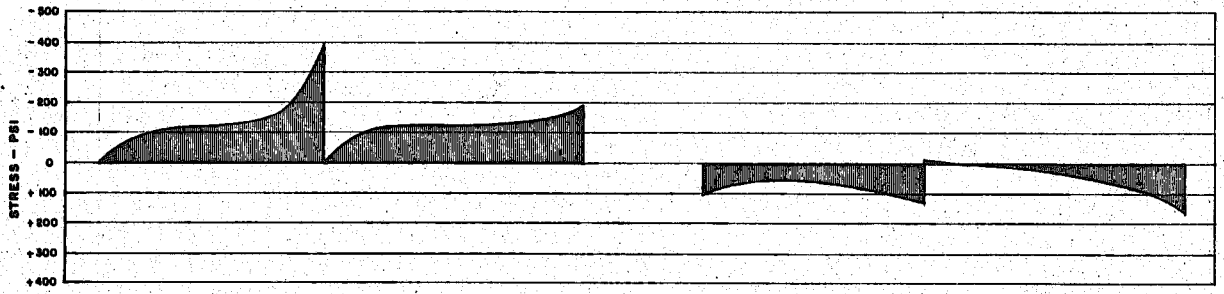

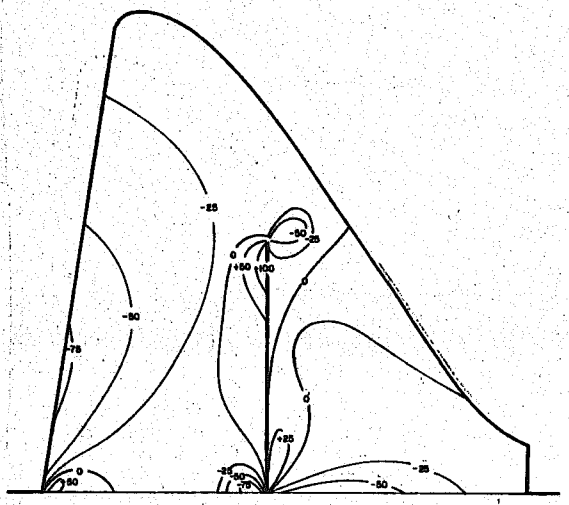

MAJOR STRESSES - σ_1

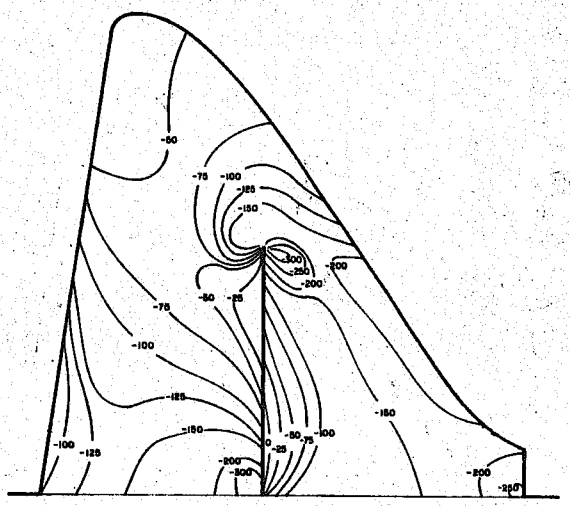

MINOR STRESSES - σ_2

UNIVERSITY OF CALIFORNIA — BERKELEY, CALIFORNIA
DIVISION OF STRUCTURAL ENGINEERING AND STRUCTURAL MECHANICS

STRESS DISTRIBUTION OF NORFORK DAM

STRESS CONTOURS

CASE	LOADING	UPLIFT
H	DL & LL	None
CRACK HEIGHT 45	FOUNDATION ORTHOTROPIC	FIG. NO. 80

Case L-1 and L-2 (Fig. 24 and 25)-- The effect of uplift pressures at the heel of the dam is shown by a comparison of Cases L and J. The principal effect of the uplift condition is the upward movement of the heel of the dam, and the consequent rotation of this upstream portion of the dam. This rotation causes a significant increase in the compressive stress at the base of the dam on the upstream side of the crack, and also causes increases in the stress concentrations near the upper end of the crack.

Cases L-1 and L-2 differ only in the extent of the uplift crack assumed at the heel of the section. In Case L-1 it extended downstream for three nodal points (about 32 ft.), in Case L-2 it extended 3½ nodal points (about 42 ft.). The additional uplift in Case L-2 caused an increased stress condition as would be expected; however, Case L-1 is considered more realistic because a system of drains and a grout curtain provided in the prototype should be effective in limiting uplift effects to about the first three nodal points.

The maximum stresses observed in Case L-1, the most critical case considered (except for L-2), amounted to over 400 psi compression at the base upstream of the crack and on the downstream face of the upper end of the crack. At the same time a tensile stress of about 150 psi was observed on the upstream face near the upper end of the crack. The tension at the heel of the dam which was noted in Case J has been eliminated, of course, by the opening of the crack at this location, and in its place is the 100 psi hydrostatic uplift pressure. Similarly, the shear stress near the heel has been eliminated by the crack and the entire shear acting on the upstream block is resisted by the remaining uncracked portion of the base.

Case M (Fig. 26)-- This case is comparable with Case H in that it represents the condition of dead plus live load acting on the system with the orthotropic foundation. The only difference between this and Case H is the extension of the crack to the 7/9 height. As might be expected, the result of this extension is a slight increase of the stress values at all points of concentration. Of greater interest is the comparison with Case J, which demonstrates the effect of the orthotropic foundation. In this comparison it is quite evident that the softening of the foundation tends to reduce the bending constraint acting at the base of the blocks, upstream and downstream of the crack. Thus the σ_y stress gradient across the base in Case M is considerably less than in Case J. This softening affect of the orthotropic foundation is considerably more evident here in the 7/9 crack height case than it was with the 2/3 crack height (Case H).

Case N (Fig. 27)-- In this case, the crack has been assumed to extend upward from 2/9 height rather than from the base. Otherwise conditions are identical with Case L-1. As would be expected, the stress concentrations here are greatly reduced, with maximum compressive normal stresses of only about 250 psi rather than 400 psi as in Case L-1. In effect, the portion of the dam up to the base of the crack acts in combination with the foundation as a single unit. The remaining portion which is subject to the crack effect is considerably smaller and therefore is stressed less. The form of the stress distribution, however, is entirely consistent with that observed before.

Cases O-1 and O-2 (Figs. 28 and 29)-- As was noted previously, these cases were included to provide a direct comparison between results obtained by the finite element method and those computed by D. McHenry of the

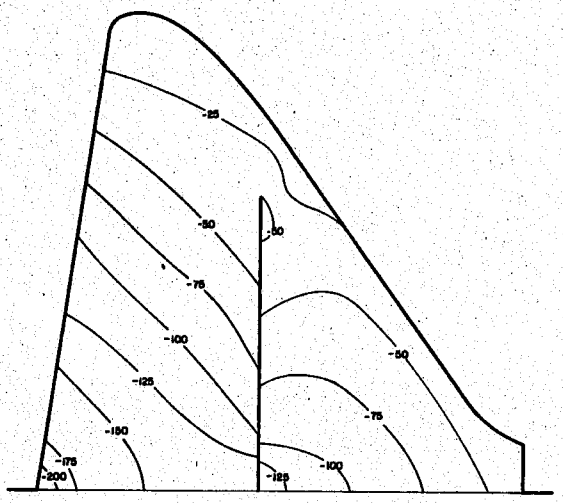

VERTICAL STRESSES – σ_y

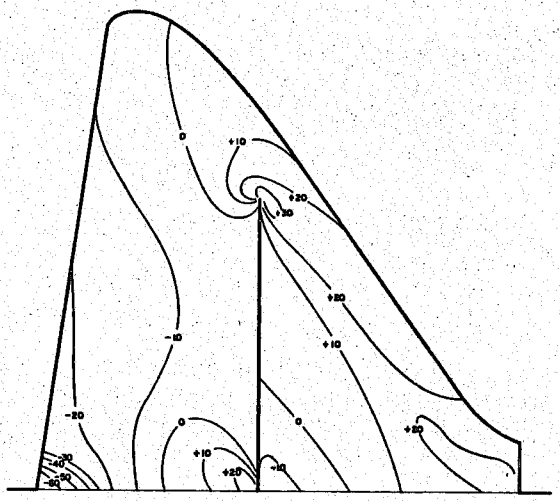

SHEAR STRESSES – σ_{xy}

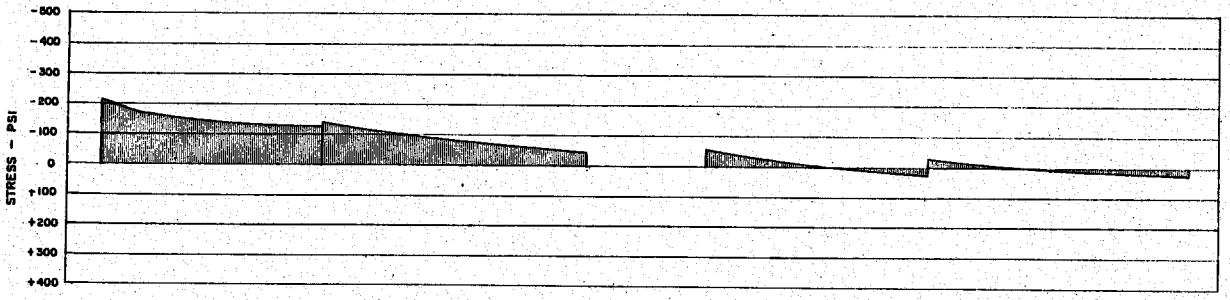

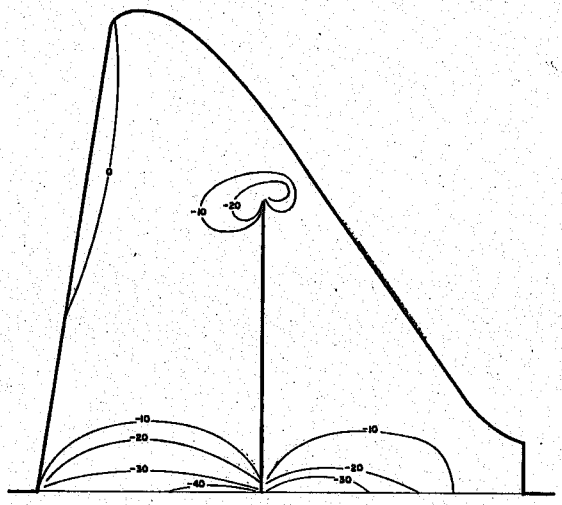

MAJOR STRESSES – σ_1

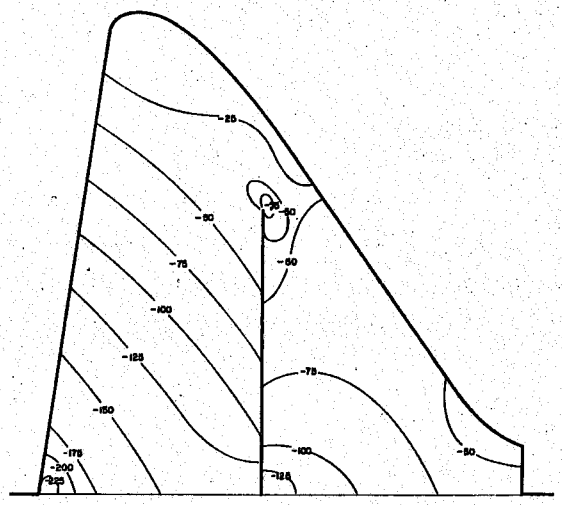

MINOR STRESSES – σ_2

UNIVERSITY OF CALIFORNIA – BERKELEY, CALIFORNIA DIVISION OF STRUCTURAL ENGINEERING AND STRUCTURAL MECHANICS		
STRESS DISTRIBUTION OF NORFORK DAM *STRESS CONTOURS*		
CASE *I*	LOADING *OL*	UPLIFT *NONE*
CRACK HEIGHT *1/3*	FOUNDATION *ISOTROPIC*	FIG. NO. *21*

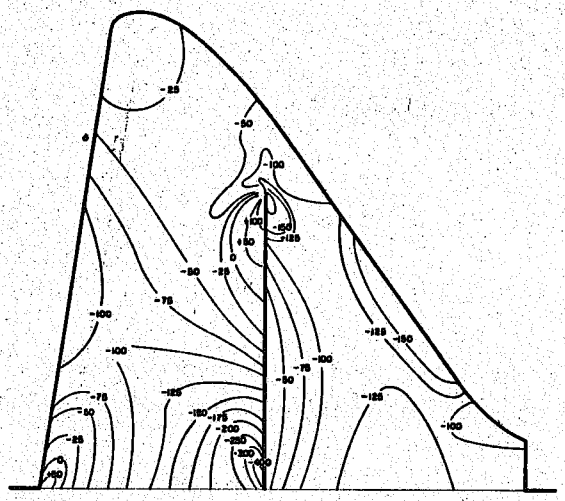

VERTICAL STRESSES - σ_y

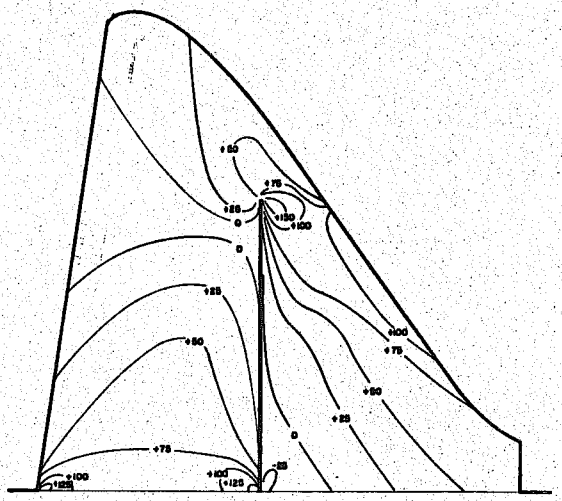

SHEAR STRESSES - σ_{xy}

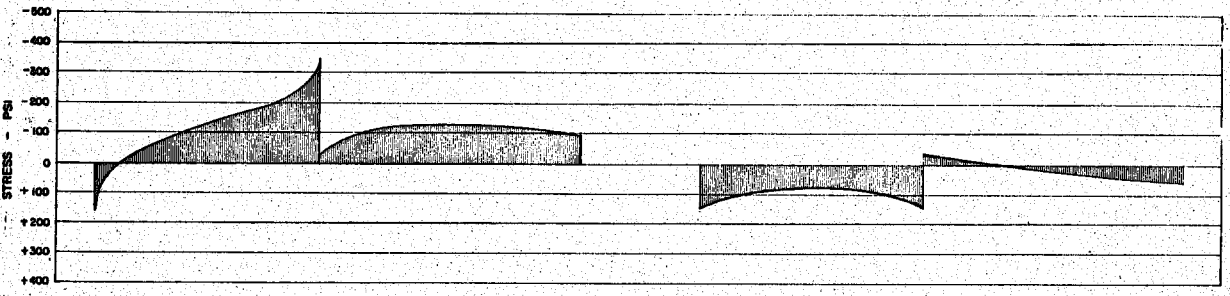

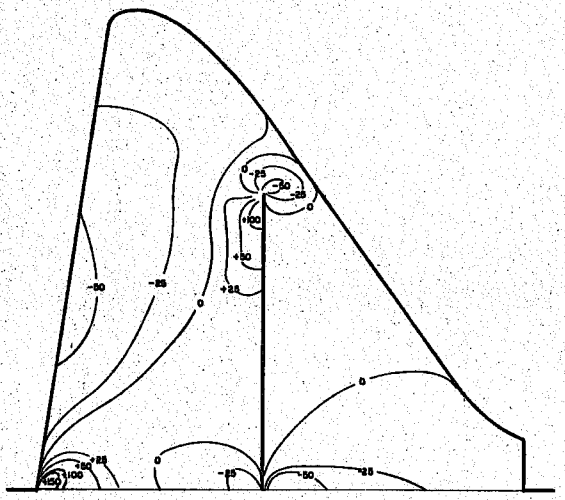

MAJOR STRESSES - σ_1

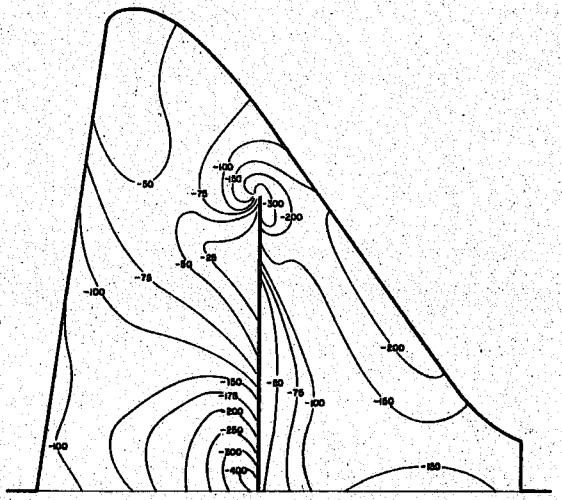

MINOR STRESSES - σ_2

UNIVERSITY OF CALIFORNIA - BERKELEY, CALIFORNIA
DIVISION OF STRUCTURAL ENGINEERING AND STRUCTURAL MECHANICS

STRESS DISTRIBUTION OF NORFORK DAM

STRESS CONTOURS

CASE	LOADING	UPLIFT
J	DL & LL	NONE
CRACK HEIGHT 1/9	FOUNDATION ISOTROPIC	FIG. NO. 12

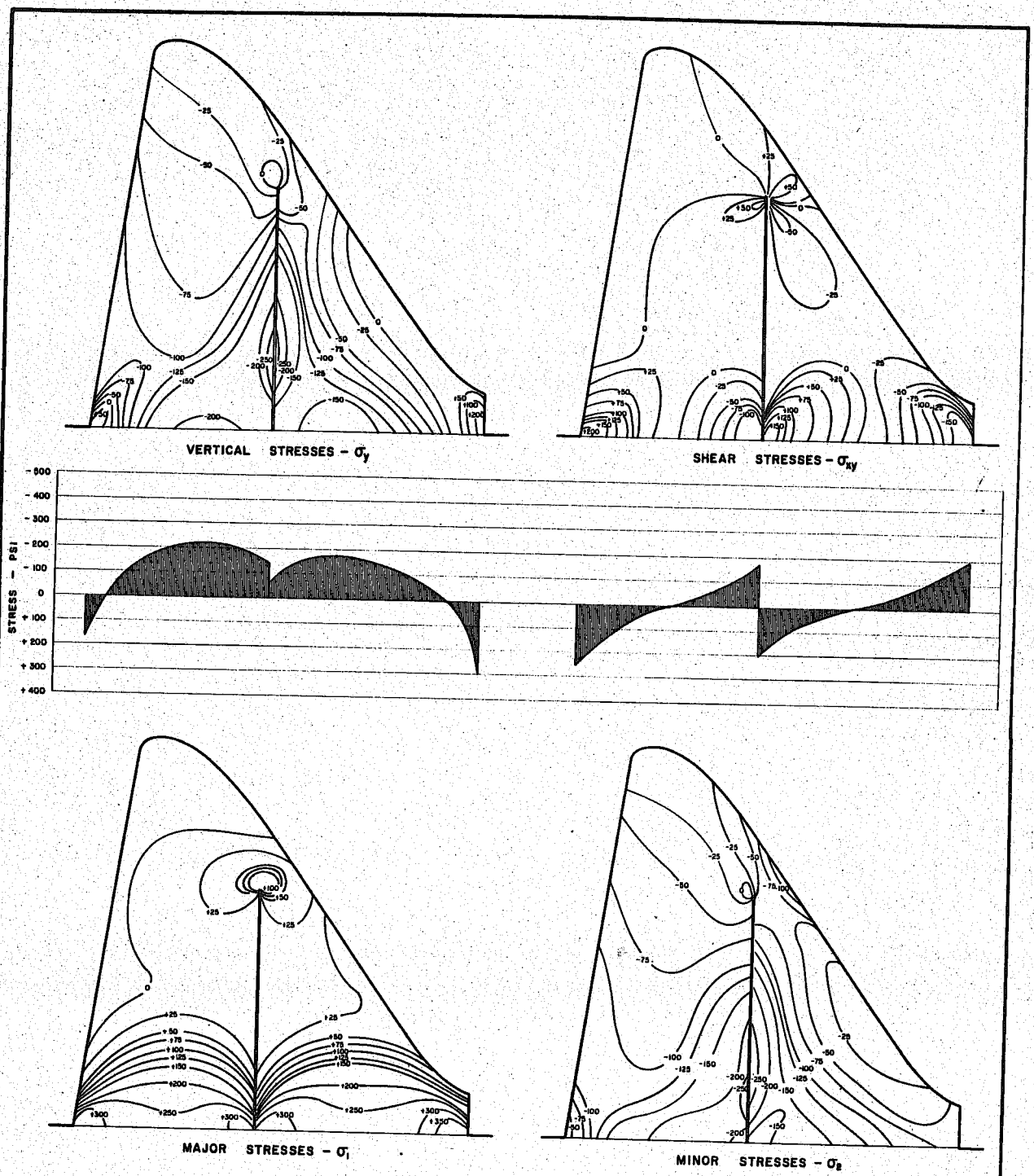

UNIVERSITY OF CALIFORNIA – BERKELEY, CALIFORNIA DIVISION OF STRUCTURAL ENGINEERING AND STRUCTURAL MECHANICS		
STRESS DISTRIBUTION OF NORFORK DAM *STRESS CONTOURS*		
CASE *K*	LOADING *OL & TH*	UPLIFT *NONE*
CRACK HEIGHT *1/9*	FOUNDATION *ISOTROPIC*	FIG. NO. *23*

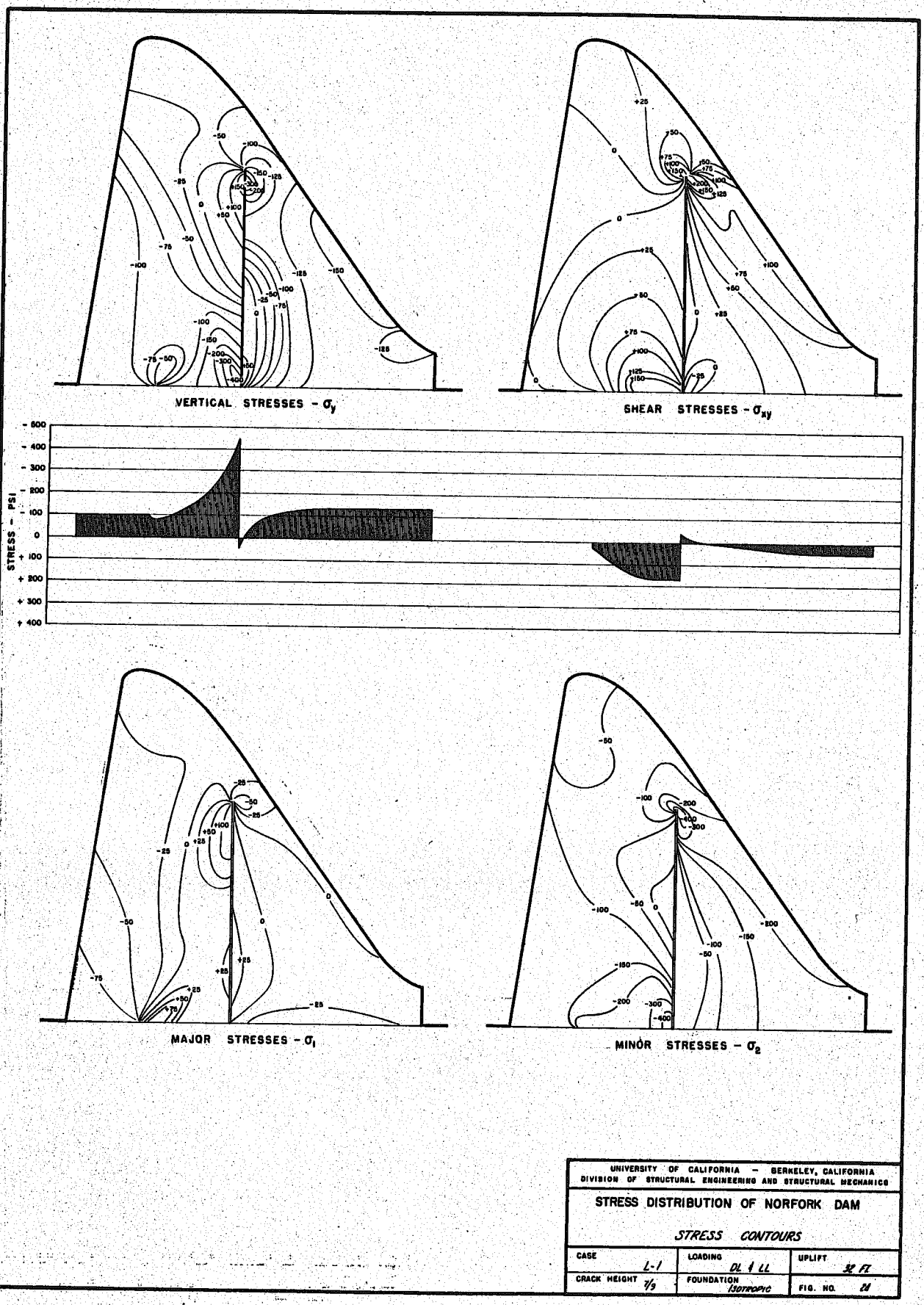

UNIVERSITY OF CALIFORNIA – BERKELEY, CALIFORNIA
DIVISION OF STRUCTURAL ENGINEERING AND STRUCTURAL MECHANICS

STRESS DISTRIBUTION OF NORFORK DAM

STRESS CONTOURS

CASE	LOADING	UPLIFT
L-1	DL + LL	32 FT
CRACK HEIGHT 7/9	FOUNDATION ISOTROPIC	FIG. NO. 28

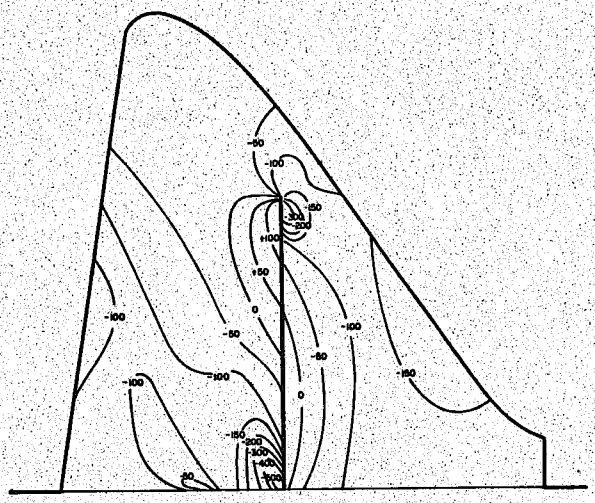

VERTICAL STRESSES – σ_y

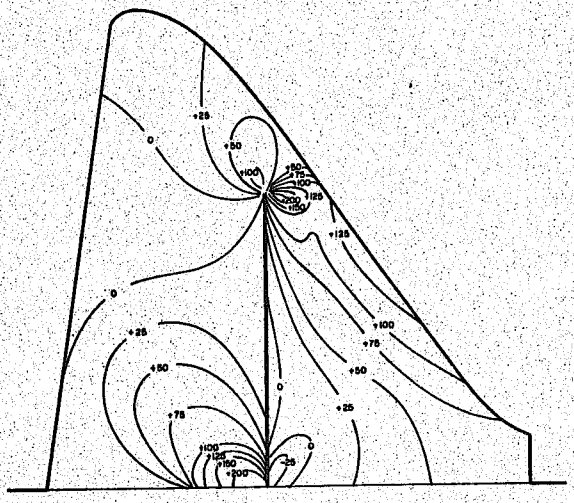

SHEAR STRESSES – σ_{xy}

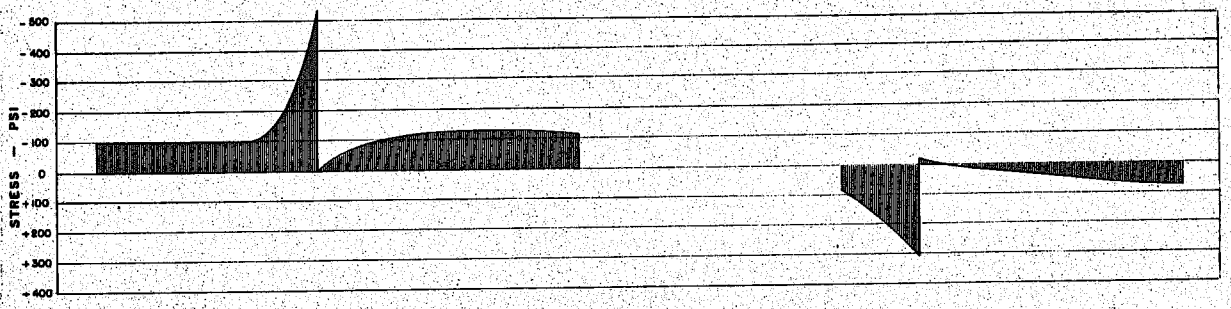

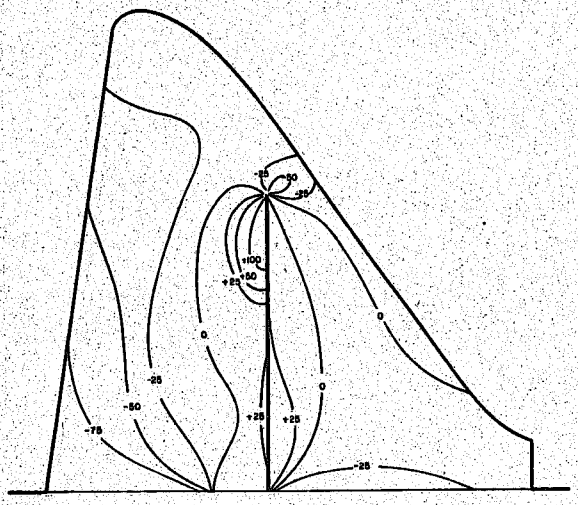

MAJOR STRESSES – σ_1

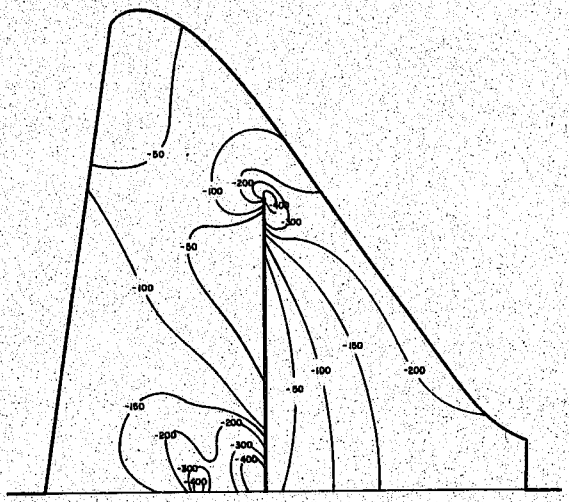

MINOR STRESSES – σ_2

UNIVERSITY OF CALIFORNIA – BERKELEY, CALIFORNIA DIVISION OF STRUCTURAL ENGINEERING AND STRUCTURAL MECHANICS		
STRESS DISTRIBUTION OF NORFORK DAM STRESS CONTOURS		
CASE L-2	LOADING DL & LL	UPLIFT 42 Ft.
CRACK HEIGHT 7/9	FOUNDATION Isotropic	FIG. NO. 23

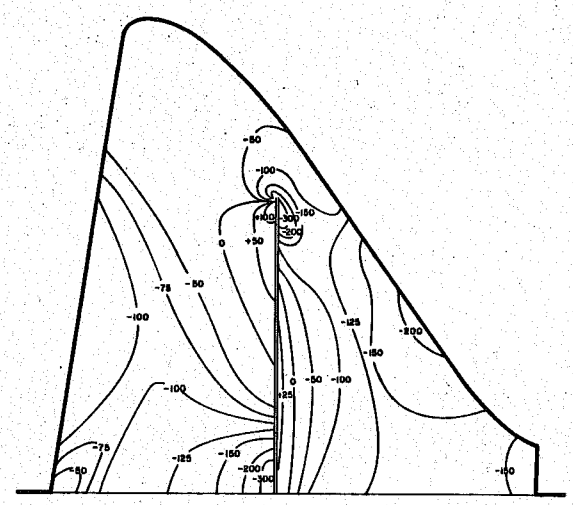

VERTICAL STRESSES - σ_y

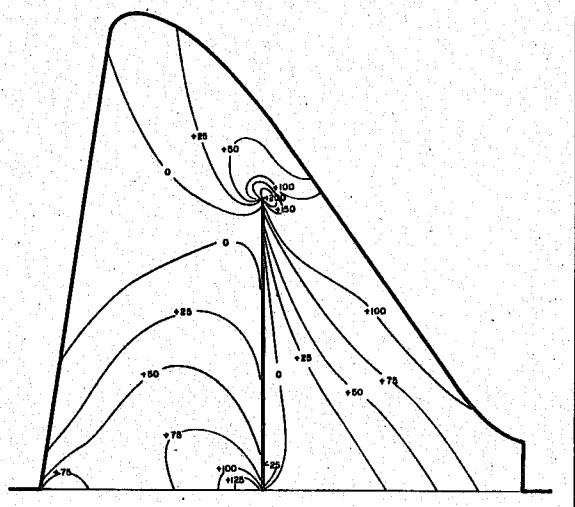

SHEAR STRESSES - σ_{xy}

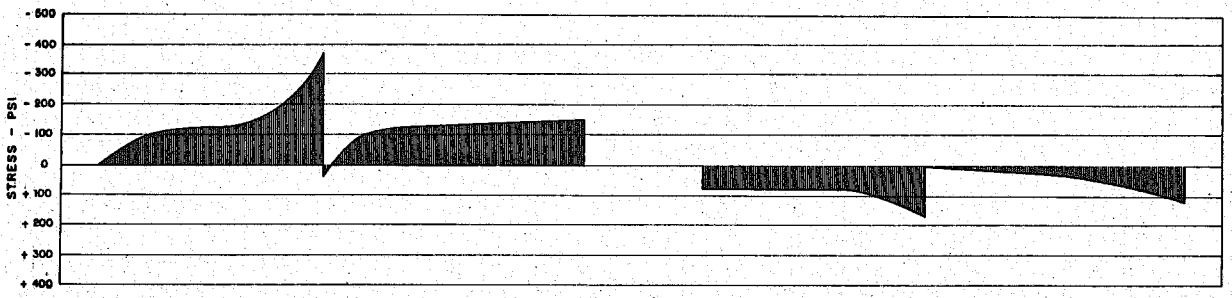

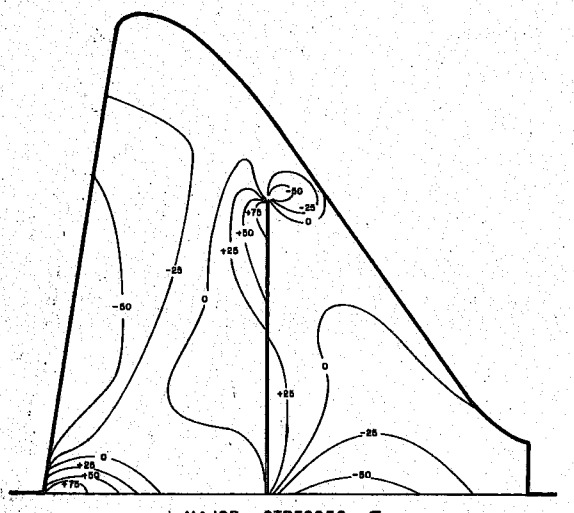

MAJOR STRESSES - σ_1

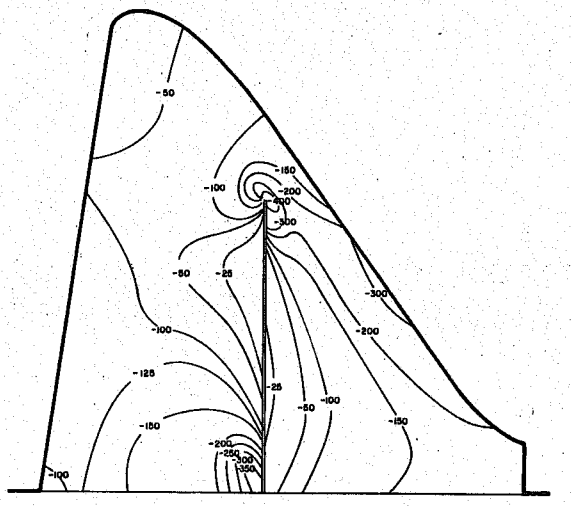

MINOR STRESSES - σ_2

UNIVERSITY OF CALIFORNIA – BERKELEY, CALIFORNIA
DIVISION OF STRUCTURAL ENGINEERING AND STRUCTURAL MECHANICS

STRESS DISTRIBUTION OF NORFORK DAM

STRESS CONTOURS

CASE	LOADING	UPLIFT
M	DL & LL	None
CRACK HEIGHT 1/3	FOUNDATION Orthotropic	FIG. NO. 26

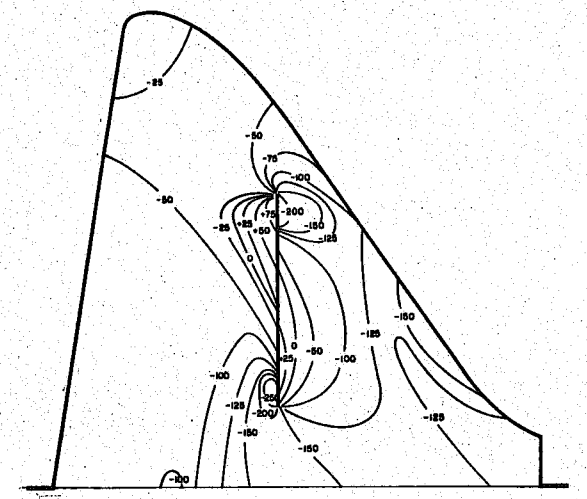

VERTICAL STRESSES - σ_y

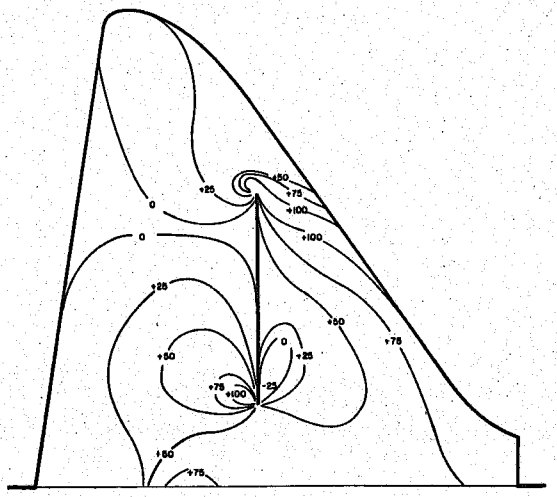

SHEAR STRESSES - σ_{xy}

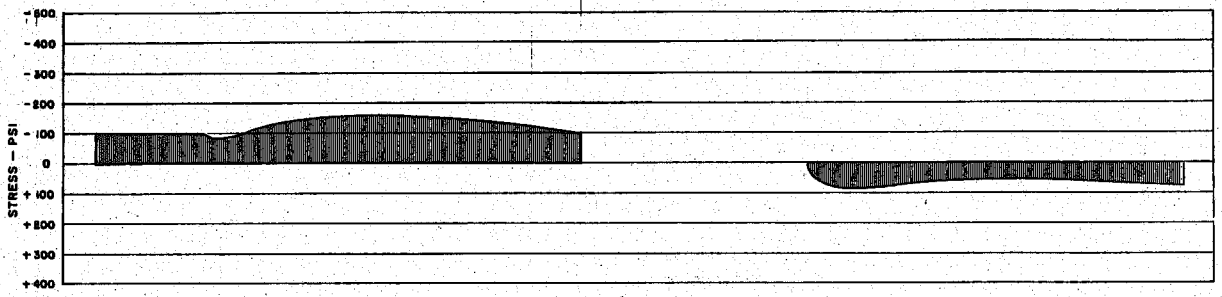

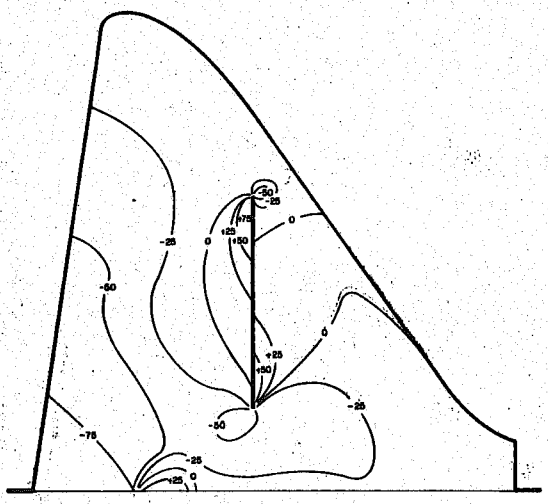

MAJOR STRESSES - σ_1

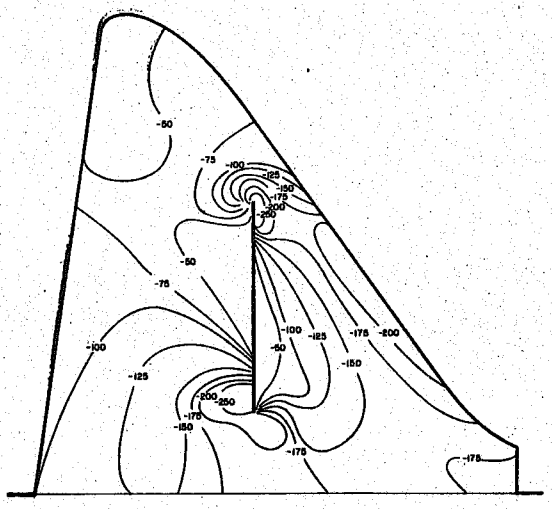

MINOR STRESSES - σ_2

UNIVERSITY OF CALIFORNIA – BERKELEY, CALIFORNIA DIVISION OF STRUCTURAL ENGINEERING AND STRUCTURAL MECHANICS		
STRESS DISTRIBUTION OF NORFORK DAM *STRESS CONTOURS*		
CASE *N*	LOADING *DL & LL*	UPLIFT *32 FT*
CRACK HEIGHT *4/3*	FOUNDATION *ISOTROPIC*	FIG. NO. *27*

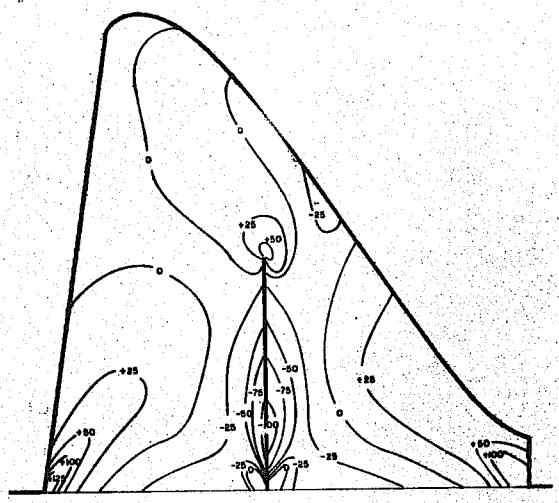

VERTICAL STRESS

FINITE ELEMENT

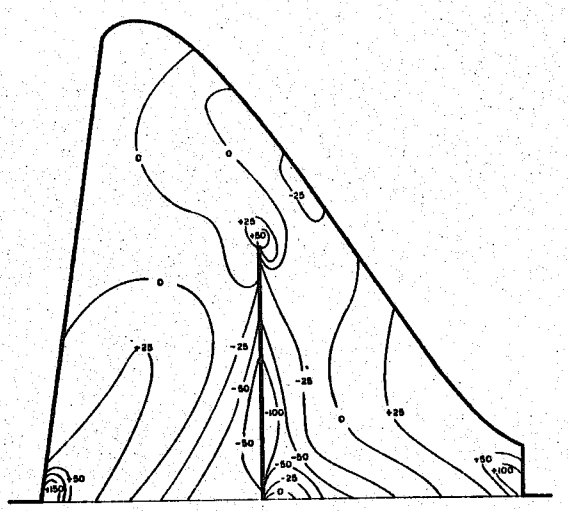

VERTICAL STRESS

LATTICE ANALOGY

UNIVERSITY OF CALIFORNIA – BERKELEY, CALIFORNIA
DIVISION OF STRUCTURAL ENGINEERING AND STRUCTURAL MECHANICS

STRESS DISTRIBUTION OF NORFORK DAM

STRESS CONTOURS

CASE 0-1	LOADING TH	UPLIFT NONE
CRACK HEIGHT 2/3	FOUNDATION ISOTROPIC	FIG. NO 28

Portland Cement Association using the lattice anology. The properties assumed by McHenry differed significantly from those employed in the analyses described above, due in part to certain limitations in his lattice analogy. Consequently it was considered desirable to employ these same property assumptions in a finite element analysis for the purpose of making this comparison. Different properties were assumed in each of the comparison cases, and each is discussed separately.

Case 0-1 (Thermal loading only):

Temperature change:	$T = -23^{o}F$	(uniform in dam, no change in foundation)
Moduli of Elasticity:	Foundation	$E = 5.0 \times 10^{6}$ psi
	Dam	$E_c = 1.90 \times 10^{6}$ psi
Poisson's Ratio:		$\nu = 0.33$

The σ_y stresses computed by the two methods are seen in Fig. 28 to be equivalent for all practical purposes. The stress contours are generally the same, and show appreciable differences only at the points of stress concentration along the base of the dam. At the toe and the heel of the section, these differences are due primarily to the boundary approximations imposed by the lattice analogy used by McHenry. The structure actually analyzed by that approach is one in which the sloping surfaces of the dam are represented by steps in the rectangular mesh. Thus at each step a stress concentration is found which is not representative of the prototype system. The minor differences which may be seen in the base stress concentrations upstream and downstream from the crack may be due to differences in the methods of representing the crack. In any case, the substantial agreement between results obtained by methods as different as these is good evidence of the reliability of both methods.

Case O-2 (dead and live load):

Modulus of Elasticity: Dam and foundation $E = 4.0 \times 10^6$ psi

Poisson's Ratio: $\upsilon = 0.33$

Unit Weight: Concrete $\gamma_c = 150$ pcf

The principal stress distributions for this loading (Fig. 29) are seen to be remarkably similar, with only very slight differences to be noted in the stress concentrations at the toe and the heel. These are due undoubtedly to the step-wise approximation of the sloping faces which was used in the lattice analogy, and are of no practical importance.

Static Checks of Force Resultants

In applying the finite element method, the digital computer automatically satisfies the equilibrium requirements imposed on the structure; in other words, internal forces are determined which exactly balance the external loads acting at each nodal point. Thus, there is no question that each portion of the finite element idealization is in equilibrium. However, a further stage of approximation is involved in establishing the element stresses, and particularly in constructing the stress contours representing these element stresses. Thus it is of some interest to compare the resultant forces represented by the calculated stress distributions with the external load resultants applied across the same sections. Such checks were made at the base of the dam section for all cases considered, and also with respect to the small triangular block above the tip of the crack for one case.

Base Force Resultants- A comparison of the resultant forces, determined from the calculated base normal and shear stress distributions, with the total vertical and horizontal applied load components, F_y and F_x respectively, is presented in Table III.

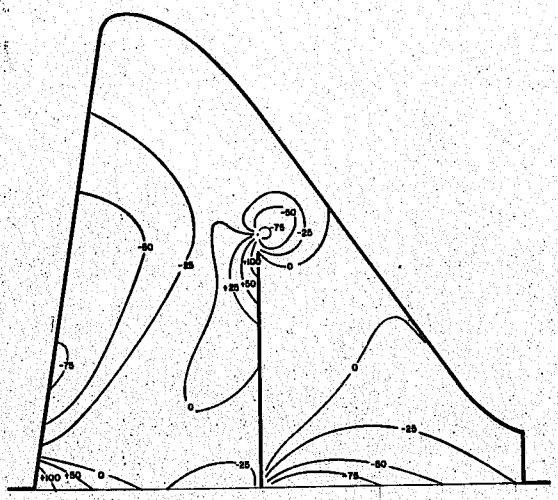

MAJOR STRESSES - σ_1

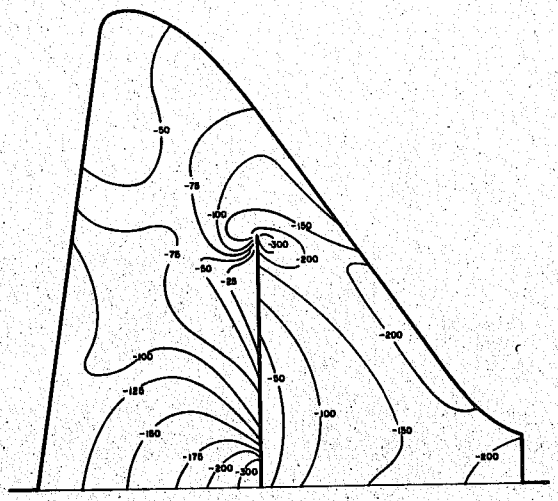

MINOR STRESSES - σ_2

FINITE ELEMENT

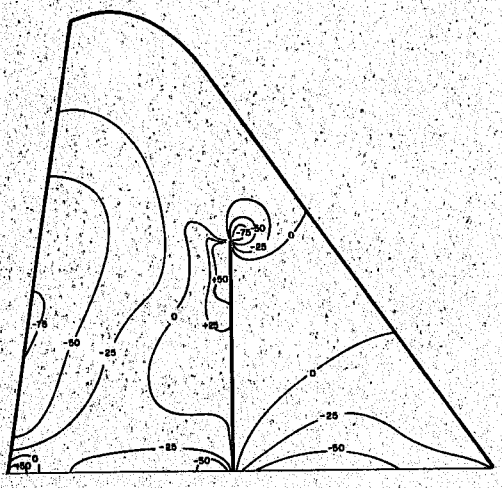

MAJOR STRESSES - σ_1

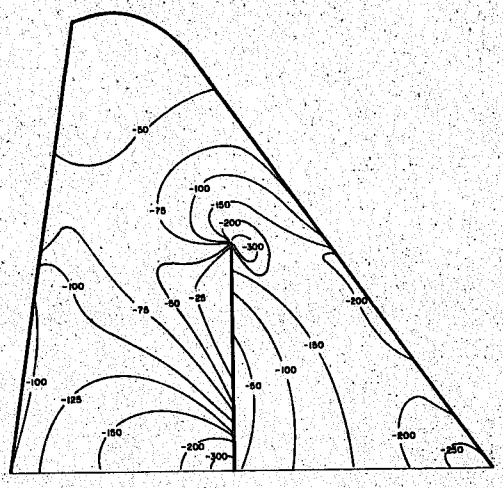

MINOR STRESSES - σ_2

LATTICE ANALOGY

UNIVERSITY OF CALIFORNIA – BERKELEY, CALIFORNIA DIVISION OF STRUCTURAL ENGINEERING AND STRUCTURAL MECHANICS		
STRESS DISTRIBUTION OF NORFORK DAM *STRESS CONTOURS*		
CASE *O-2*	LOADING *DL + LL*	UPLIFT *NONE*
CRACK HEIGHT *2/3*	FOUNDATION *ISOTROPIC*	FIG. NO. *29*

TABLE III. CHECK OF BASE FORCE EQUILIBRIUM

Case	$\int \sigma_y dx$	F_y	Error	$\int \tau_{xy} dx$	F_x	Error
A	3300^T	3350^T	-1.5%	0	0	0
B	3740	3650	2.5	1570	1530	2.6
C	3780	3650	3.6	1640	1530	7.2
D	3400	3350	1.5	0	0	0
E	3650	3650	0	1640	1530	7.2
F	3250	3350	-3.0	0	0	0
G	3800	3650	4.1	1540	1530	0.7
H	3650	3650	0	1620	1530	5.9
I	3350	3350	0	0	0	0
J	3600	3650	-1.4	1590	1530	3.9
K	3280	3350	-2.1	0	0	0
L-1	3700	3650	1.4	1520	1530	-0.6
L-2	3600	3650	-1.4	1520	1530	-0.6
M	3700	3650	1.4	1550	1530	1.3
N	3700	3650	1.4	1560	1530	2.0

In general it is believed that these results represent a very satisfactory degree of agreement, and that the triangular element mesh size which was employed is justified. A finer definition of the stresses could have been achieved, of course, by using smaller elements, but at a considerable cost in computational effort. It is believed that no greater precision could be justified for the purpose of this project.

Block Above Crack- From the complete stress distribution information provided by these analyses it is possible to evaluate the equilibrium of forces acting on any desired portion of the cross-section. Of particular interest in this regard is the small triangular block above the tip of the crack, which transmits all of the forces acting between the two basic portions of the dam. Fig. 30 shows the normal and shear stress distributions in this zone of the cross-section for Case J, the case with the seven-ninths crack height subjected to dead plus live loads. The normal and shear stress distributions acting on the vertical and horizontal surfaces bounding this little block are shown, in addition to their resultant forces. The resultant forces acting on the block are seen to balance to within about 4 per cent, which is a very satisfactory result, especially considering the rather small number of elements used to define the state of stress in this local region.

Effect of Crack on Base Stress Distribution- In the discussion of the stress contours above, it was noted that the effect of the crack on the stress distribution was indicated directly by a comparison of cracked section results with the uncracked section results for like loading conditions. It would have been relatively simple to arrange the program so that the digital computer would automatically make such a comparison, subtracting stress results for the uncracked case from those for the cracked section. This was not done for the present investigation because it was considered that the results would not be of sufficient interest to justify the programming effort. However, to indicate the character of such an analysis, the effect of the crack on the base stress distribution for a typical loading was evaluated by manually taking the difference between the base stresses for Cases B and J. The results, shown in Fig. 31, depict

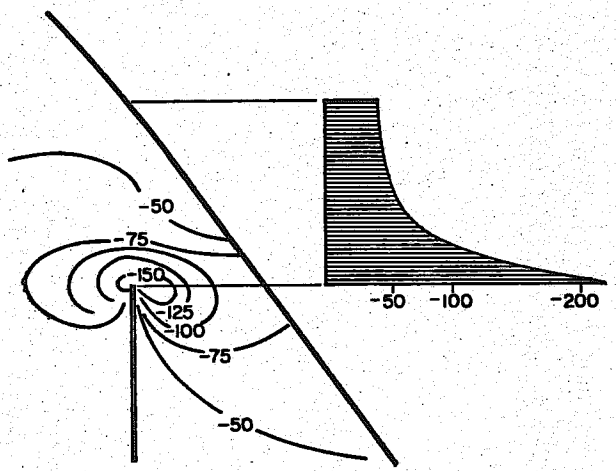

HORIZONTAL STRESS - σ_x

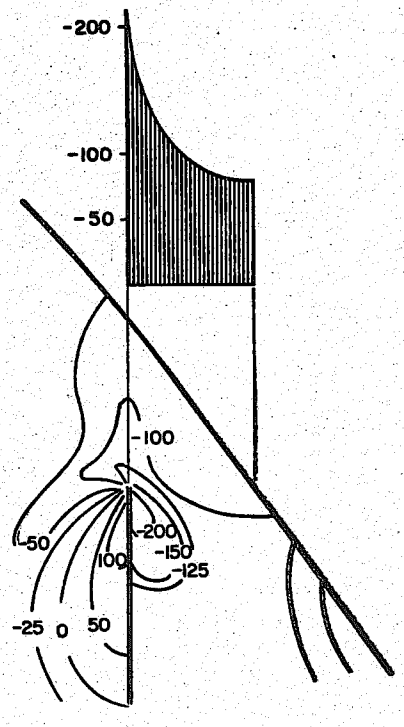

VERTICAL STRESS - σ_y

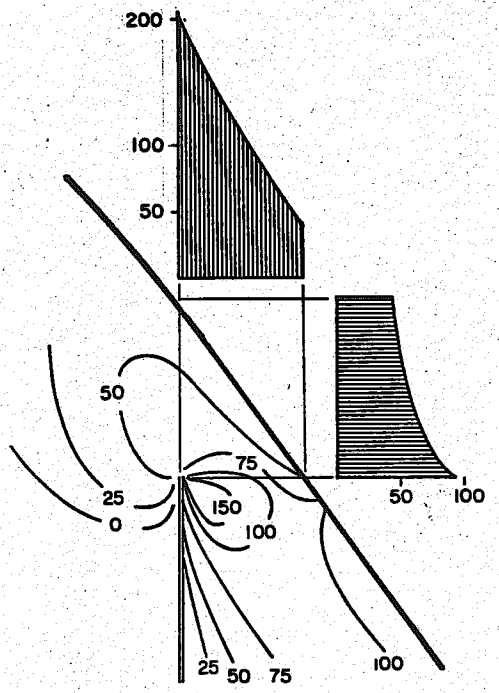

SHEARING STRESS - τ_{xy}

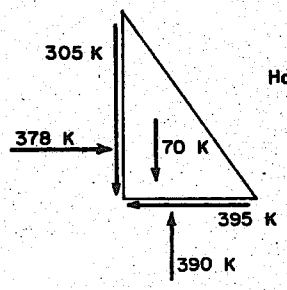

Vertical Force Check
305 + 70 = 375 ≈ 390

Horizontal Force Check
378 ≈ 395

UNIVERSITY OF CALIFORNIA — BERKELEY, CALIFORNIA
DIVISION OF STRUCTURAL ENGINEERING AND STRUCTURAL MECHANICS

STRESS DISTRIBUTION OF NORFORK DAM

EQUILIBRIUM OF BLOCK AT TOP OF CRACK

CASE	LOADING	UPLIFT
J	DL & LL	NONE
CRACK HEIGHT 7/9	FOUNDATION ISOTROPIC	FIG. NO. 30

the base normal and shear stresses caused by the 7/9 crack when the section is subjected to live plus dead loading. The stress concentrations due to the crack, amounting to a maximum of about 200 psi in compression, are quite evident in this plot.

Boundary Displacements

The displacement vectors of each of the boundary nodal points have been plotted for the most significant cases which were treated. Lines connecting the end points of these vectors show the deformed shape of the structure, to a greatly exaggerated deformation scale. The reference base with respect to which all displacements have been computed is the base of the coarse mesh foundation elements (Fig. 10), thus foundation deformations as well as those of the concrete structure are represented.

Uncracked Section (Fig. 32)- The only notable result presented in this figure is the relative magnitude of the thermal deformations as compared with those due to dead and live loads. The fact that serious cracking has been observed in the structure is not at all surprising in view of these very large thermal strains.

Two-Thirds Crack Height (Fig. 33)- Comparing Figs. 32 and 33, it is apparent that the only effect of the crack on the boundary deformations is a very slight increase in downstream displacement resulting from the live load. Thus it is evident that the cracked structure behaving as two blocks is slightly more flexible than the uncracked system, as would be expected. The introduction of the orthotropic foundation leads to the expected large increase in the vertical displacement of the structure, but has no other apparent effect on the boundary displacements.

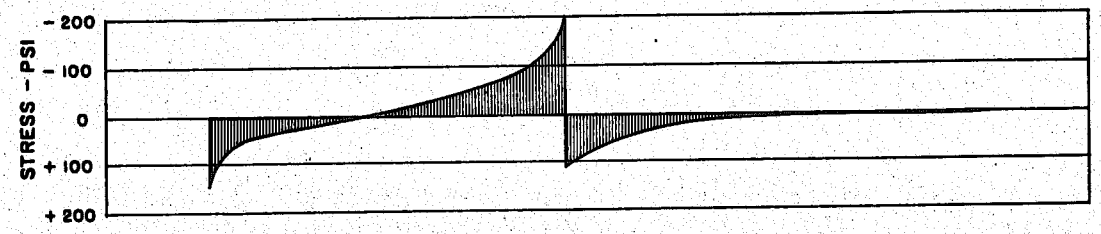

VERTICAL STRESS - σ_y

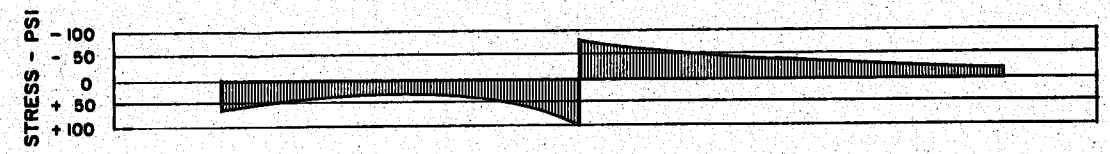

SHEARING STRESS - τ_{xy}

UNIVERSITY OF CALIFORNIA - BERKELEY, CALIFORNIA
DIVISION OF STRUCTURAL ENGINEERING AND STRUCTURAL MECHANICS

STRESS DISTRIBUTION OF NORFORK DAM

EFFECT OF CRACK ON BASE STRESSES

CASE J	LOADING DL & LL	UPLIFT NONE
CRACK HEIGHT 1/9	FOUNDATION ISOTROPIC	FIG. NO. 31

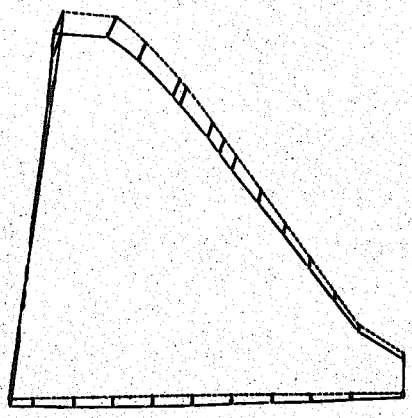

DEAD LOAD

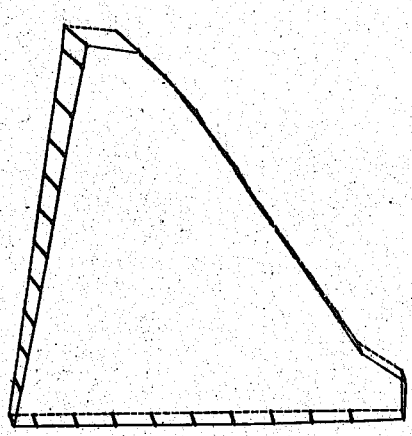

DEAD LOAD AND LIVE LOAD

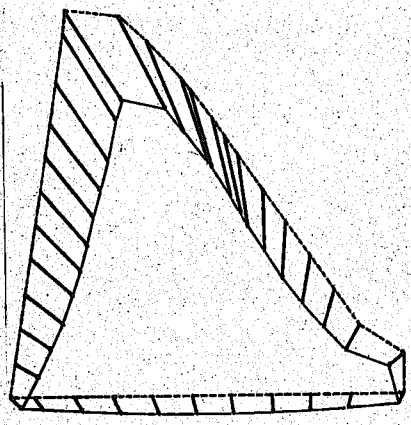

DEAD LOAD, LIVE LOAD AND TEMPERATURE

SCALE

UNIVERSITY OF CALIFORNIA — BERKELEY, CALIFORNIA
DIVISION OF STRUCTURAL ENGINEERING AND STRUCTURAL MECHANICS

STRESS DISTRIBUTION OF NORFORK DAM

BOUNDARY DISPLACEMENTS

CASE	LOADING	UPLIFT
CRACH HEIGHT 80 FEET	FOUNDATION	FIG. NO. 32

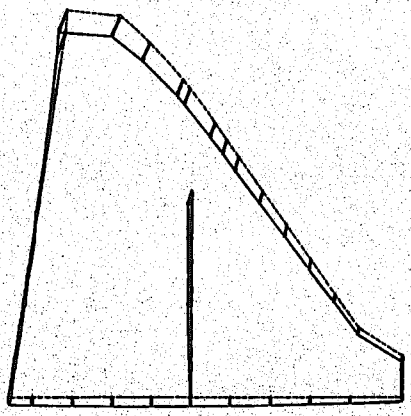

DEAD LOAD

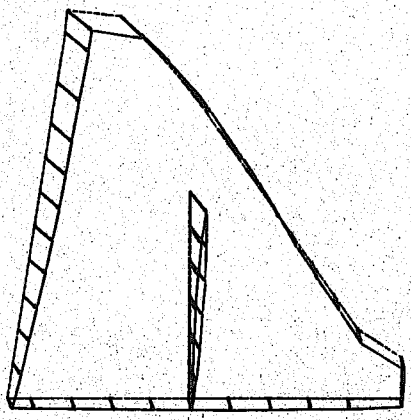

DEAD LOAD AND LIVE LOAD

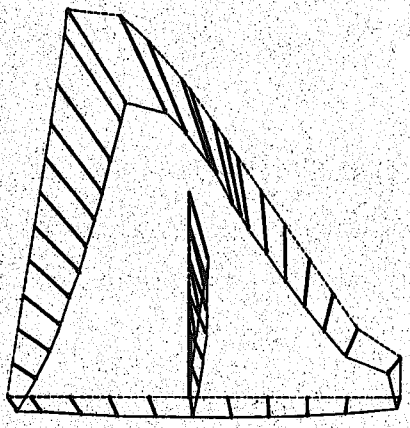

DEAD LOAD, LIVE LOAD AND TEMPERATURE

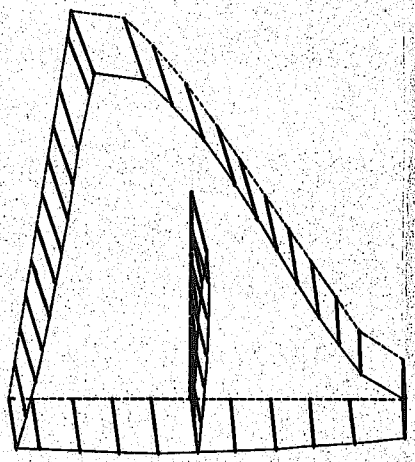

DEAD LOAD AND LIVE LOAD
(ORTHOTROPIC FOUNDATION)

SCALE

UNIVERSITY OF CALIFORNIA — BERKELEY, CALIFORNIA
DIVISION OF STRUCTURAL ENGINEERING AND STRUCTURAL MECHANICS

STRESS DISTRIBUTION OF NORFORK DAM

BOUNDARY DISPLACEMENTS

CASE	LOADING	UPLIFT
CRACH HEIGHT 4/9	FOUNDATION	FIG. NO. 33

Seven-Ninths Crack Height (Fig. 34)- Remarks similar to the above apply equally to the first two cases presented in Fig. 34; the additional crack height considered here has a very small influence on the boundary displacement. The addition of uplift pressures at the heel of the section causes an additional downstream rotation of the dam, as is shown in the third sketch. The increased stiffness provided by closing the crack for the lower two nodal points is demonstrated by the reduced downstream displacement to be noted in the fourth sketch in this figure.

Crack Opening (Fig. 35)

The displacements of the upstream and downstream faces of the crack were generally of more interest than the outer boundary displacements. In the first place, the amount of opening of the crack was used as a check on the properties assumed for the concrete (i.e. its thermal coefficient and modulus of elasticity) as well as on the assumed temperature changes. Because the opening of the crack rather than its actual displacement was of principal interest, only the horizontal components were plotted in this figure, relative to the original position of the crack.

Two sets of results are presented in this figure, those for the 2/3 crack height, and those for the 7/9 crack height. For each system, the crack opening due to temperature alone was determined by taking the difference between dead load plus temperature and the dead load (alone) results. The maximum width of the opening due to temperature was found to be over 1/8 inch for the 2/3 crack height case and over 3/16 of an inch for the 7/9 case, the increase in opening due to the vertical extension of the crack being quite notable. These values decreased to about 1/8 inch and just under 3/16 inch respectively when dead load was included,

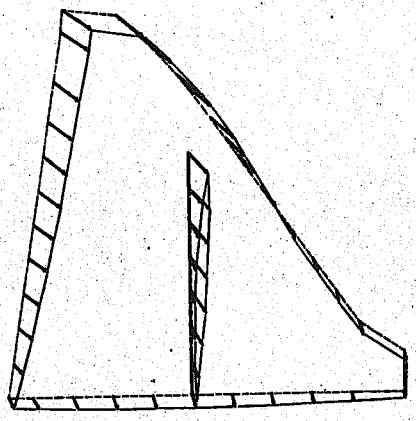

DEAD LOAD AND LIVE LOAD

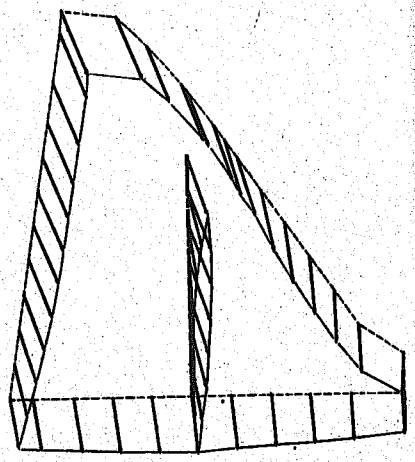

DEAD LOAD AND LIVE LOAD
(ORTHOTROPIC FOUNDATION)

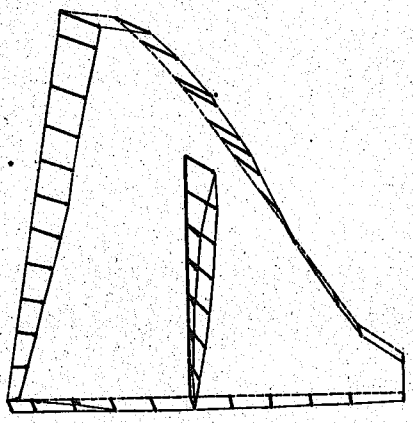

DEAD LOAD AND LIVE LOAD
(UPLIFT)

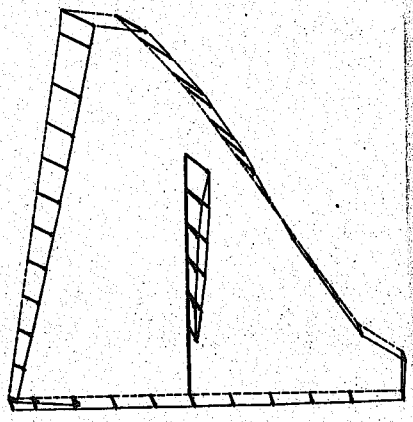

DEAD LOAD AND LIVE LOAD
(UPLIFT)
BASE OF CRACK AT 2/9 POINT

SCALE

UNIVERSITY OF CALIFORNIA - BERKELEY, CALIFORNIA
DIVISION OF STRUCTURAL ENGINEERING AND STRUCTURAL MECHANICS

STRESS DISTRIBUTION OF NORFORK DAM

BOUNDARY DISPLACEMENTS

CASE	LOADING	UPLIFT
CRACK HEIGHT 2/9	FOUNDATION	FIG. NO. 39

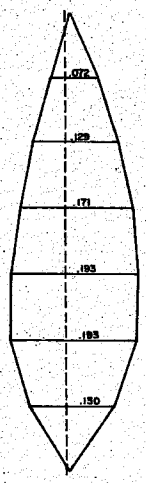

TEMPERATURE

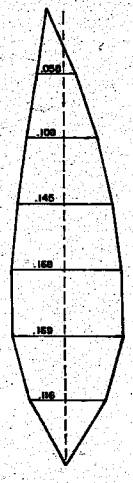

DEAD LOAD
TEMPERATURE

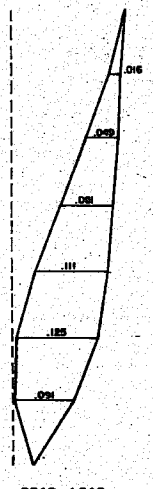

DEAD LOAD
LIVE LOAD
TEMPERATURE

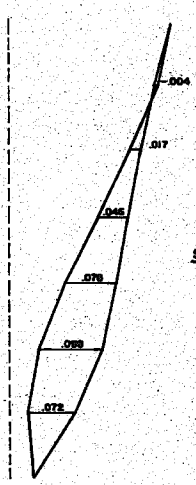

DEAD LOAD
LIVE LOAD
TEMPERATURE
(UPLIFT)

SECTION CRACKED TO 7/9 HEIGHT

NOTE:
DASHED LINE INDICATES ORIGINAL CRACK AXIS

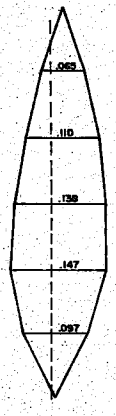

TEMPERATURE

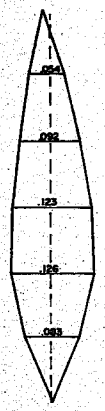

DEAD LOAD
TEMPERATURE

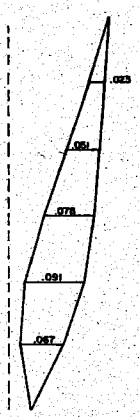

DEAD LOAD
LIVE LOAD
TEMPERATURE

SECTION CRACKED TO 2/3 HEIGHT

UNIVERSITY OF CALIFORNIA — BERKELEY, CALIFORNIA
DIVISION OF STRUCTURAL ENGINEERING AND STRUCTURAL MECHANICS

STRESS DISTRIBUTION OF NORFORK DAM

HORIZONTAL CRACK DISPLACEMENTS

CASE	LOADING	UPLIFT
CRACK HEIGHT	FOUNDATION	FIG. NO. 33

a more realistic condition, of course. Addition of the live load then caused both a large downstream displacement of the crack, as well as tendencies toward closing near the upper end (where the base constraint was less effective). The amount of closure was somewhat greater in the 7/9 case, but even here it did not completely close at any point.

However, when the uplift pressures were added, it was found that the crack did actually close at the top nodal point in the 7/9 case. The calculations show an excess of closure of 0.004 inches, thus the displacements actually would have been slightly less than these computed values, and results obtained in this case may be considered slightly conservative. In other words, contact pressures across the upper nodal point of the crack would have carried some of the stress, and results would revert back slightly toward those obtained for the 2/3 crack height case.

It should be noted, however, that only in the most severe conditions assumed did any crack closing develop, and since the crack probably does not extend all the way from the base to 7/9 height, it is probable that no closure actually has been produced on the prototype structure.

CONCLUSIONS

The results obtained in this investigation permit several conclusions to be drawn with regard to a number of different aspects of the study. It should be pointed out that the investigators were not requested to establish the adequacy of the structure and no conclusions of this type will be reported (though it should also be mentioned that none of the results indicate an overstressed or unsafe condition). Specific conclusions are discussed consecutively, below.

Method of Analysis

One of the most important results derived from the study was the demonstration of the effectiveness and versatility of the finite element method and of the digital computer program which was developed to implement the method. Stress distributions and deformations were obtained for a variety of complex plane stress systems subjected to some rather awkward loading conditions. The input data required to define any problem is easily prepared; the most time consuming part of the task is the choice of the most suitable finite element mesh and the evaluation of the coordinates of the nodal points of the system. When the input data has been prepared properly, the operation of the program is automatic and the analysis can be carried to any suitable degree of convergence. Computer time requirements are quite reasonable, even for the treatment of complex cases such as these.

The comparison of this method with the lattice analogy employed by D. McHenry demonstrated that both methods give reliable results. The lattice analogy idealization utilized a much finer mesh than was considered desirable in the finite element system. In any analysis of this type it

is necessary to weigh the advantage of increased precision of the results against the cost in computer time, which increases rapidly with the number of elements. In general, it is best to use only enough elements to obtain the necessary accuracy; this is particularly true when a large number of cases are to be treated. Comparisons of the computer time requirements of the two methods are relatively meaningless because the IBM 704 used in this study is a much faster and more powerful machine than the LGP30 used by McHenry, though it may be noted that the analysis of a single case by McHenry took about 200 times as long as to do a similar problem on the IBM 704.

The most obvious advantage of the finite element method over the lattice analogy is the ease with which it can account for arbitrary boundary conditions(e.g. sloping surfaces), arbitrary material properties (Poissons' ratio must be taken as 1/3 in the lattice analogy) and arbitrary thermal variations. Such special conditions as the orthotropic foundation, which would be quite difficult to represent in the lattice analogy, also may be included without difficulty.

Effect of Crack

The principal reason for initiating this investigation was the question as to how a centrally located crack would affect the stress behavior of a gravity dam. These studies showed clearly that, although several rather significant stress concentrations might be associated with the crack, the magnitudes of the total stresses were not excessive for the section geometry considered here, being less than 500 psi in all cases. The principal stress concentration zones were at the upper and lower ends of the crack and at the heel of the dam. Tensile stress was developed at

the heel of the cracked section, and at the upstream face of the crack near its upper end. It is of interest to note that cracking was observed in the prototype at this latter location, and it is presumed to be present in the vicinity of the heel also.

Thermal Loading

The finite element analysis described in this report indicates stresses due to thermal changes which are consistent with the assumed behavior of the structure. However, it is believed that the magnitude of the computed stresses, which exceeds 500 psi near the heel of the cracked section or 350 psi at the base of the section with the crack extending to 7/9 height, is considerably greater than the actual thermal stresses developed in these initial zones because several of the assumptions on which the analysis is based are not satisfied.

The principal differences between the assumed and the actual conditions are as follows:

1) It was assumed that there was no horizontal temperature gradient, whereas it is known that the temperature rise (and subsequent cooling) must be significantly smaller near the exposed surface of the section. Tensile stresses near the surface therefore would be significantly less than computed.
2) It was assumed that the entire section was subjected to dead weight and cooling effects as a unit, whereas the structure actually was built over an extended period of time, and cooling deformations of the earliest construction took place before the

final sections were built. Resistance to thermal deformation (thermal stress) must therefore be less than computed.

3) It was assumed that the section acted as a homogeneous, isotropic elastic system except for the specified vertical and uplift cracks, whereas it is known that many additional smaller cracks developed in the structure, particularly near the base. These additional cracks would have the effect of relieving tensile stresses wherever the computed tensile stresses were high enough to induce cracking. Specifically, it would be expected that the horizontal (σ_x) tensile stress over the entire base section, and the vertical (σ_y) tensile stress near the heel would be reduced by this effect.

Because of these several factors tending to reduce thermal stess, it is believed that the computed thermal stresses are significantly higher than the actual values in the critical stress regions. Therefore it was deemed advisable to base the principal stress analysis conclusions of the study on dead and live load effects, and to take account of the thermal analysis with regard to its deformation effects only. This is equivalent to assuming that all thermal stress was dissipated by creep and cracking.

Orthotropic Foundation

Although the orthotropic foundation was found to contribute to large vertical displacements of the section, the effect of the orthotropy on the stress distribution was inconsequential. Thus any question as to

whether the assumed foundation properties are correct or realistic is of little importance; it seems clear that the results don't depend upon this factor.

ACKNOWLEDGMENTS

A number of individuals and groups of people made significant contributions to the work described in this report, and the author wishes to thank them all for their participation. Most important were Messrs. Edward L. Wilson and Ian King, graduate students of the University of California, who actually carried out all of the analyses discussed herein--from the initial preparation of data to the plotting of the final results. In addition, Mr. Wilson was responsible for the development of the digital computer program which made the investigation possible.

The Little Rock District Office of the Corps of Engineers, under Mr. E. F. Rutt, and its Board of Consultants: Messrs. R. W. Carlson, R. E. Davis, and Byram Steele, were very helpful in establishing the properties of the system and in selecting the loading conditions to be considered. It was particularly convenient to have Prof. Davis and Dr. Carlson available locally for consultation at various intervals during the course of the study, and their continued interest and cooperation is greatly appreciated.

Finally, acknowledgment is due the University of California Computer Center which provided the computer on which the computations were carried out, and to the National Science Foundation whose research grant supported the original development of the finite element computer program, prior to the initiation of this study.

REFERENCES

1. Zienkiewicz, O. C., "The Stress Distribution in Gravity Dams", Journal, Institution of Civil Engineers, Vol. 27, 1946-47.
2. Raphael, J. M., "The Development of Stresses in Shasta Dam", Trans. ASCE, Vol. 118, 1953.
3. Boulder Canyon Project, Final Reports; Part V, Technical Investigations; U.S. Bureau of Reclamation, Denver, Colorado, 1938-1940.
4. Clough, R. W., "The Finite Element Method in Plane Stress Analyses", Proceedings, ASCE 2nd Conference on Electronic Computation, Pittsburgh, Pa., September 1960.
5. Turner, M. J., Clough, R. W., Martin, H. C., and Topp, L. J., "Stiffness and Deflection Analyses of Complex Structures", Journal of the Aeronautical Sciences, Vol. 23, No. 9, September 1956, p. 805.
6. Hrennikoff, A., "Solution of Problems of Elasticity by the Framework Method", Journal of Applied Mechanics, December 1941.
7. McHenry, D., "A Lattice Analogy for the Solution of Stress Problems", Journal, Institution of Civil Engineers, December 1943, pp. 59-82.
8. Clough, R. W., "Structural Analysis by Means of a Matrix Algebra Program", Proceedings, ASCE Conference on Electronic Computation, Kansas City, November 1958.
9. Lehman, F. G., "Simultaneous Equations Solved by Over-Relaxation", Proceedings, ASCE 2nd Conference on Electronic Computation, Pittsburgh, Pa., September 1960.

SUPPLEMENTARY INVESTIGATION

INTRODUCTION

Objectives of the Supplementary Investigation

During the course of the original investigation regarding the stress distribution in Norfork Dam, a number of topics came up which were of interest, but were beyond the scope of the contract. Accordingly, the contract was modified to permit the extension of the investigation into two of these areas, and this supplementary report describes the work done under the extended contract. This supplement is intended merely as an addition to the original report and is not complete in itself.

One of the topics considered here involves a simple extension of the analyses performed in the original work, to include a case not previously treated. In this new case, which is designated N-2, the central crack is assumed to extend from the first to the seventh nodal points (i.e., from 1/9 to 7/9 height). Thus it lies midway between cases L-1 and N of the original investigation. It is now believed that this new case is closer to the actual conditions in the dam than any of the previous cases. Case N-3 is identical with N-2 except that the reservoir level has been set at 573 ft. elev. rather than 584 ft as was assumed for all other live load cases. It represents the state of stress developed by

the maximum water level yet permitted in the reservoir.

The other subject of this supplementary study is the case of a crack extending through to the upper surface of the dam. Examination of the dam indicates that no such crack exists; however, this condition is of interest as a limiting case as well as a subject of scientific curiosity. The physical properties of the dam were assumed the same for this case as before, and a similar finite element idealization was adopted. As before, the thermal changes were used merely to establish the initial crack opening (under dead load plus thermal conditions). The thermal stresses were considered to be unrealistic, due to creep effects, and were not included in the final stress distributions. Isotropic foundation conditions were assumed in all of the new analyses, and the calculations were carried out both with and without uplift pressures.

The principal difference between these new cases and the previous analyses is that, with the crack extending to the surface, the section becomes so flexible that addition of the live load causes the upstream block to deflect into contact with the downstream block. This "crack closing" condition makes the structure non-linear and requires a major modification of the analysis procedure in order to account for it. Thus, an additional result of this supplementary study was the demonstration of a procedure for the analysis of non-linear problems by the finite element method.

Cases Considered

A complete listing of the analyses considered in this supplementary investigation is presented in Table IIa, below.

Table IIa SUPPLEMENTARY SCHEDULE OF ANALYSIS

Case	Crack Heights	Loading	Uplift	Fig. No.
N-2	1/9 to 7/9	Dead + Live	32 ft.	36
N-3	1/9 to 7/9	Dead + Live (573ft.)	32 ft.	36a
P-1	Full	Dead + Temp	None	37 & 38
P-2	Full	Dead + Live	None	39
P-3	Full	Dead + Temp	32 ft.	
P-4	Full	Dead + Live	32 ft.	40
Q-1	1/9 to full	Dead + Temp	None	
Q-2	1/9 to full	Dead + Live	None	41
Q-3	1/9 to full	Dead + Temp	32 ft.	
Q-4	1/9 to full	Dead + Live	32 ft.	42

Cases P & Q involve the new full crack height configuration in which the crack closed under live loading. The 1st and 3rd analysis for each case considered dead plus thermal stresses in order to establish the initial crack opening. The stresses due to thermal changes were not considered significant, however, as was noted above, and stress contours are presented only for the 2nd and 4th analysis for each case.

METHOD OF ANALYSIS FOR CRACK CLOSING

General Comments

If a gravity dam section is cracked all the way to the

surface, the crack will open over its entire length under the action of gravity loads and thermal changes. As the reservoir is filled, however, the increasing hydrostatic pressures will gradually force the crack closed at the top; and as more water is added the crack will close further and further down. As the crack closes and contact is made between the two sides, the behaviour of the dam changes. Opposite sides of the crack are no longer free to move independently; in fact, because of the roughness of the crack surface, it may be assumed that the two sides lock together upon contact and subsequently displace as a continuous medium.

This changing character of the structure with crack closing makes it infinitely non-linear in reality. However, in the finite element idealization only a finite number of nodal points can come into contact along the crack surface. Thus an incremental approach to the non-linear problem becomes feasible. The reservoir is filled by increments and each time a nodal point closes, they are locked together and the modified structure is subjected to further increments of load. For the purpose of this analysis, a pair of nodal points facing each other across the crack (see Fig. 11, Final Report) is assumed to have closed when their relative horizontal displacement under live load just equals their initial horizontal displacement due to dead load plus thermal changes.

The stresses and displacements developed in each element of the dam due to each increment of loading may be superimposed to obtain the total stress in the non-linear system at any stage of loading. Thus the treatment of the crack closing problem reduces to the analysis of a succession of varying structures due to load increments and the superposition of the stresses (and displacements) calculated for each increment.

Uplift pressures, where considered in these analyses, were assumed to act over the first 3 nodal points of the base (32 feet) and were applied at the full hydrostatic pressure appropriate to each load increment. It should be noted that the extent of opening of the uplift pressure crack was not assumed to increase incrementally; it was active over its full extent throughout the loading.

Because of the incremental nature of the loading applied to the dam in these studies, it was not feasible to establish initial foundation displacements with a coarse mesh system as has been done previously. For this reason a larger foundation zone was included with the dam section in order that the foundation deformations might be treated realistically.

As was noted earlier, the thermal stresses computed in establishing the initial crack displacement condition of the structure were not considered to be realistic. Thus these stresses were stored during the incremental live load analysis

and then subtracted off prior to printing the final stress distribution. This is equivalent to assuming that the thermal stresses were eliminated by creep and plastic flow.

The Computer Program

The plane stress program used in all the previous analyses formed the basis of the crack-closing analysis program. However, it was modified by the addition of sub-routines which accomplished the incremental loading and structural modification operations described above. The basic flow sequence of the modified analysis is as follows:

1) The dead plus thermal loading case is solved, for the section cracked to the surface.
2) The displacements and stresses due to this loading are stored and the loading is erased.
3) After checking that the water level is not at the prescribed maximum, the loads due to a specified increment of water level are computed.
4) The structure, in its existing crack configuration, is analyzed for the incremental water loads.
5) The resulting horizontal crack displacements are checked against the previously existing crack openings to see if closure develops at any nodal point.

6a) If no closure occurs, the stresses and displacements are superposed on the previously existing results, the loads are erased, and the procedure is repeated from

Step 3.

6b) If exact closure occurs at any nodal point, the structure is modified by altering element connections so that the structural form is that of a section with the crack height lowered. Then stresses and displacements are superposed into storage, the loads are erased, and the procedure is repeated from Step 3.

6c) If overclosing occurs at any nodal point, the loads are scaled so as to cause exact closing* and the structure is modified as above. The remaining proportion of the loads is saved for superposing with the new load increment. The scaled stresses and displacements are superposed into storage, and the procedure is repeated from Step 3.

7) When the maximum water level is reached, the prevailing stresses and displacements in storage are printed.

8) Finally the stresses due to thermal changes are subtracted and the residual stresses (due to dead plus live load) are printed.

Because essentially the same basic program was used for each increment of loading, the analysis of a single case

---

*It will be noted that this scaling of loads is not exactly equivalent to taking a smaller water level increment. However, for small increments of water level, the difference is negligible.

involving crack closing was equivalent to approximately 10 analyses of the previous type. However, the high speed IBM 7090 digital computer became available for these analyses, and in addition certain modifications were made in the basic plane stress program which permitted faster operation. As a result, a complete crack closing case - involving approximately 1200 cycles of iterations in all - could be solved in about 12 minutes.

RESULTS AND DISCUSSION

Cases N-2 and N-3

As was noted earlier these cases are intermediate between Cases L-1 and N of the original investigation report, in that the crack extends from 1/9 height to 7/9 height rather than from the base and from 2/9 height respectively in the previous studies. The stress contours for Case N-2, presented in Fig. 36, show that the maximum stresses fall between the values given for the previous studies in Fig. 24 and 27 respectively. Thus the compressive stresses at the upstream side of the base of the crack are reduced from L-1 but are greater than N, while similar effects are observed with respect to the tensile stresses near the top of the crack.

The stress contours for Case N-3 (shown in Fig. 36a) are so similar to Fig. 36 that differences can be noted only by careful scrutiny. The loading for this case is reduced by about 10 per cent from Case N-2, and the apparent changes in stress

are of this order of magnitude.

Crack Closing Cases (P and Q)

Because the stress distribution of the systems subjected to crack closing depends so directly upon the extent of crack closing, it is advantageous to consider just the crack displacement history during the incremental loading. These results are presented in Fig. 37 for Case P (cracked to the base) and in Fig. 38 for Case Q (cracked to 1/9 above the base).

Case P-2, in which no uplift is considered, shows a regular relative displacement effect of the two sides of the crack as the load is increased, with a final condition in which the crack is closed from the top to 7/9 height. Thus its final configuration is quite similar to Case J (Fig. 22).

Case P-4, which includes the uplift crack is considerably more flexible (due to the redirection of base constraint). In fact, in the initial dead load plus thermal change condition, the analysis indicates that the uplift crack would develop negative displacements, which accounts for the wide opening of the vertical crack for this condition. This is an impossible situation, of course, but as live load is added the upstream block tilts rapidly and long before the top of the vertical crack closes, the uplift crack has opened. Thus the analysis is correct for an initial condition consisting of dead plus thermal plus partial water loading, and is valid for all subsequent stages of loading. The greater flexibility of the P-4

case (as compared with P-2) is indicated by the fact that closure developed from the top to 5/9 height of the crack.

The principal difference in crack displacements shown for Case Q in Fig. 38 is due to the increased stiffness caused by the base of the crack starting at 1/9 height. This additional connection at the base of the crack inhibits its initial opening under dead plus thermal loading. Subsequent live loading then is able to cause greater closure than developed in Case P-2, i.e. from the top to 6/9 height. The uplift crack produced approximately the same result in Case Q-4 as in Case P-4, including both the overclosing effect of the uplift crack before live loading (to a reduced degree) and the closing of the vertical crack from the top to 5/9 height under full live load.

The stress contours for Cases P-2, P-4, Q-2, and Q-4 are shown in Figs. 39, 40, 41 and 42 respectively. Comparison of the results for Case P-2 with Case J (Fig. 22) is of considerable interest in that the final crack configuration is the same in both cases but vertical adjustment took place in Case P-2 before the crack closed at the top. Consequently the shearing forces transmitted across the crack from 7/9 height to the top are much less in this case than for the corresponding zone in Case J. As a result, the live load is carried more by the upstream block in Case P-2 with corresponding increases in the stress concentrations at the base of the block (exceeding

600 psi compression and 300 psi tension).

Addition of the uplift pressures in Case P-4 eliminates the tensile stress concentrations at the heel of the section, of course, and permits a greater part of the live load to be transferred to the downstream block. The compressive stress concentration at the base is seen to be reduced from Case P-2 (to less than 600 psi).

Similar results are evident in Cases Q-2 and Q-4, except that having the crack closed to the first nodal point causes a much more favorable distribution of load between the two segments of the structure. In Case Q-2, the maximum tensile and compressive stresses at the critical horizontal section are only about 150 and 450 psi respectively. Addition of the uplift forces in Case Q-4 again reduces the maximum compressive stress at the critical section to only about 350 psi.

One of the basic assumptions made in the "crack closing" analyses was that the two sides of the crack locked together upon contact, and that no relative sliding of the two surfaces was permitted. This assumption is valid, of course, only if the coefficient of friction between the surfaces is sufficient to prevent slip. In order to assess these frictional force requirements the shear and normal stresses developed along the part of the crack which had closed were evaluated for Cases P-4 and Q-4. The results, shown in Fig. 43, demonstrate that the normal and shear stresses average about 50 psi in Case P-4

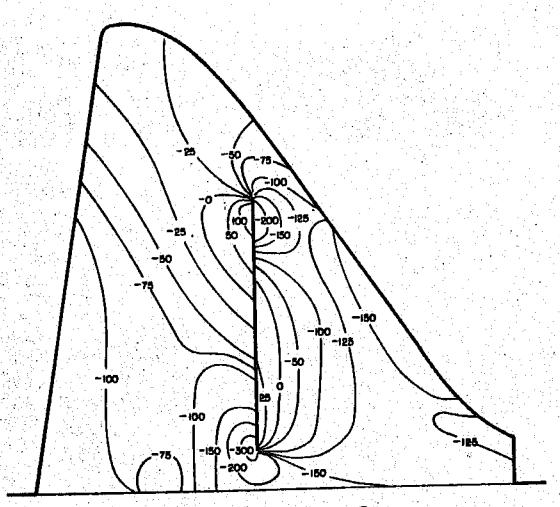

VERTICAL STRESSES – σ_y

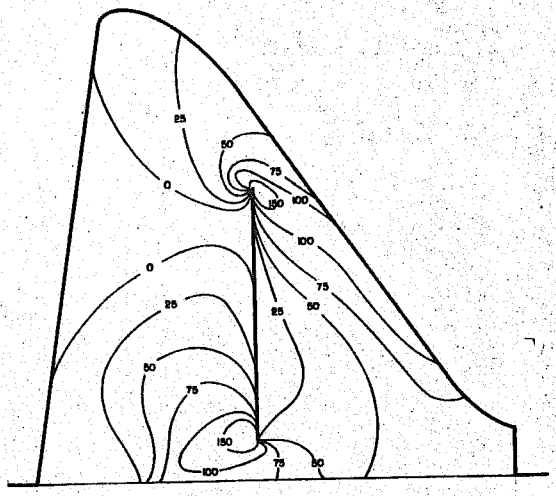

SHEAR STRESSES – σ_{xy}

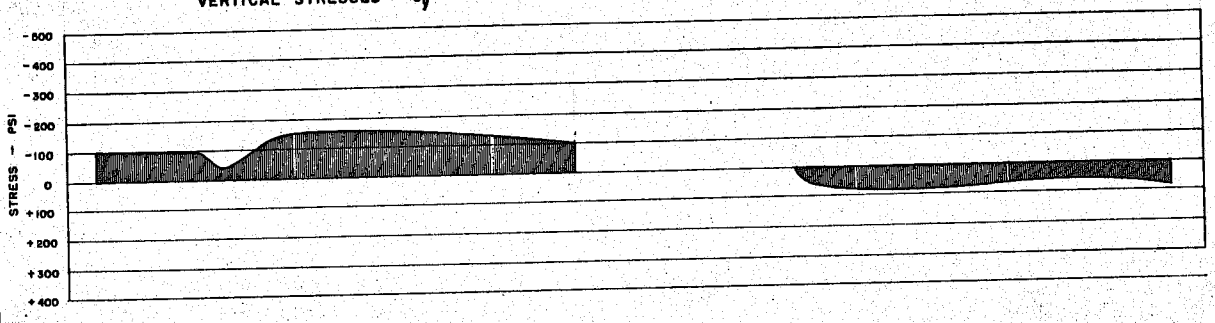

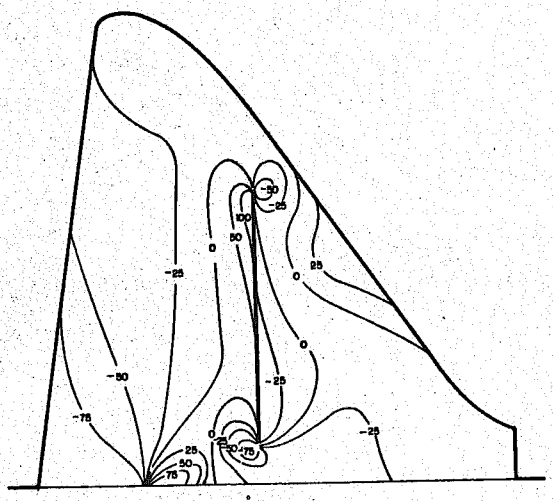

MAJOR STRESSES – σ_1

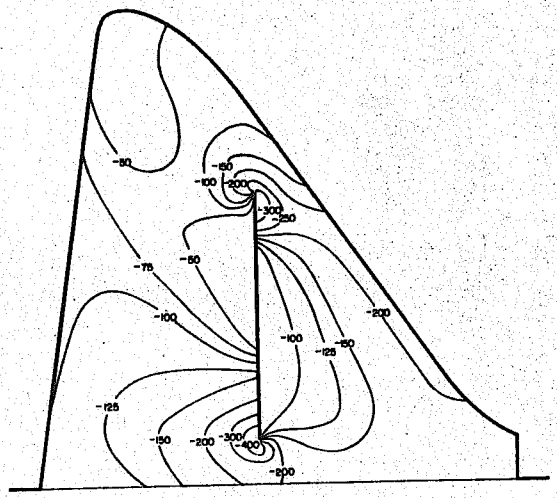

MINOR STRESSES – σ_2

UNIVERSITY OF CALIFORNIA – BERKELEY, CALIFORNIA DIVISION OF STRUCTURAL ENGINEERING AND STRUCTURAL MECHANICS		
STRESS DISTRIBUTION OF NORFORK DAM *STRESS CONTOURS*		
CASE *N-2*	LOADING *DL+LL*	UPLIFT *32 Ft.*
CRACK HEIGHT *1/9 TO 7/9*	FOUNDATION *ISOTROPIC*	FIG. NO. *36*

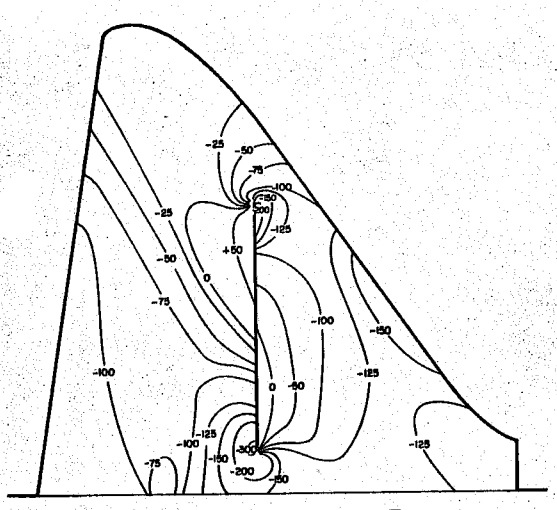

VERTICAL STRESSES – σ_y

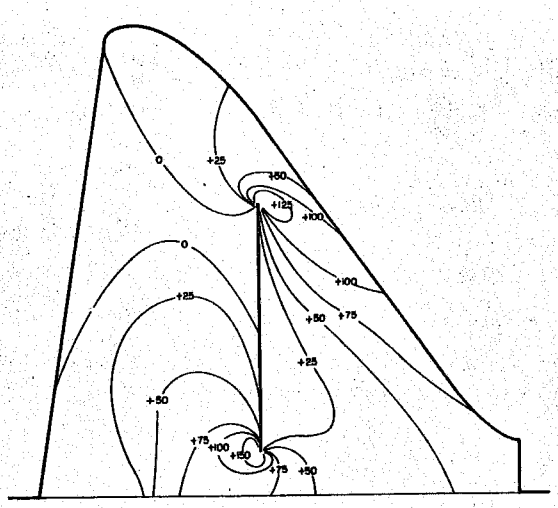

SHEAR STRESSES – σ_{xy}

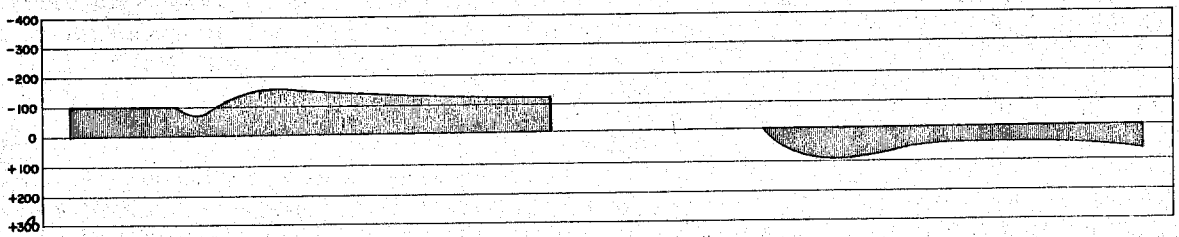

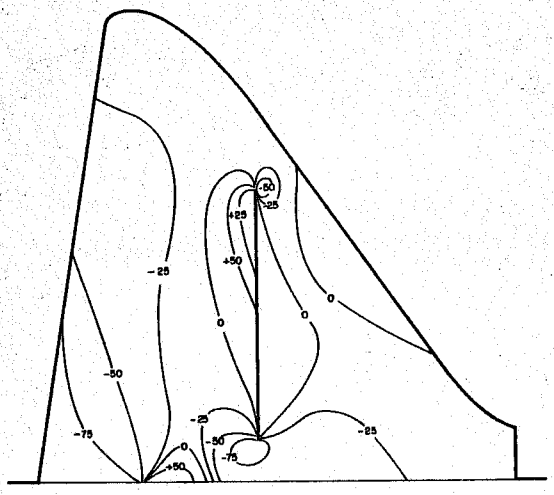

MAJOR STRESSES – σ_1

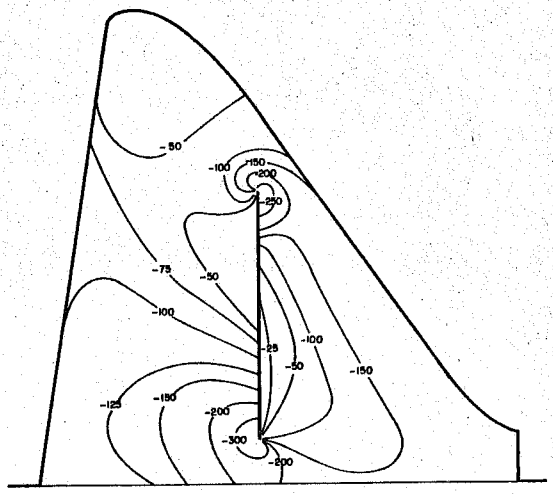

MINOR STRESSES – σ_2

UNIVERSITY OF CALIFORNIA – BERKELEY, CALIFORNIA DIVISION OF STRUCTURAL ENGINEERING AND STRUCTURAL MECHANICS		
STRESS DISTRIBUTION OF NORFORK DAM *STRESS CONTOURS*		
CASE *N 3*	LOADING *DL + LL*	UPLIFT *32 FT.*
CRACK HEIGHT *1/9 TO 7/9*	FOUNDATION *ISOTROPIC*	FIG. NO. *36a*

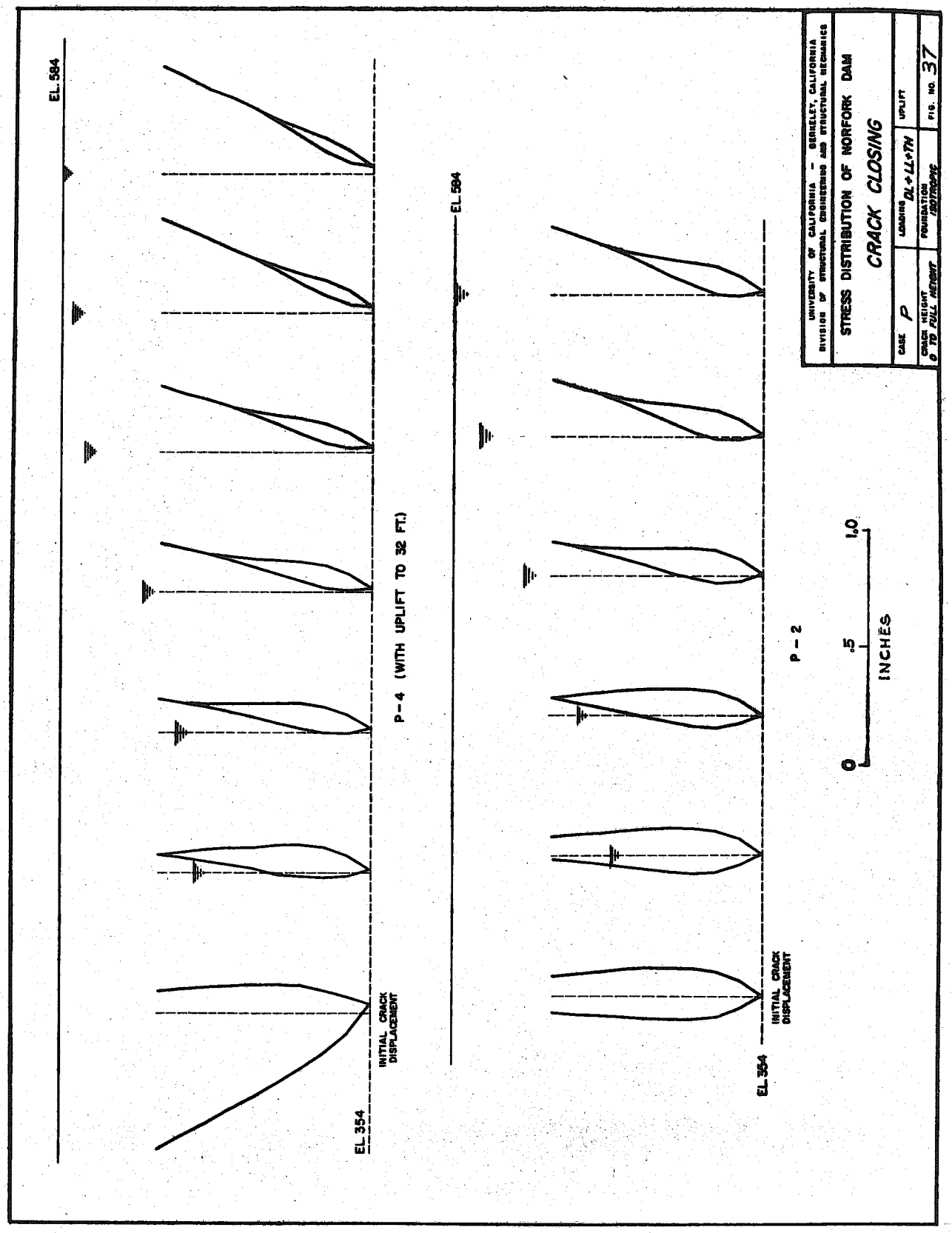
EL 584
EL 354
INITIAL CRACK DISPLACEMENT
P - 4 (WITH UPLIFT TO 32 FT.)
EL 584
EL 354
INITIAL CRACK DISPLACEMENT
P - 2
0
.5
1.0
INCHES
UNIVERSITY OF CALIFORNIA - BERKELEY, CALIFORNIA
DIVISION OF STRUCTURAL ENGINEERING AND STRUCTURAL MECHANICS
STRESS DISTRIBUTION OF NORFORK DAM
CRACK CLOSING
CASE P
LOADING DL+LL+TH
UPLIFT
CRACK HEIGHT @ TO FULL HEIGHT
FOUNDATION ISOTROPIC
FIG. NO. 37

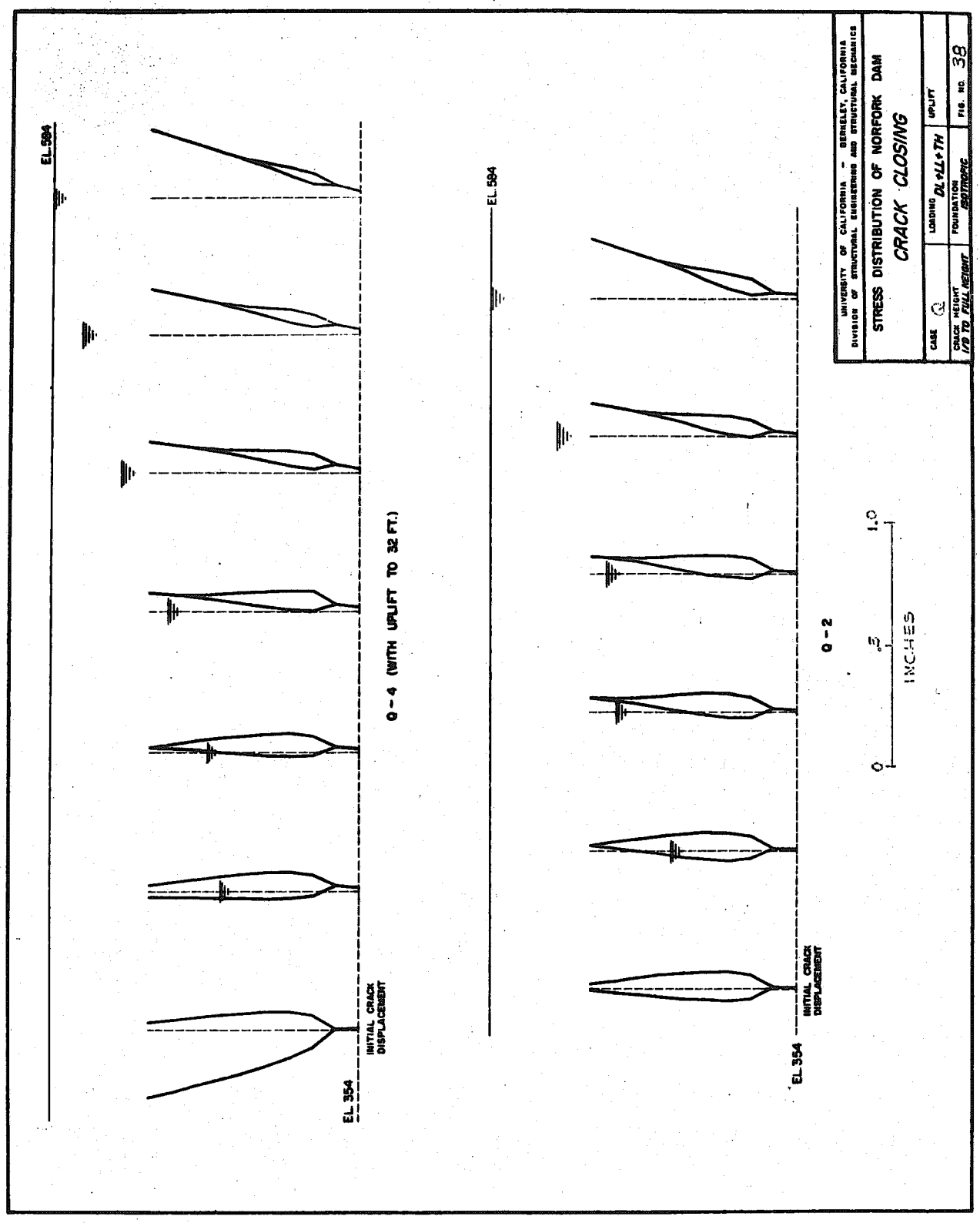
EL. 584
EL. 354
INITIAL CRACK DISPLACEMENT
0 - 4 (WITH UPLIFT TO 32 FT.)
EL. 584
EL. 354
INITIAL CRACK DISPLACEMENT
0 - 2
0
.5
1.0
INCHES
UNIVERSITY OF CALIFORNIA - BERKELEY, CALIFORNIA
DIVISION OF STRUCTURAL ENGINEERING AND STRUCTURAL MECHANICS
STRESS DISTRIBUTION OF NORFORK DAM
CRACK CLOSING
CASE Q
LOADING DL+LL+TH
UPLIFT
CRACK HEIGHT 1/3 TO FULL HEIGHT
FOUNDATION ISOTROPIC
FIG. NO. 38

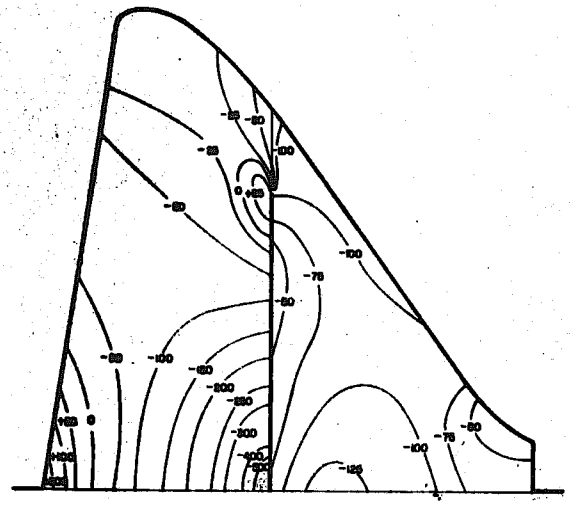

VERTICAL STRESSES – σ_y

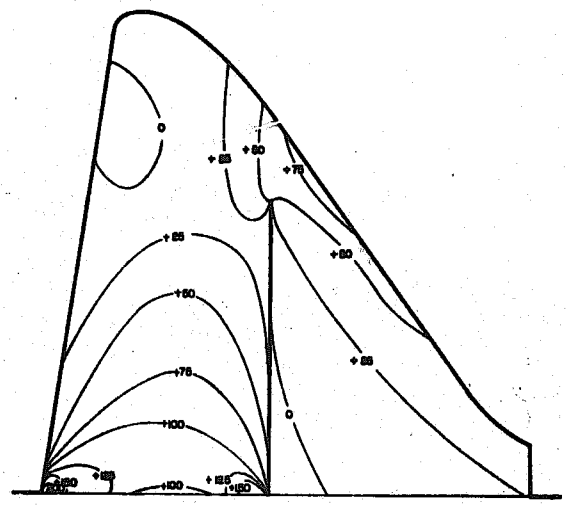

SHEAR STRESSES – σ_{xy}

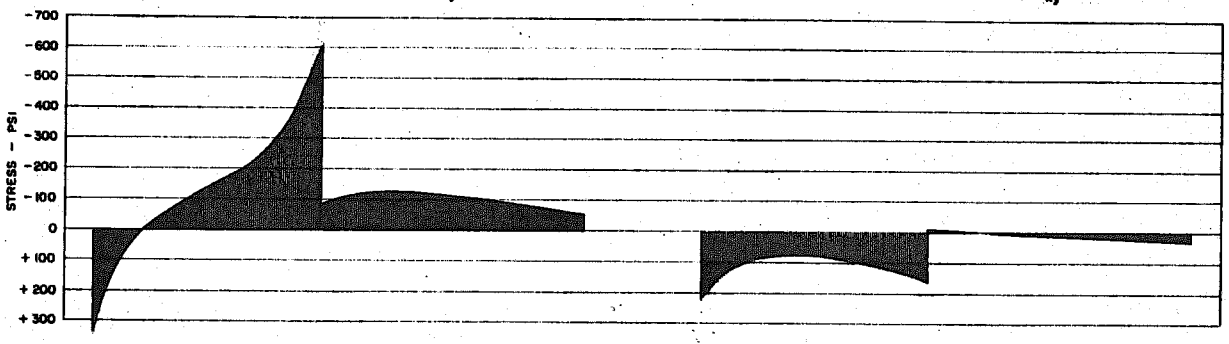

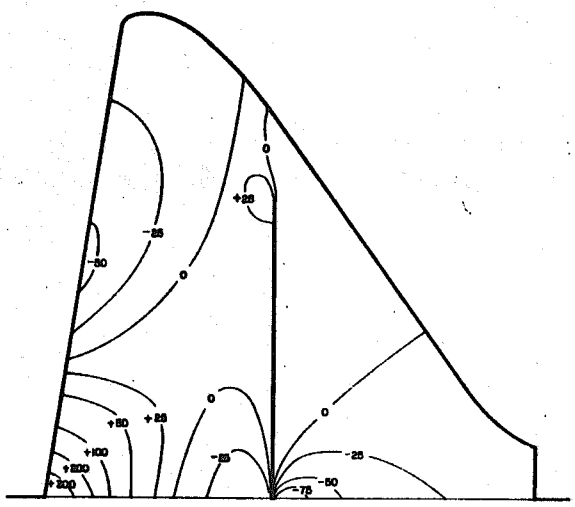

MAJOR STRESSES – σ_1

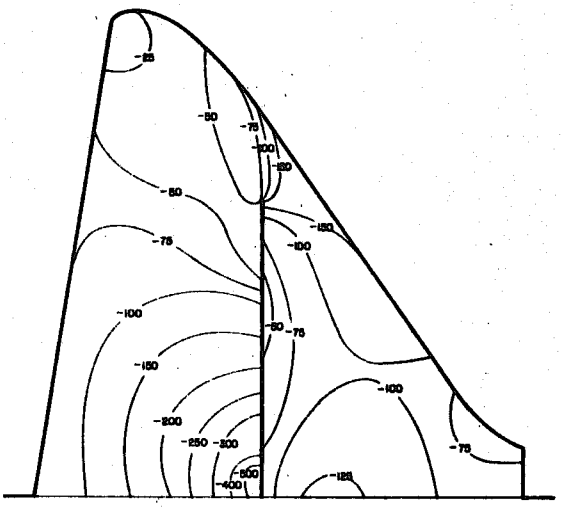

MINOR STRESSES – σ_2

UNIVERSITY OF CALIFORNIA – BERKELEY, CALIFORNIA
DIVISION OF STRUCTURAL ENGINEERING AND STRUCTURAL MECHANICS

STRESS DISTRIBUTION OF NORFORK DAM

STRESS CONTOURS

CASE *P-2*	LOADING *DL+LL*	UPLIFT *None*
CRACK HEIGHT *0 TO FULL HEIGHT*	FOUNDATION *ISOTROPIC*	FIG. NO. *39*

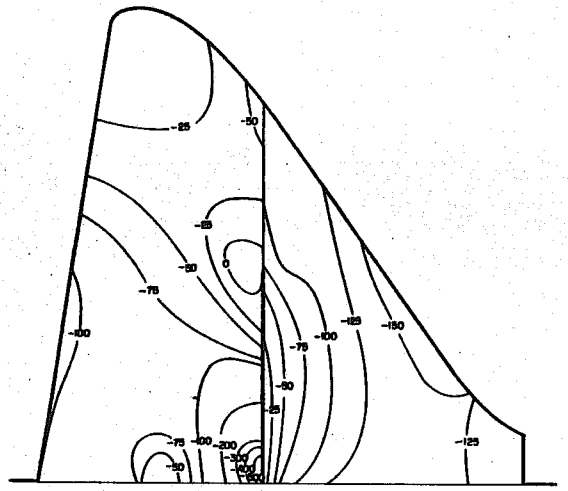

VERTICAL STRESSES – σ_y

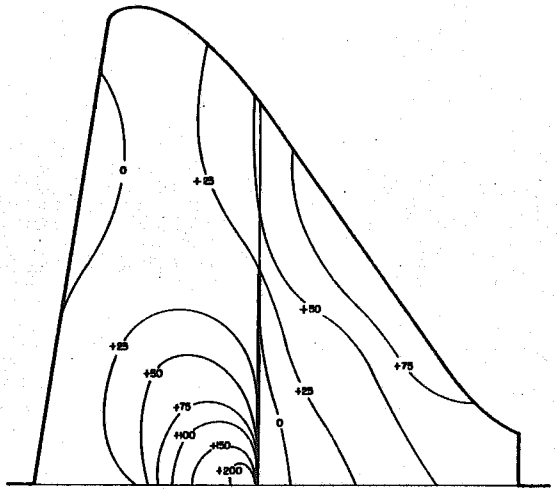

SHEAR STRESSES – σ_{xy}

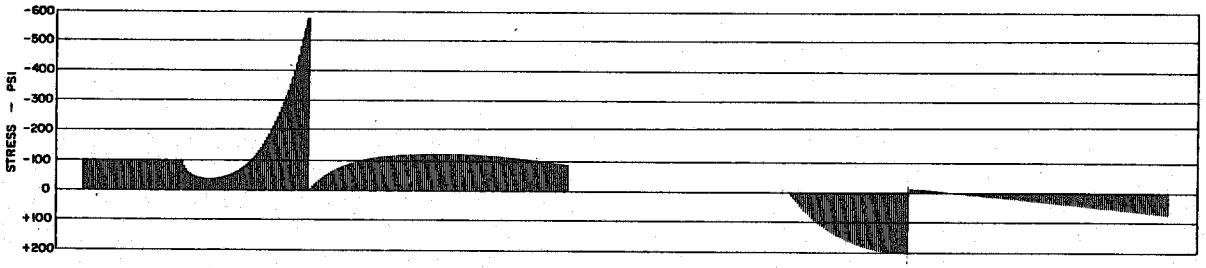

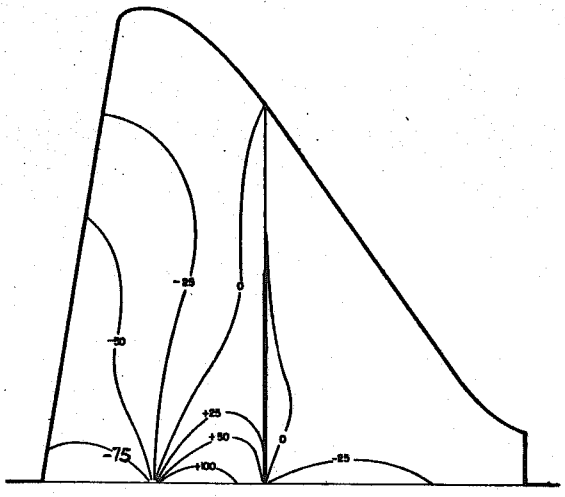

MAJOR STRESSES – σ_1

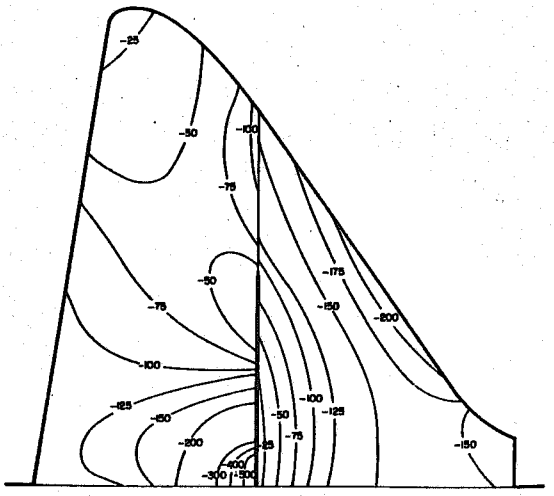

MINOR STRESSES – σ_2

UNIVERSITY OF CALIFORNIA – BERKELEY, CALIFORNIA DIVISION OF STRUCTURAL ENGINEERING AND STRUCTURAL MECHANICS		
STRESS DISTRIBUTION OF NORFORK DAM *STRESS CONTOURS*		
CASE *P-4*	LOADING *DL + LL*	UPLIFT *32 Ft.*
CRACK HEIGHT *0 TO FULL HEIGHT*	FOUNDATION *ISOTROPIC*	FIG. NO. *40*

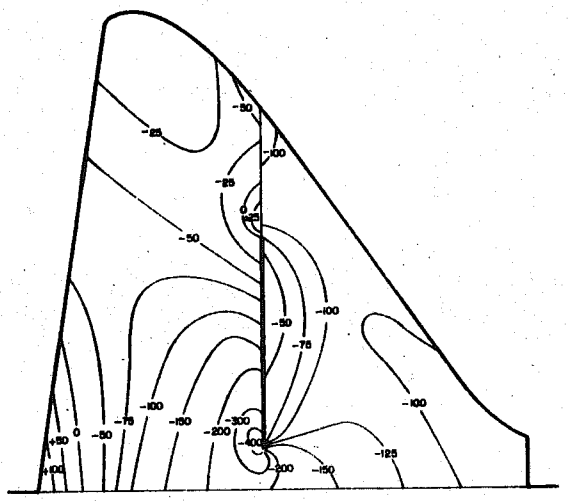

VERTICAL STRESSES – σ_y

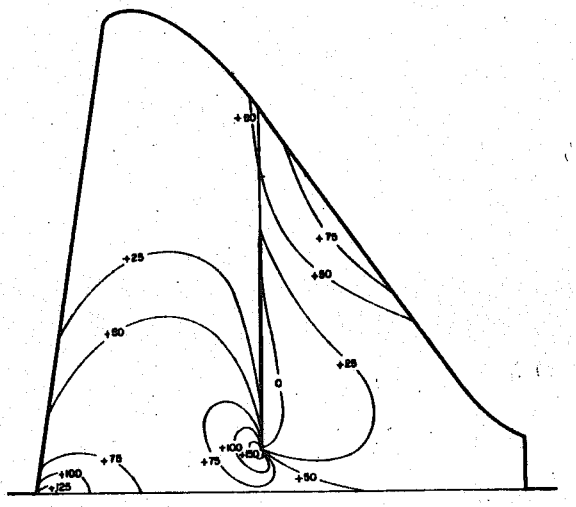

SHEAR STRESSES – σ_{xy}

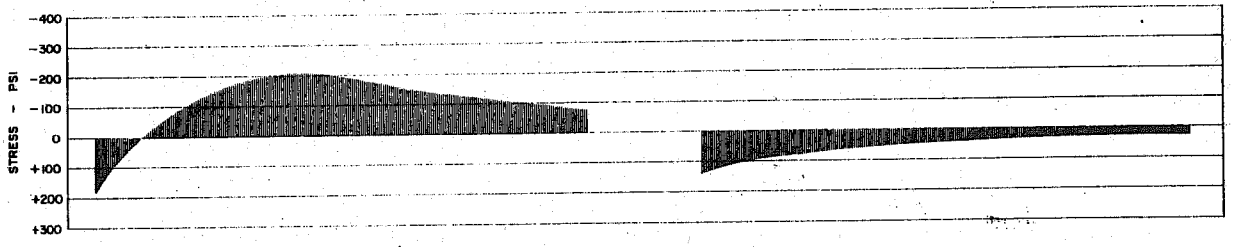

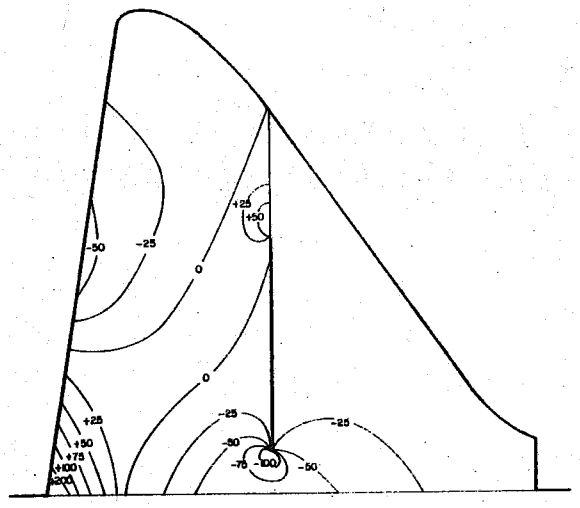

MAJOR STRESSES – σ_1

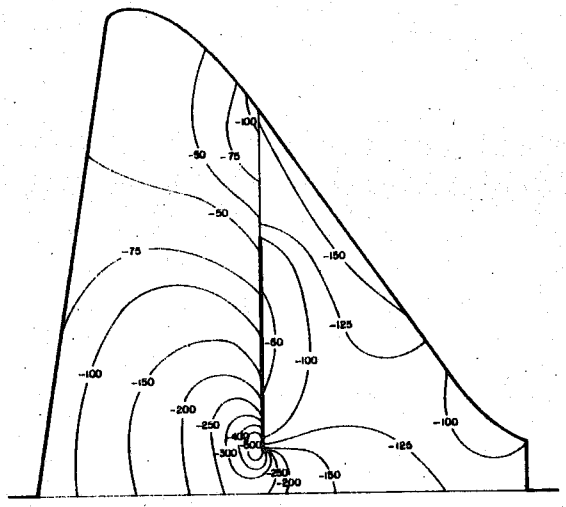

MINOR STRESSES – σ_2

UNIVERSITY OF CALIFORNIA – BERKELEY, CALIFORNIA
DIVISION OF STRUCTURAL ENGINEERING AND STRUCTURAL MECHANICS

STRESS DISTRIBUTION OF NORFORK DAM
STRESS CONTOURS

CASE *O – 2*	LOADING *DL + LL*	UPLIFT *None*
CRACK HEIGHT *1/9 TO FULL HEIGHT*	FOUNDATION *ISOTROPIC*	FIG. NO. *41*

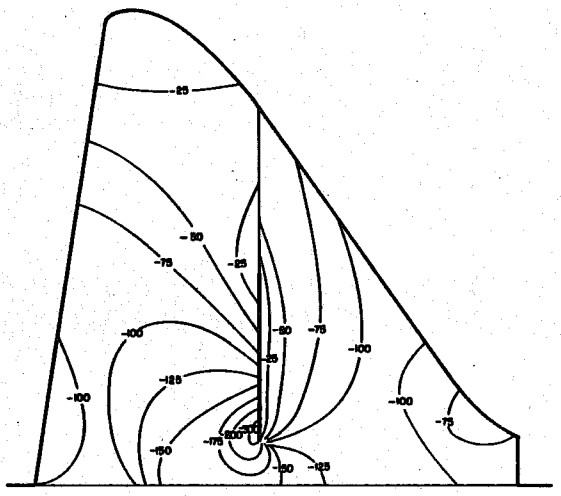

VERTICAL STRESSES - σ_y

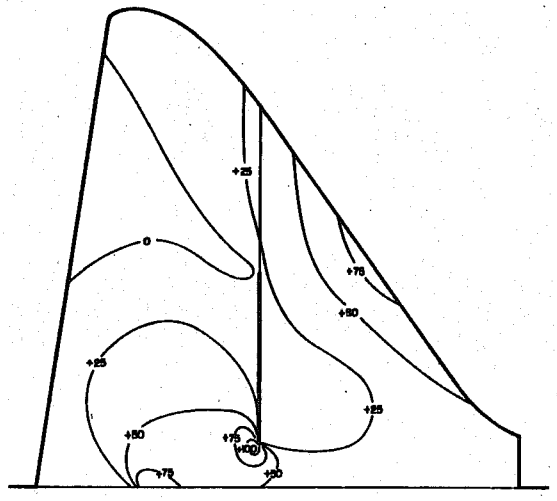

SHEAR STRESSES - σ_{xy}

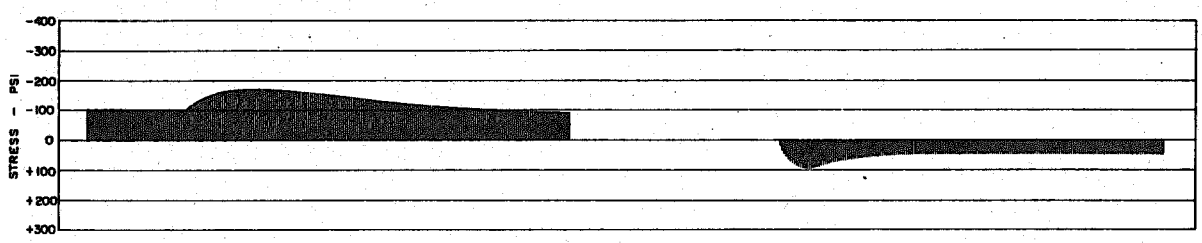

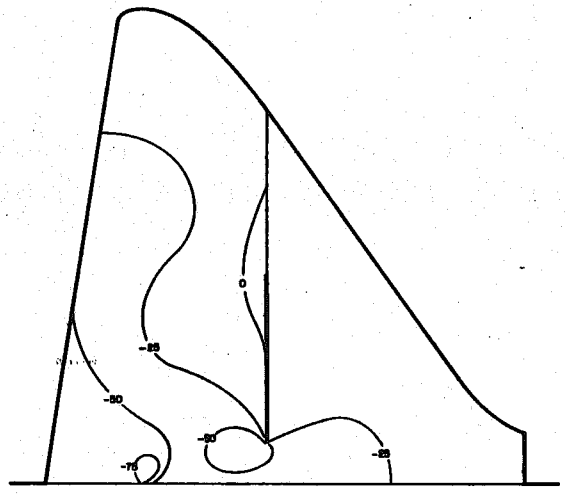

MAJOR STRESSES - σ_1

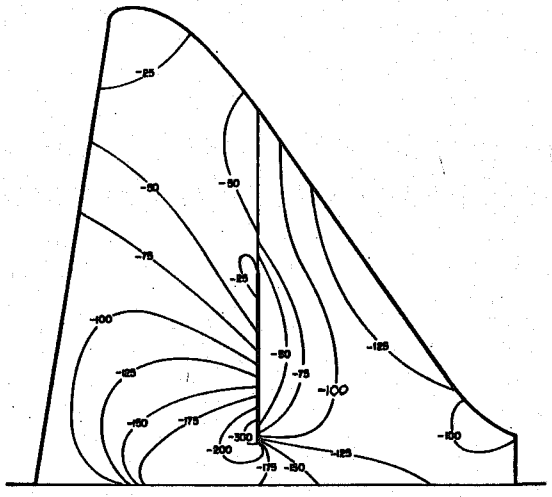

MINOR STRESSES - σ_2

UNIVERSITY OF CALIFORNIA - BERKELEY, CALIFORNIA DIVISION OF STRUCTURAL ENGINEERING AND STRUCTURAL MECHANICS		
STRESS DISTRIBUTION OF NORFORK DAM *STRESS CONTOURS*		
CASE *Q - 4*	LOADING *DL+LL*	UPLIFT *32 Ft.*
CRACK HEIGHT *1/3 TO FULL HEIGHT*	FOUNDATION *ISOTROPIC*	FIG. NO. *42*

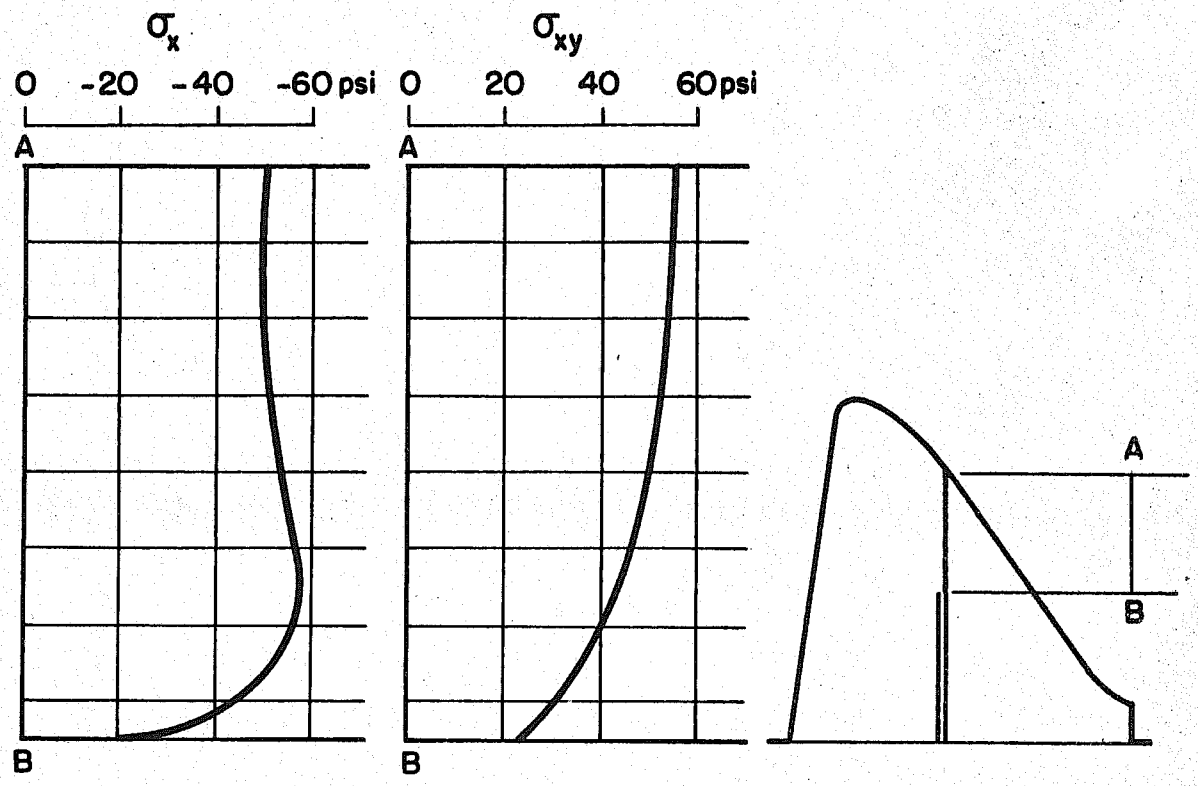

CASE P-4

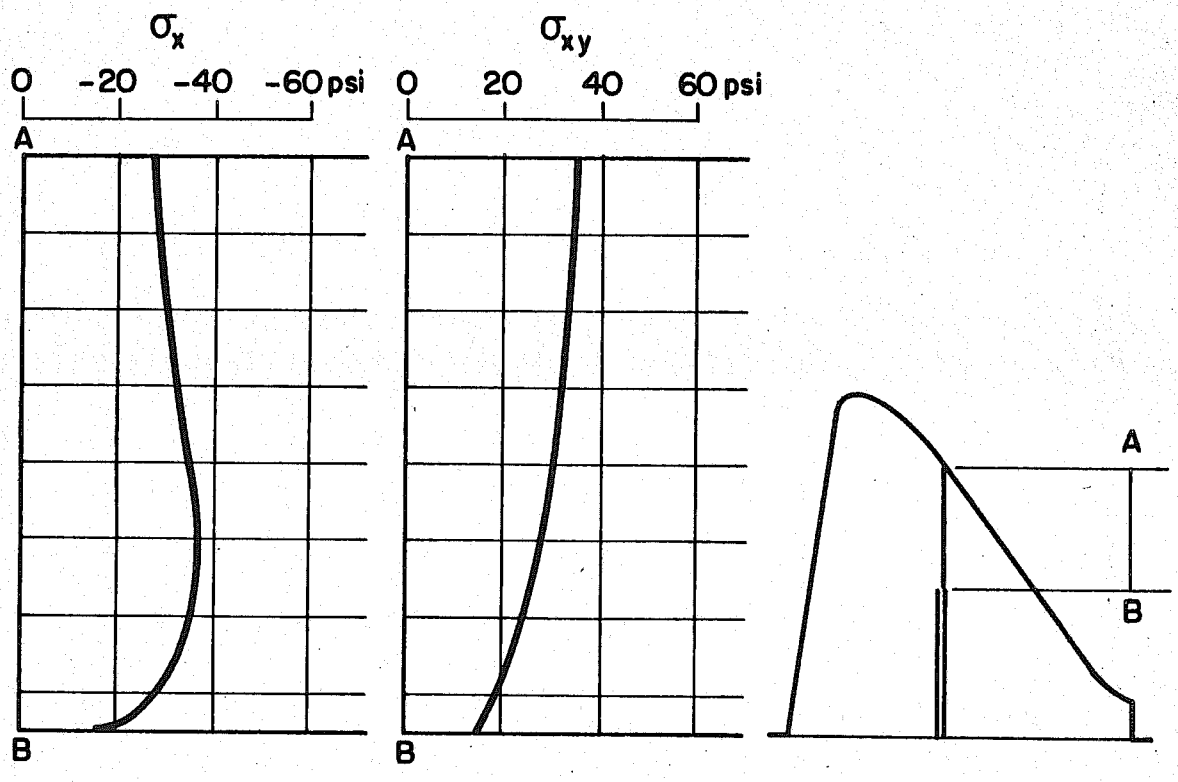

CASE Q-4

FIG. 43

STRESS TRANSFER ACROSS TOP SECTION OF CRACK

and about 30 psi in Case Q-4. In both cases the shear and normal stresses are nearly of equal value thus the required coefficient of friction is about 1. For the low stress values and rough concrete surface involved here this seems quite reasonable and the assumed behavior is believed justified.

CONCLUSIONS

The principal contribution of this supplementary investigation was the development of the incremental analysis procedure which made possible the treatment of crack closing conditions. Although the incremental loading increases the computational effort by a factor of about 10, with the present high speed program and digital computer such problems may be handled easily. Data preparation for an incremental analysis is not much more complicated than for a simple plane stress analysis, and it is expected that this new program may find application in future investigations on other aspects of gravity dam behavior.

The results obtained from the crack closing analysis of the Norfork Dam do not indicate extremely severe stress values, although the maximum stresses are increased somewhat over corresponding cases which do not have the full crack height. In general, redistribution of stress which might result from cracking or creep effects in regions of overstress has a favorable influence on the stress distribution. Deformation adjustments tend to distribute the stress more uniformly to the entire system, and since the structure is very massive, these

average stresses are quite safe. Even the addition of uplift pressures tends to have a favorable effect on the system as a result of eliminating the region of tensile overstress.

TABLE IIIa. CHECK OF BASE FORCE EQUILIBRIUM

Case	$\int dx$	F_y	Error	$\int xy\,dx$	F_x	Error
N-2	3560^k	3650^k	-2.5%	1610	1530	5.2
N-3	3550	3640	-2.5	1500	1460	2.7
P-2	3620	3650	-0.8	1650	1530	7.8
P-4	3650	3650	0	1530	1530	0
Q-2	3580	3650	-1.9	1620	1530	5.9
Q-4	3610	3650	-1.1	1440	1530	-5.9

APPENDIX

STRESS VECTORS FOR ALL CASES

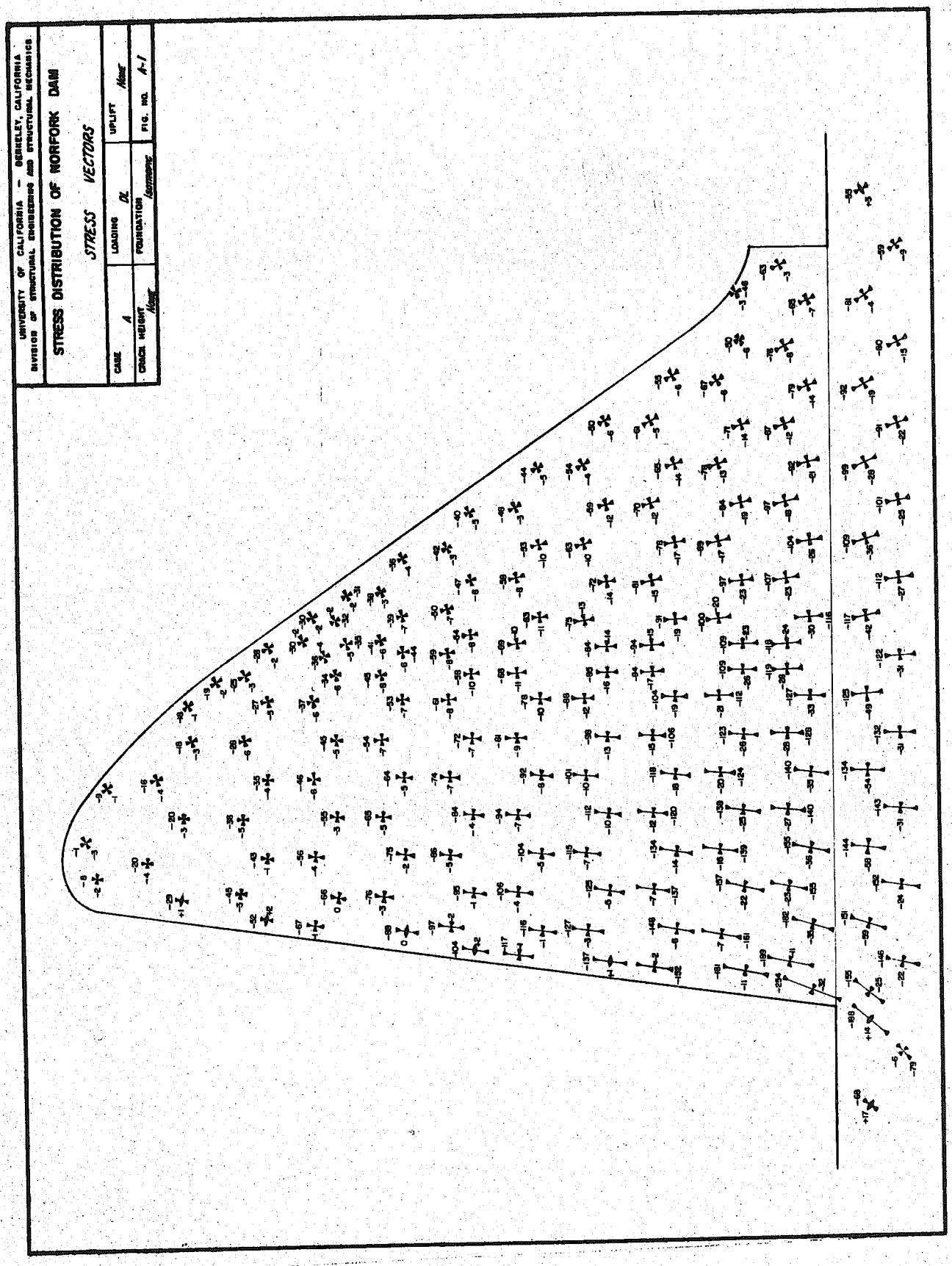
UNIVERSITY OF CALIFORNIA — BERKELEY, CALIFORNIA
DIVISION OF STRUCTURAL ENGINEERING AND STRUCTURAL MECHANICS
STRESS DISTRIBUTION OF NORFORK DAM
STRESS VECTORS
CASE A
LOADING DL
UPLIFT None
CRACK HEIGHT None
FOUNDATION Isotropic
FIG. NO. A-1

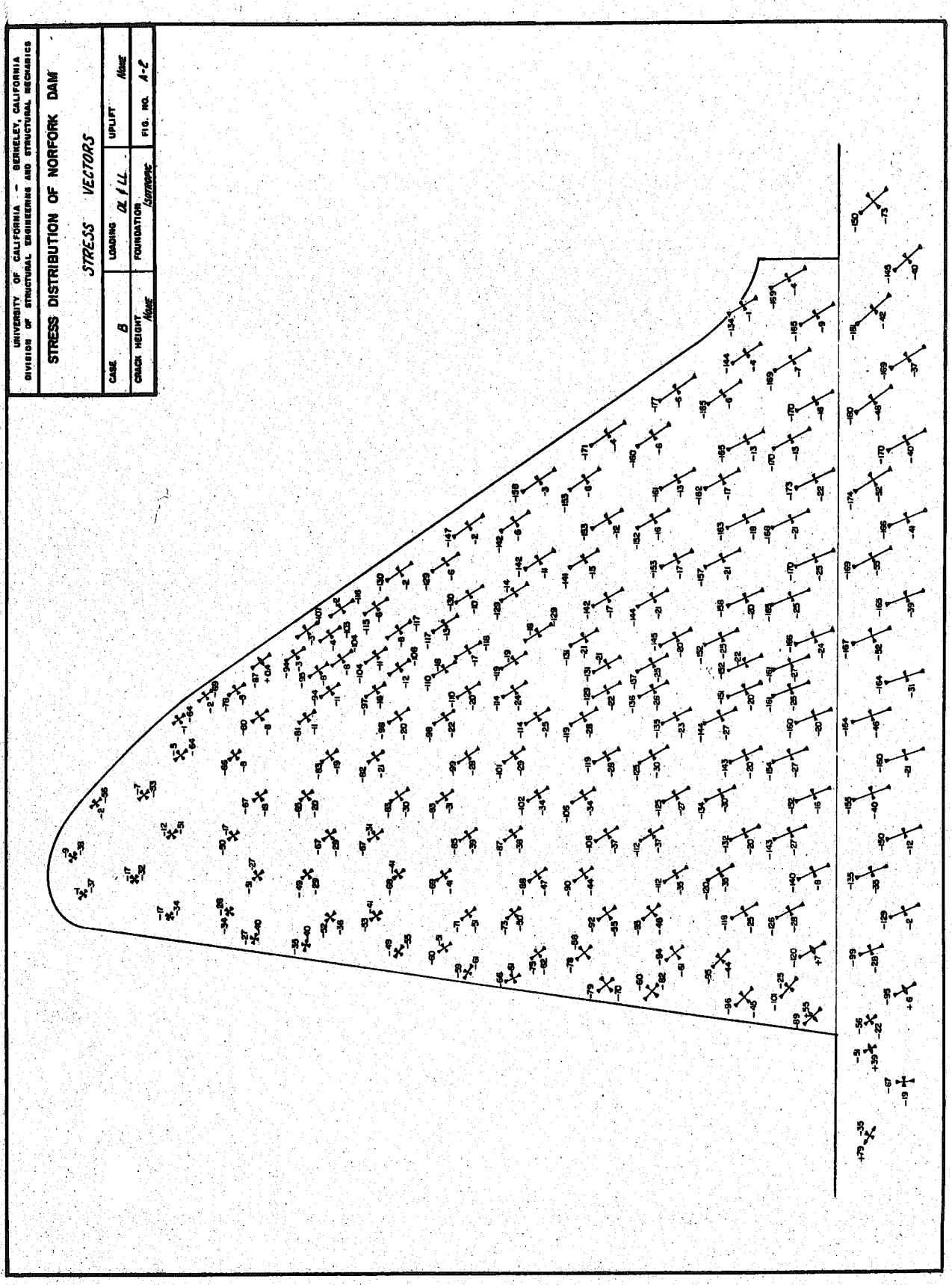
UNIVERSITY OF CALIFORNIA - BERKELEY, CALIFORNIA
DIVISION OF STRUCTURAL ENGINEERING AND STRUCTURAL MECHANICS
STRESS DISTRIBUTION OF NORFORK DAM
STRESS VECTORS
CASE B
LOADING DL + LL
UPLIFT None
CRACK HEIGHT None
FOUNDATION Isotropic
FIG. NO. A-2

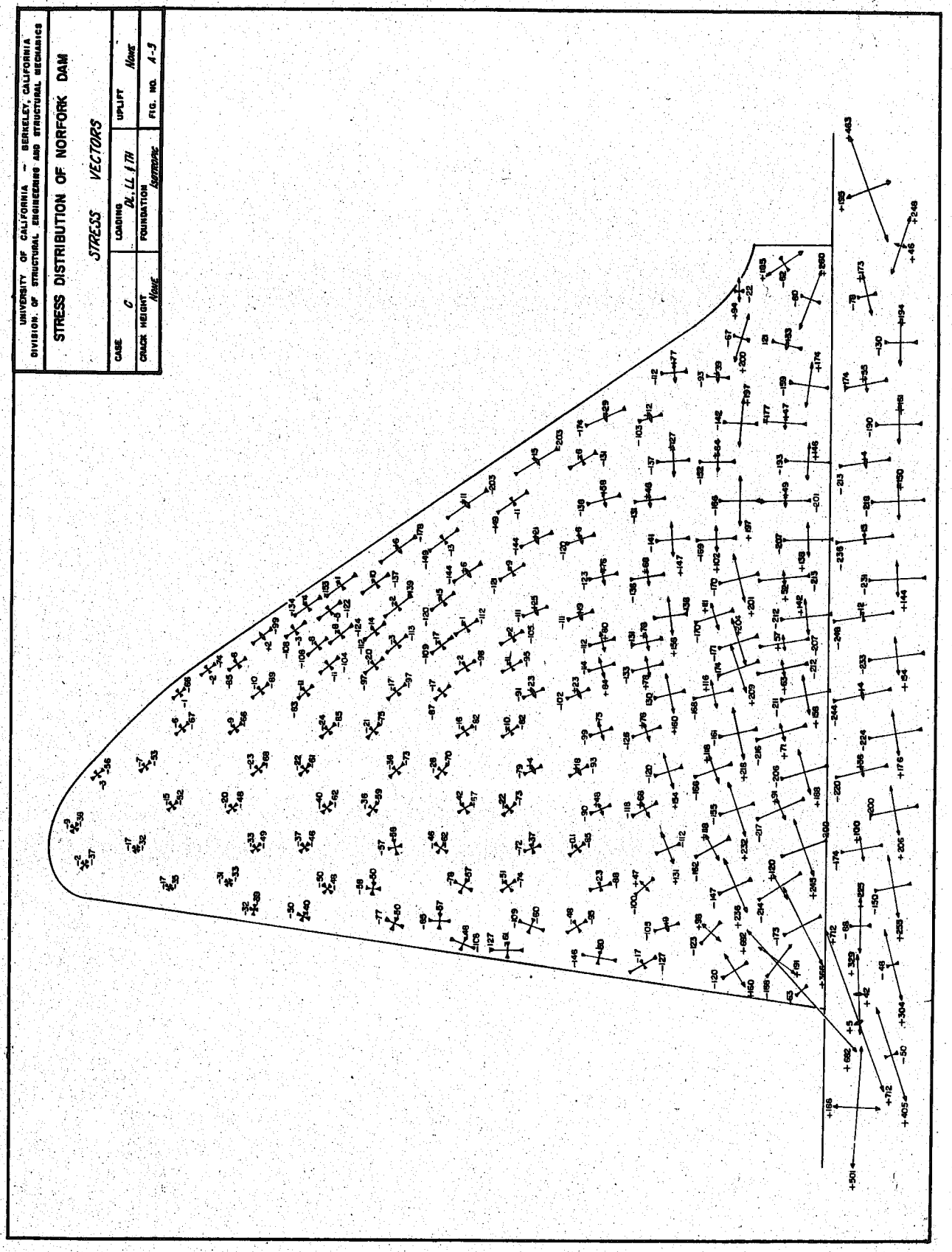
UNIVERSITY OF CALIFORNIA – BERKELEY, CALIFORNIA
DIVISION OF STRUCTURAL ENGINEERING AND STRUCTURAL MECHANICS
STRESS DISTRIBUTION OF NORFORK DAM
STRESS VECTORS
CASE C
LOADING DL. LL 17N
UPLIFT None
CRACK HEIGHT None
FOUNDATION Homogeneous
FIG. NO. A-9

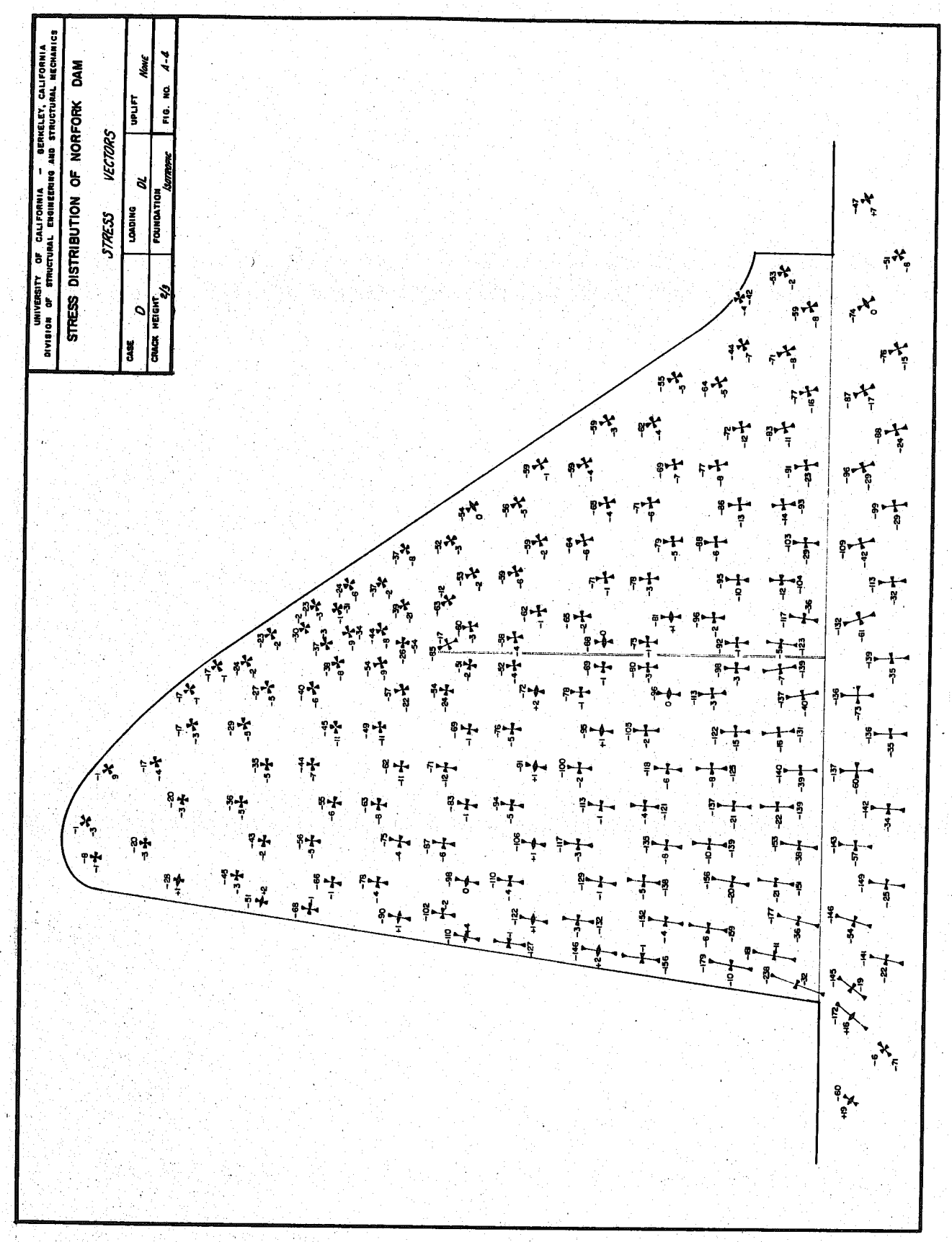
UNIVERSITY OF CALIFORNIA – BERKELEY, CALIFORNIA
DIVISION OF STRUCTURAL ENGINEERING AND STRUCTURAL MECHANICS
STRESS DISTRIBUTION OF NORFORK DAM
STRESS VECTORS
CASE D
LOADING DL
UPLIFT None
CRACK HEIGHT 4/9
FOUNDATION Isotropic
FIG. NO. A-4

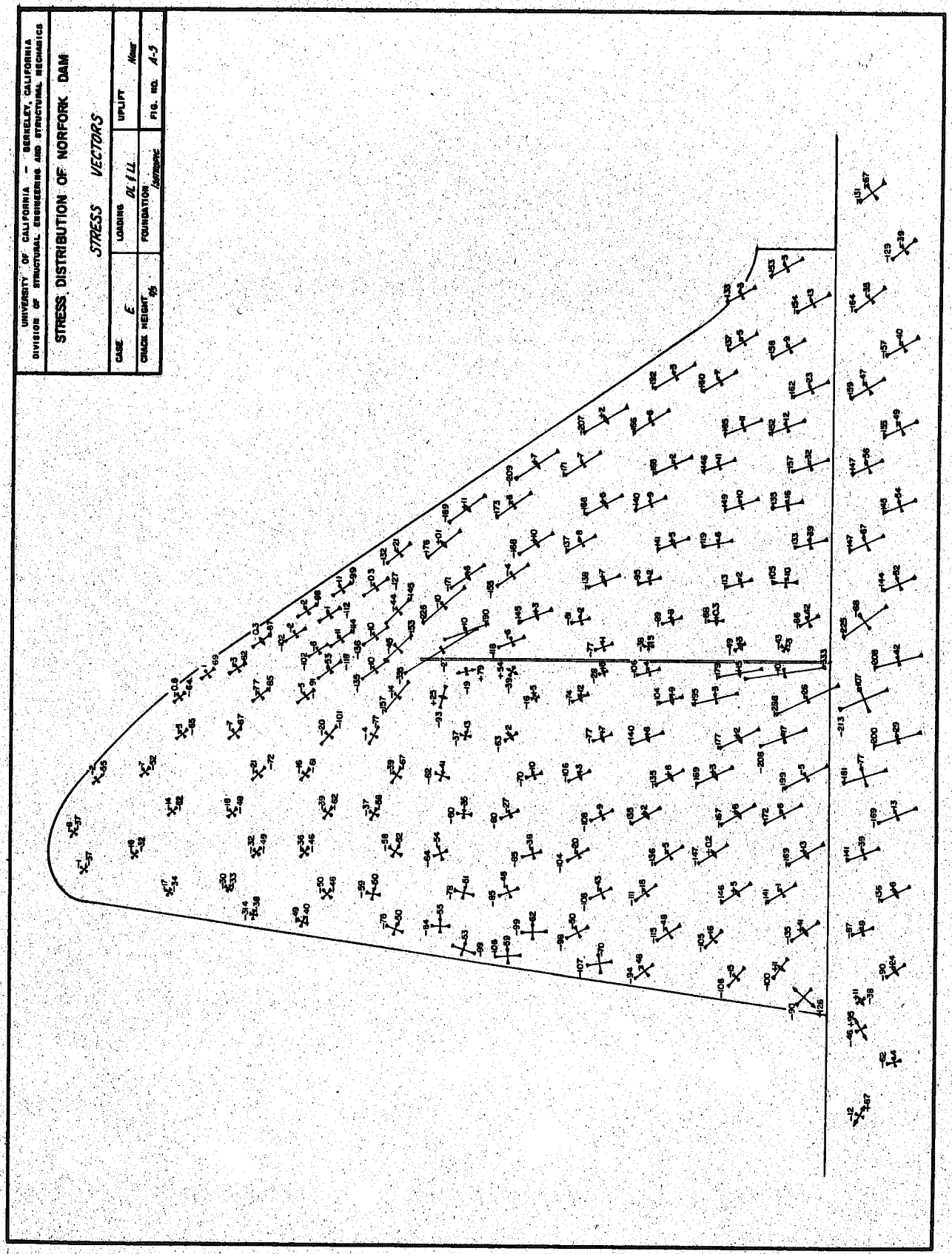
UNIVERSITY OF CALIFORNIA – BERKELEY, CALIFORNIA
DIVISION OF STRUCTURAL ENGINEERING AND STRUCTURAL MECHANICS
STRESS DISTRIBUTION OF NORFORK DAM
STRESS VECTORS
CASE E
LOADING DEAD LOAD
UPLIFT None
CRACK HEIGHT 95
FOUNDATION Isotropic
FIG. NO. A-5

UNIVERSITY OF CALIFORNIA — BERKELEY, CALIFORNIA
DIVISION OF STRUCTURAL ENGINEERING AND STRUCTURAL MECHANICS

STRESS DISTRIBUTION OF NORFORK DAM

STRESS VECTORS

CASE	LOADING	UPLIFT
F	DL & TH	None
CRACK HEIGHT 0%	FOUNDATION Isotropic	FIG. NO. A-6

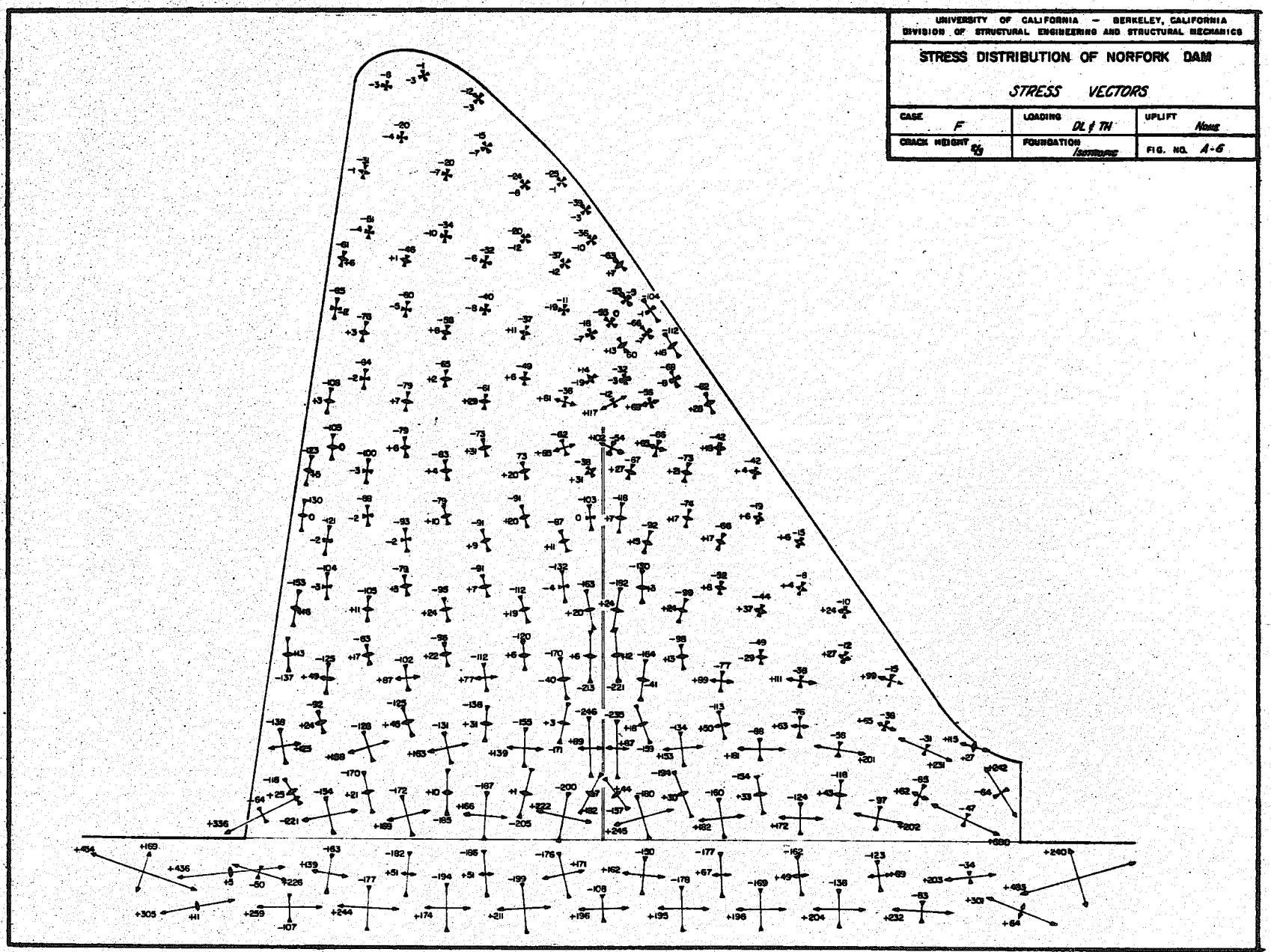

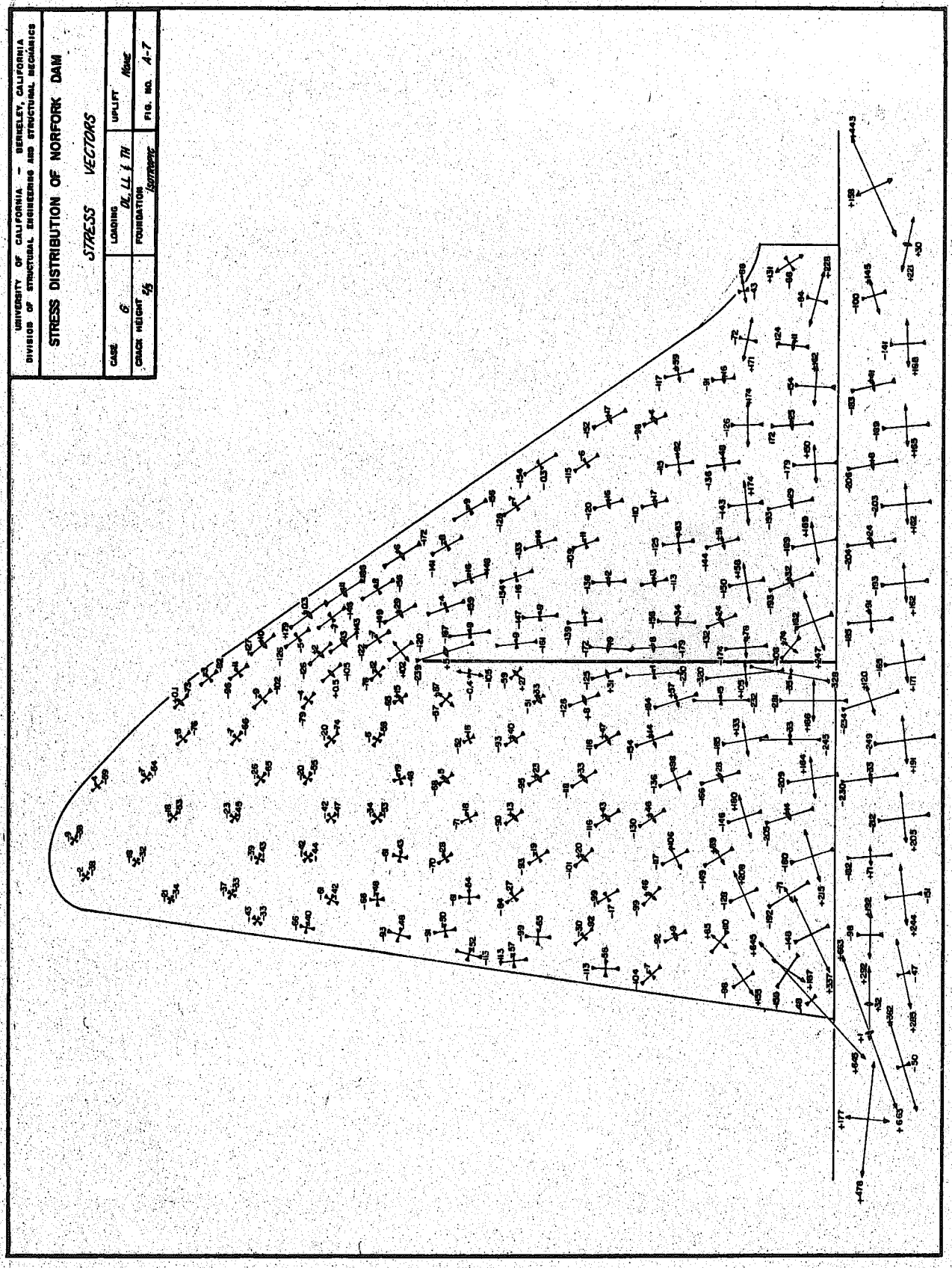
UNIVERSITY OF CALIFORNIA — BERKELEY, CALIFORNIA
DIVISION OF STRUCTURAL ENGINEERING AND STRUCTURAL MECHANICS
STRESS DISTRIBUTION OF NORFORK DAM
STRESS VECTORS
CASE 6
LOADING DL, LL & TH
UPLIFT NONE
CRACK HEIGHT 45
FOUNDATION Isotropic
FIG. NO. 4-7

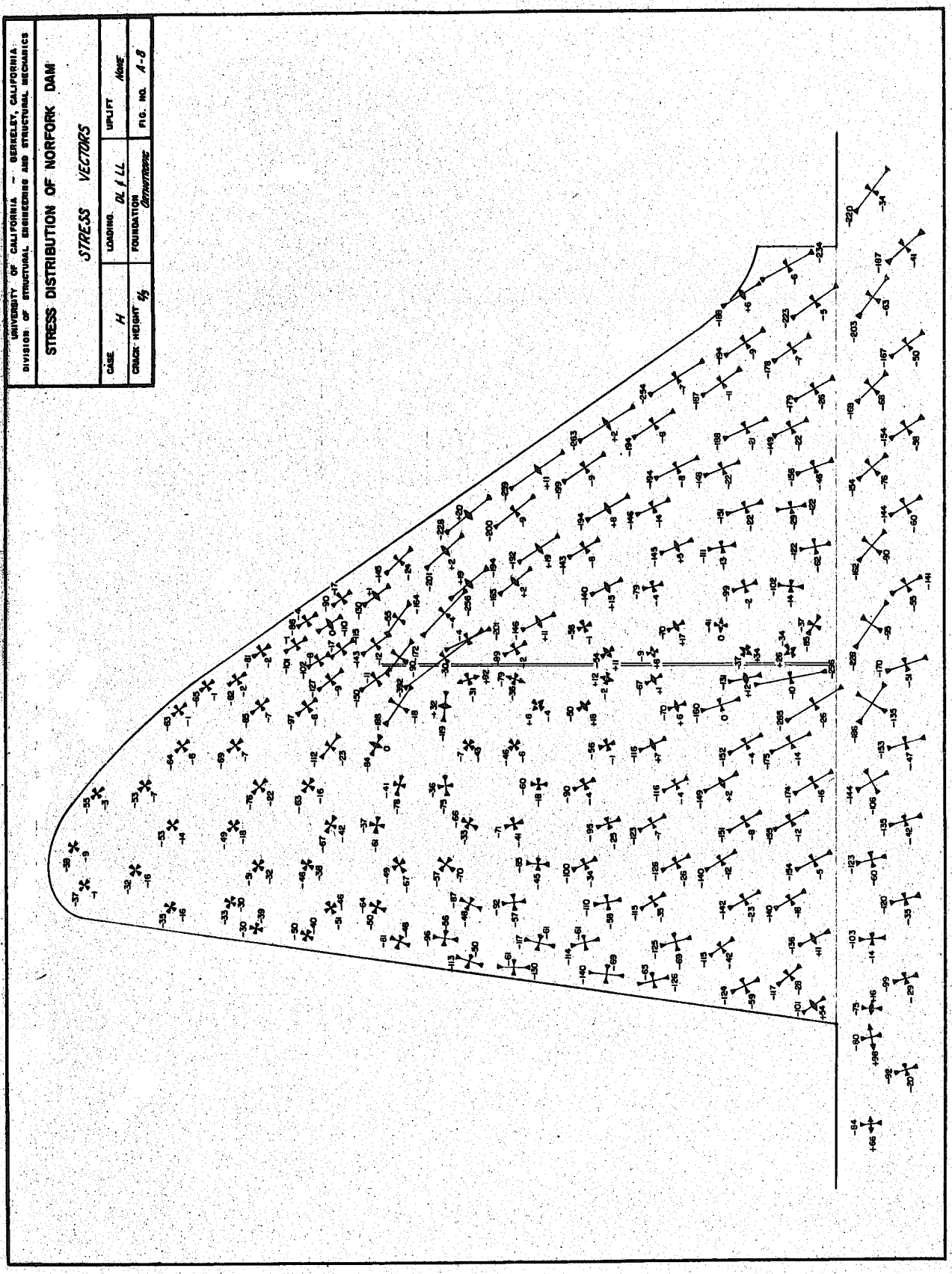
UNIVERSITY OF CALIFORNIA – BERKELEY, CALIFORNIA
DIVISION OF STRUCTURAL ENGINEERING AND STRUCTURAL MECHANICS
STRESS DISTRIBUTION OF NORFORK DAM
STRESS VECTORS
CASE H
LOADING DL & LL
UPLIFT None
CRACK HEIGHT 1/3
FOUNDATION Granite
FIG. NO. A-8

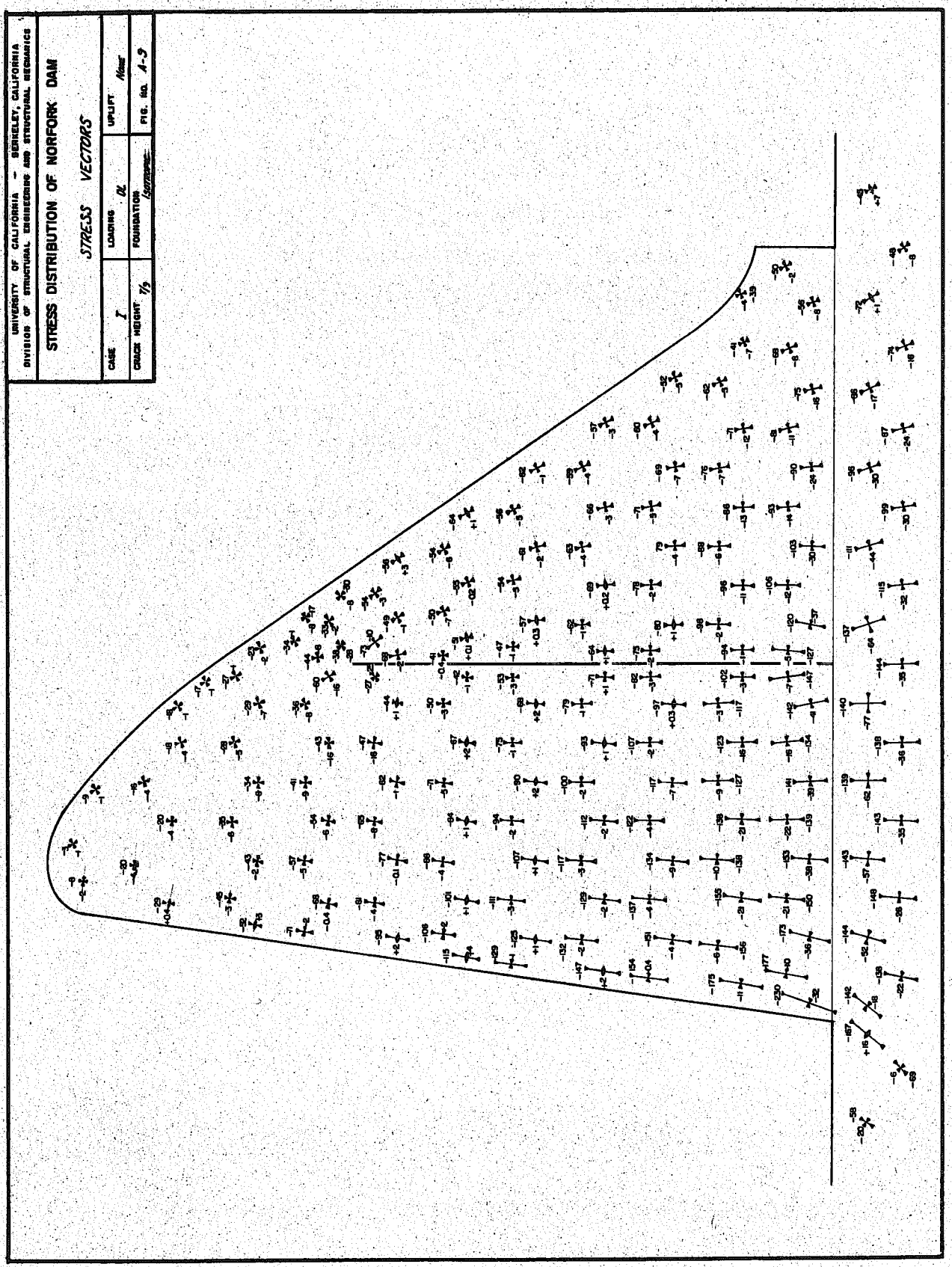
UNIVERSITY OF CALIFORNIA – BERKELEY, CALIFORNIA
DIVISION OF STRUCTURAL ENGINEERING AND STRUCTURAL MECHANICS
STRESS DISTRIBUTION OF NORFORK DAM
STRESS VECTORS
CASE 1
LOADING DL
UPLIFT Mean
CRACK HEIGHT 1/3
FOUNDATION Isotropic
FIG. NO. 4-9

UNIVERSITY OF CALIFORNIA — BERKELEY, CALIFORNIA
DIVISION OF STRUCTURAL ENGINEERING AND STRUCTURAL MECHANICS

STRESS DISTRIBUTION OF NORFORK DAM

STRESS VECTORS

CASE	LOADING	UPLIFT
J	DL & LL	None
CRACK HEIGHT 1/9	FOUNDATION Isotropic	FIG. NO. A-10

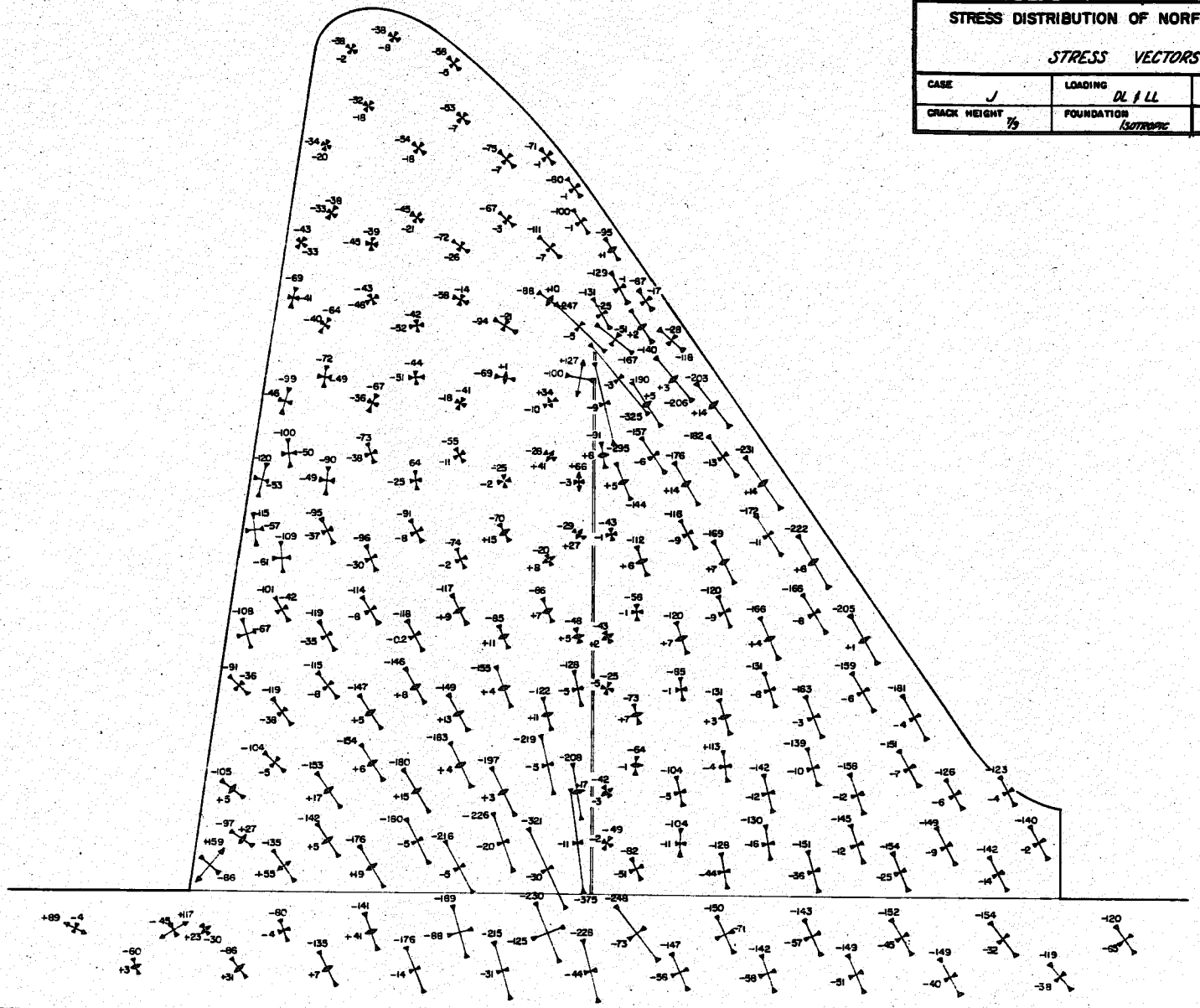

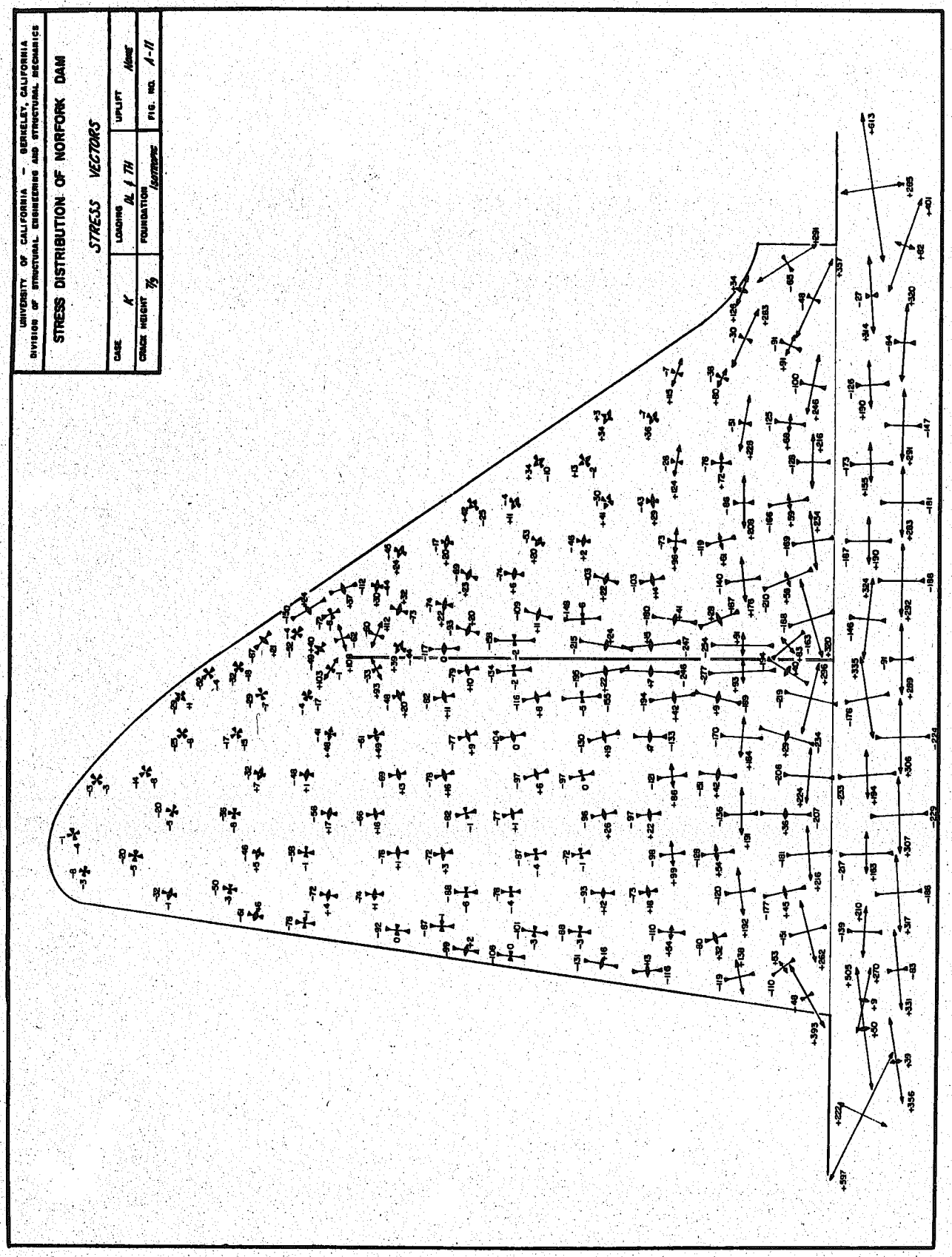
UNIVERSITY OF CALIFORNIA — BERKELEY, CALIFORNIA
DIVISION OF STRUCTURAL ENGINEERING AND STRUCTURAL MECHANICS
STRESS DISTRIBUTION OF NORFORK DAM
STRESS VECTORS
CASE K
LOADING DL + TH
UPLIFT None
CRACK HEIGHT 75
FOUNDATION Isotropic
FIG. NO. A-11

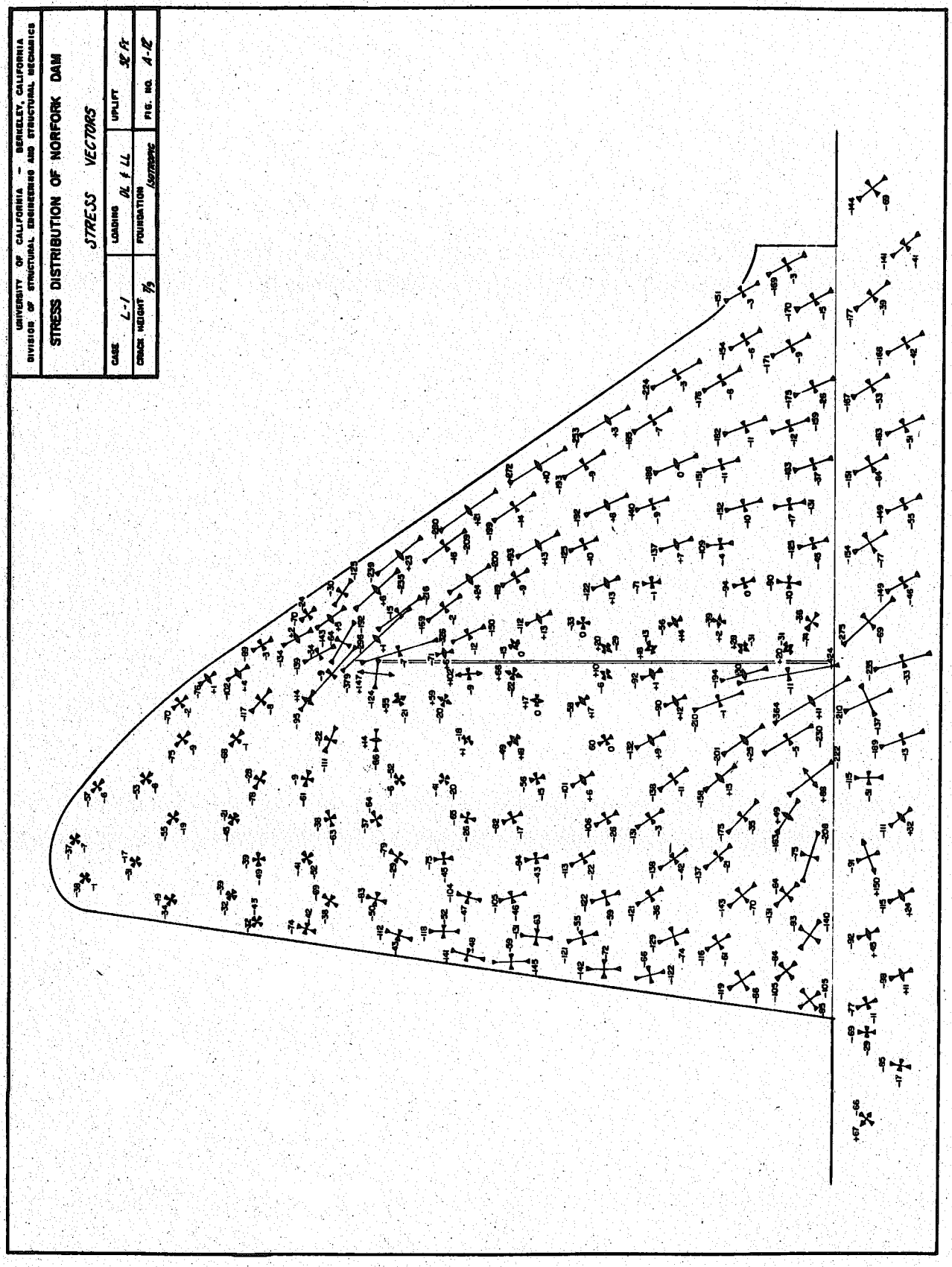
UNIVERSITY OF CALIFORNIA - BERKELEY, CALIFORNIA
DIVISION OF STRUCTURAL ENGINEERING AND STRUCTURAL MECHANICS
STRESS DISTRIBUTION OF NORFORK DAM
STRESS VECTORS
CASE L-1
LOADING DL + LL
UPLIFT 30 ft
CRACK HEIGHT 1/3
FOUNDATION HOMOGENEOUS
FIG. NO. A-12

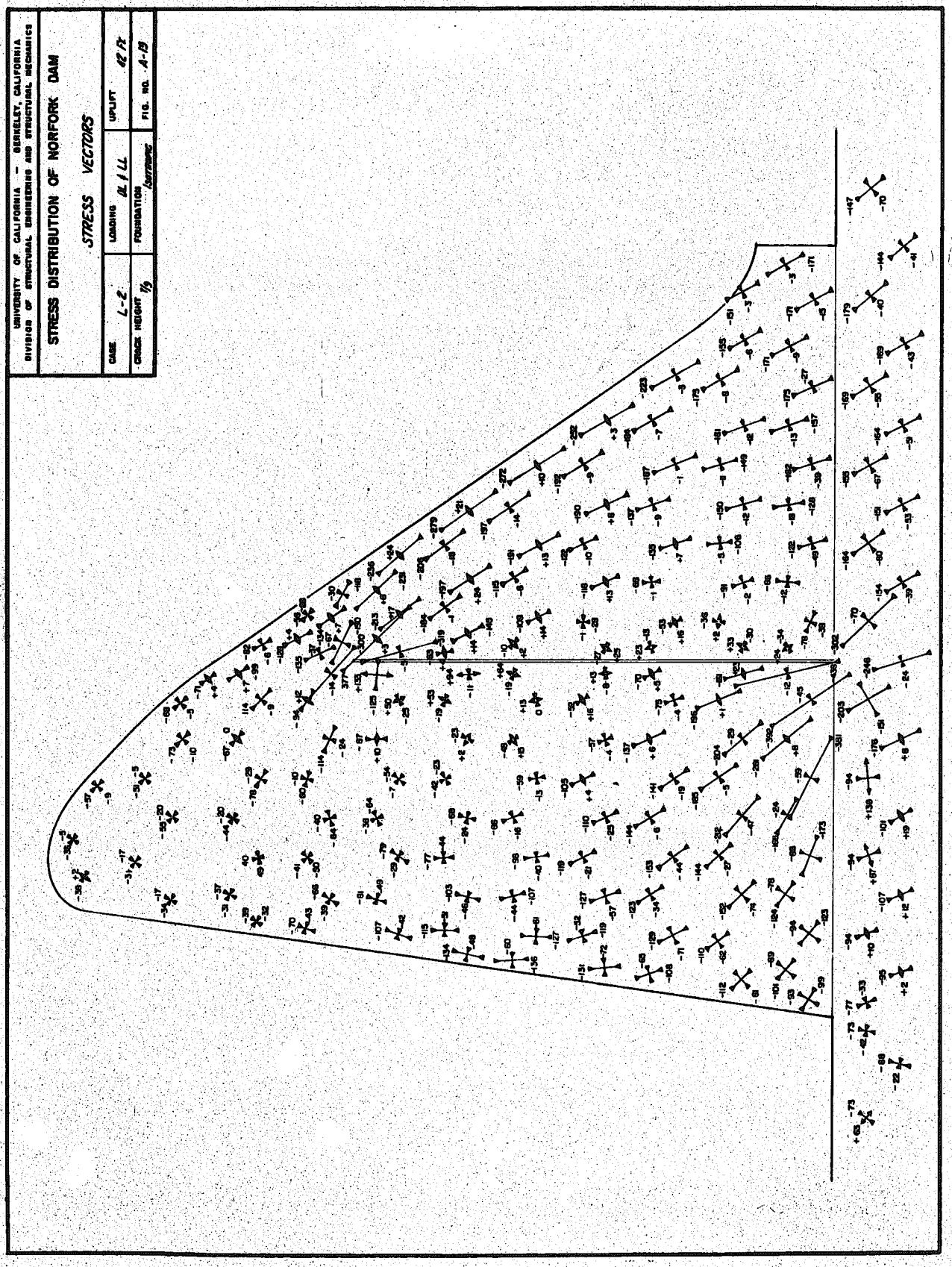
UNIVERSITY OF CALIFORNIA – BERKELEY, CALIFORNIA
DIVISION OF STRUCTURAL ENGINEERING AND STRUCTURAL MECHANICS
STRESS DISTRIBUTION OF NORFORK DAM
STRESS VECTORS
CASE L-2
LOADING ALL
UPLIFT 42 ft
CRACK HEIGHT 1/3
FOUNDATION Sandstone
FIG. NO. A-13

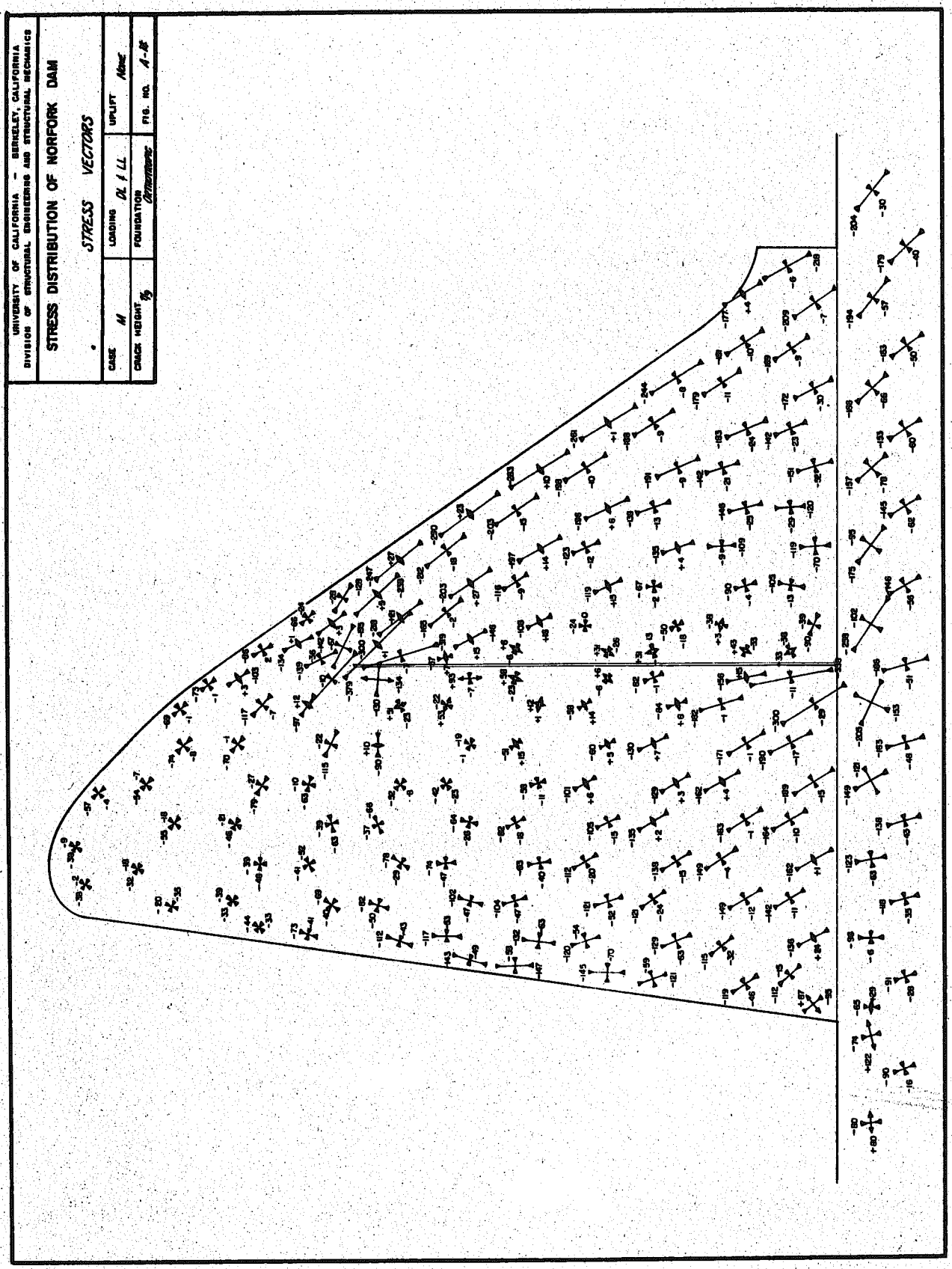
UNIVERSITY OF CALIFORNIA - BERKELEY, CALIFORNIA
DIVISION OF STRUCTURAL ENGINEERING AND STRUCTURAL MECHANICS
STRESS DISTRIBUTION OF NORFORK DAM
STRESS VECTORS
CASE M
LOADING DL + LL
UPLIFT None
CRACK HEIGHT 0%
FOUNDATION Homogeneous
FIG. NO. A-8

UNIVERSITY OF CALIFORNIA – BERKELEY, CALIFORNIA
DIVISION OF STRUCTURAL ENGINEERING AND STRUCTURAL MECHANICS

STRESS DISTRIBUTION OF NORFORK DAM

STRESS VECTORS

CASE	LOADING	UPLIFT
N	DL & LL	92 Ft
CRACK HEIGHT 5/9	FOUNDATION ISOTROPIC	FIG. NO. A-13

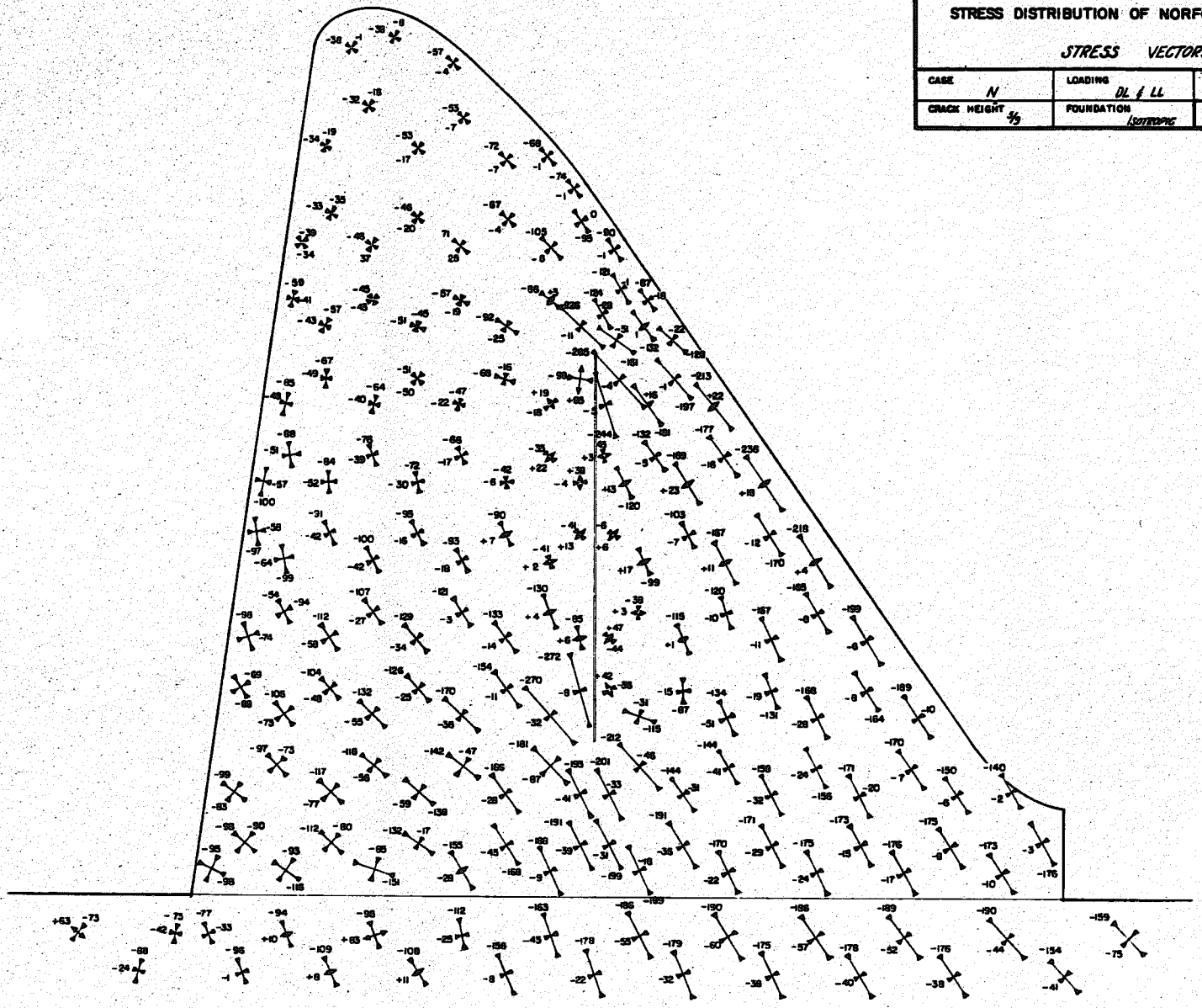

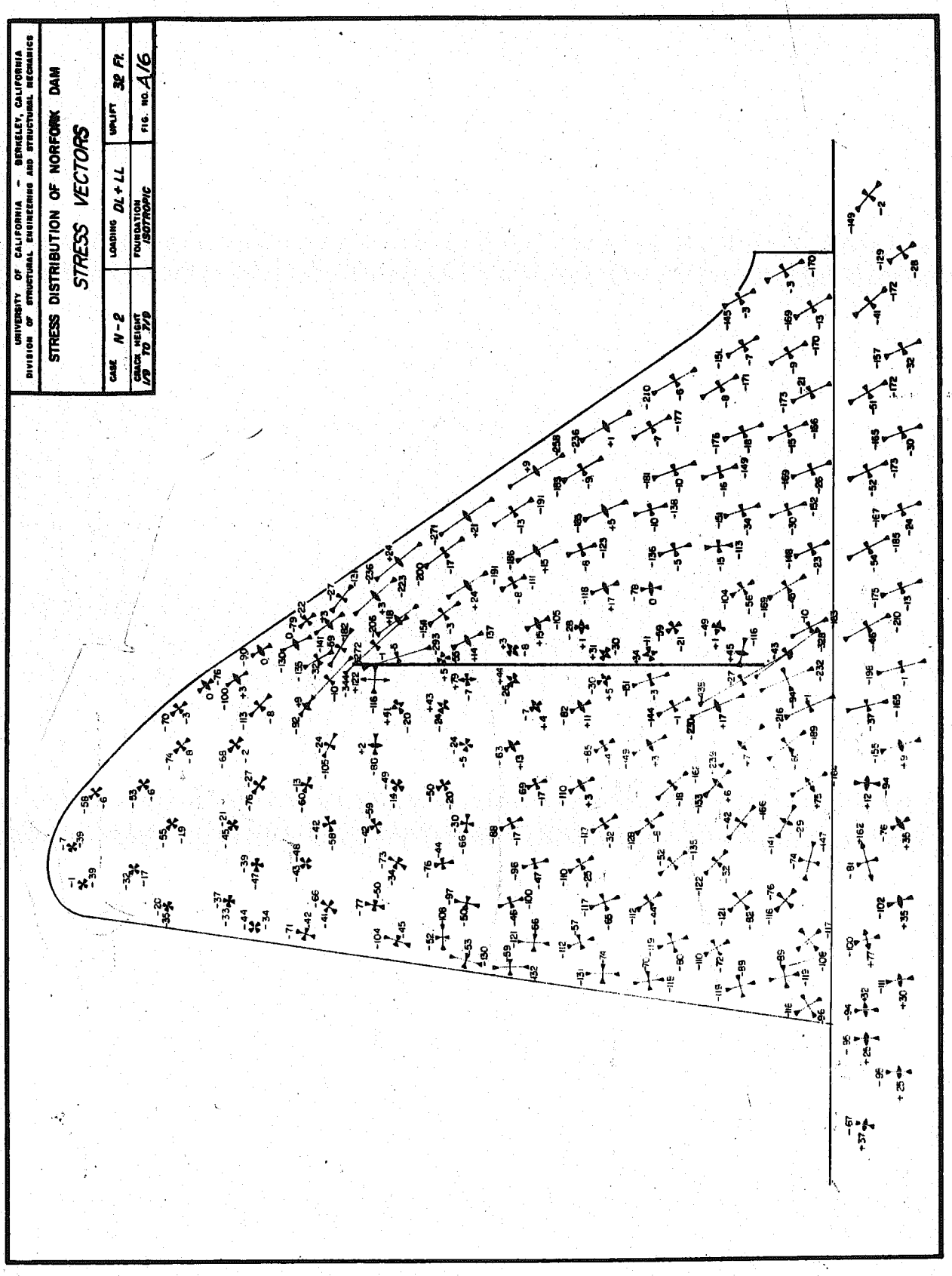
UNIVERSITY OF CALIFORNIA - BERKELEY, CALIFORNIA
DIVISION OF STRUCTURAL ENGINEERING AND STRUCTURAL MECHANICS
STRESS DISTRIBUTION OF NORFORK DAM
STRESS VECTORS
CASE N-2
LOADING DL+LL
UPLIFT 32 FT.
CRACK HEIGHT 1/8 TO 3/8
FOUNDATION ISOTROPIC
FIG. NO. A16

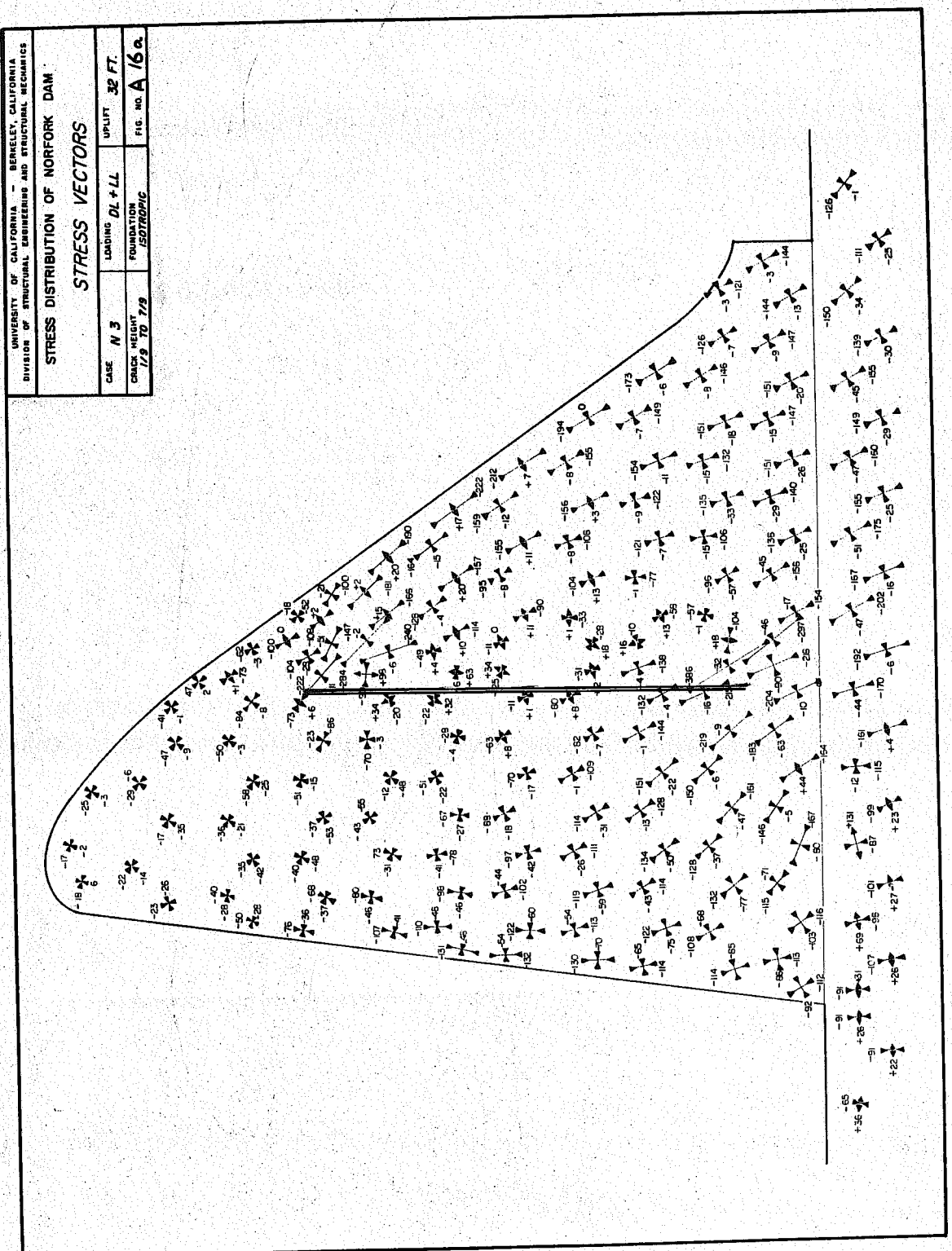
UNIVERSITY OF CALIFORNIA – BERKELEY, CALIFORNIA
DIVISION OF STRUCTURAL ENGINEERING AND STRUCTURAL MECHANICS
STRESS DISTRIBUTION OF NORFORK DAM
STRESS VECTORS
CASE N 3
LOADING DL + LL
UPLIFT 32 FT.
CRACK HEIGHT 1/3 TO 1/4
FOUNDATION ISOTROPIC
FIG. NO. A 16a

UNIVERSITY OF CALIFORNIA — BERKELEY, CALIFORNIA
DIVISION OF STRUCTURAL ENGINEERING AND STRUCTURAL MECHANICS

STRESS DISTRIBUTION OF NORFORK DAM

STRESS VECTORS

CASE P-1	LOADING DL + TH	UPLIFT None
CRACK HEIGHT 0 TO FULL HEIGHT	FOUNDATION ISOTROPIC	FIG. NO. A17

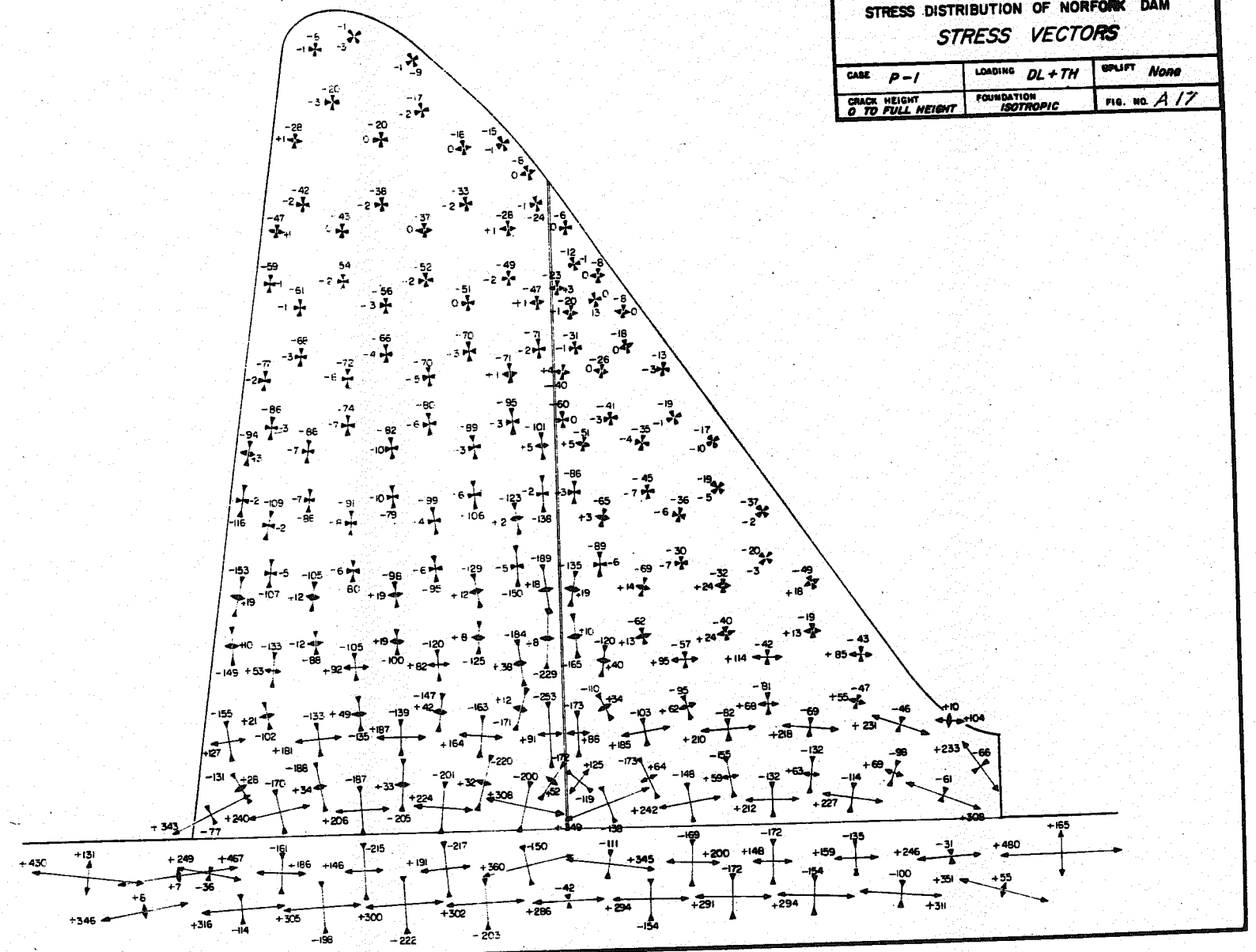

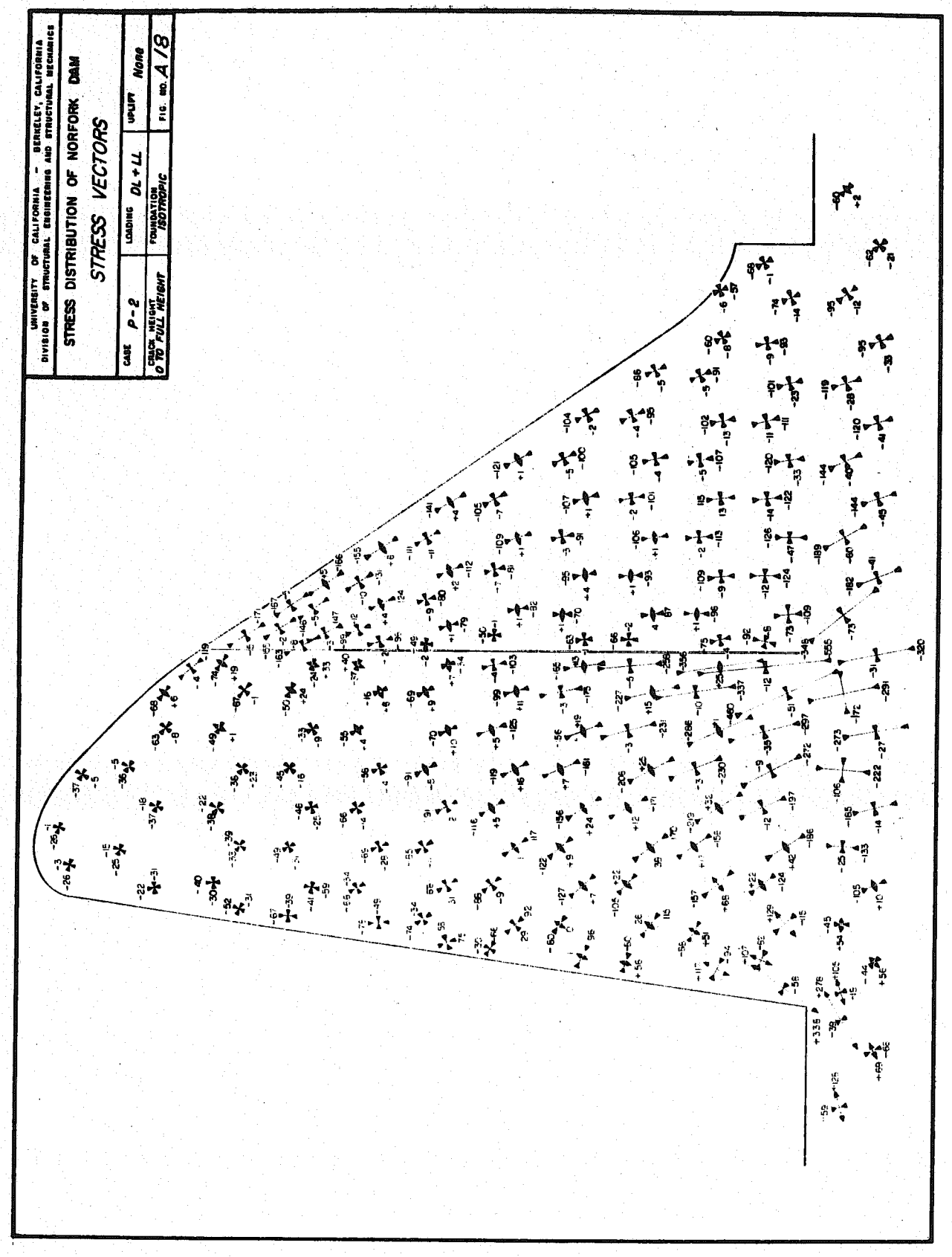
UNIVERSITY OF CALIFORNIA – BERKELEY, CALIFORNIA
DIVISION OF STRUCTURAL ENGINEERING AND STRUCTURAL MECHANICS
STRESS DISTRIBUTION OF NORFORK DAM
STRESS VECTORS
CASE P-2
LOADING DL+LL
UPLIFT NONE
CRACK HEIGHT 0 TO FULL HEIGHT
FOUNDATION ISOTROPIC
FIG. NO. A18

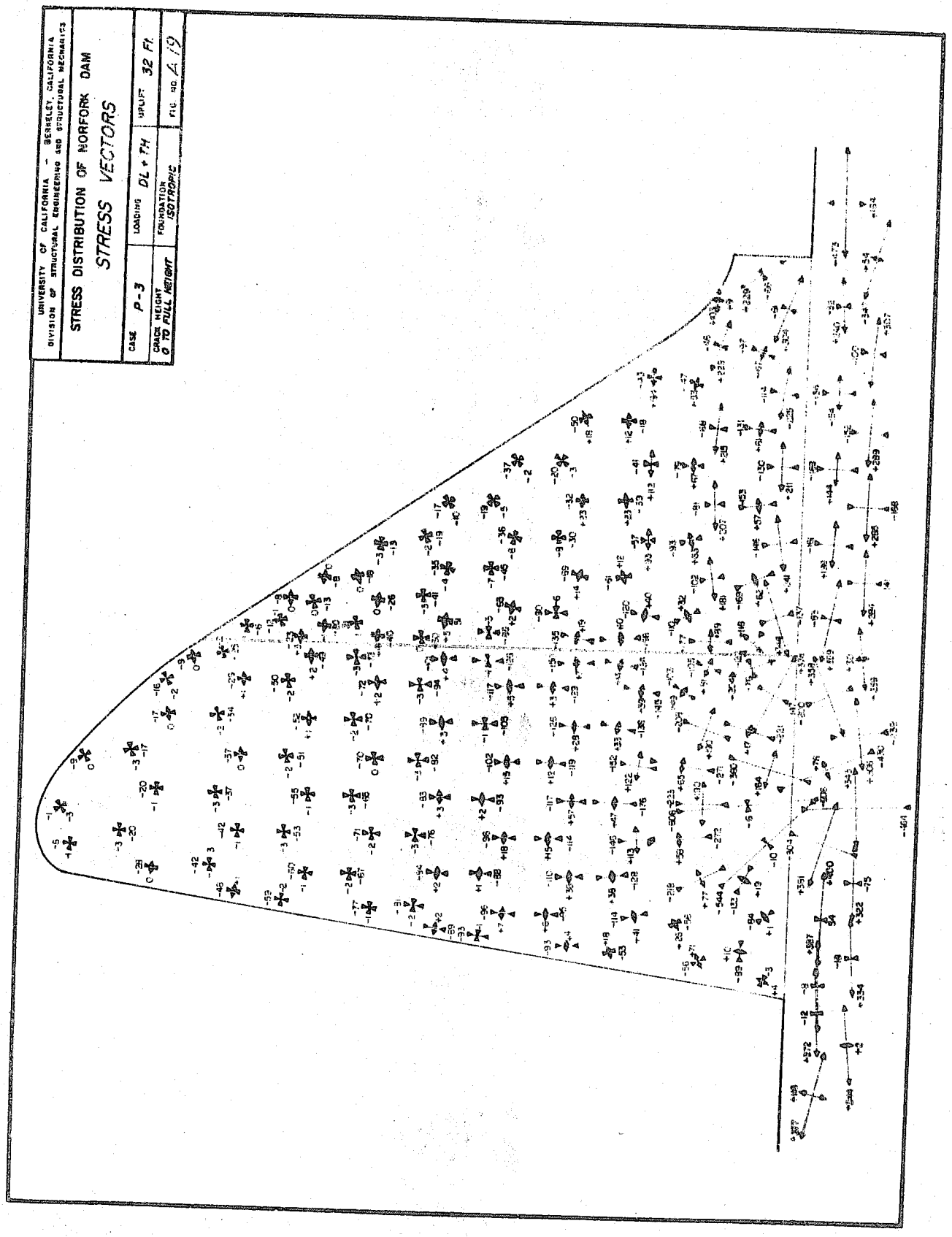
UNIVERSITY OF CALIFORNIA – BERKELEY, CALIFORNIA
DIVISION OF STRUCTURAL ENGINEERING AND STRUCTURAL MECHANICS
STRESS DISTRIBUTION OF MORFORK DAM
STRESS VECTORS
CASE P-3
LOADING DL + FH
UPLIFT 32 FT.
GRADE HEIGHT 0 TO FULL HEIGHT
FOUNDATION ISOTROPIC
FIG. NO. 4.19

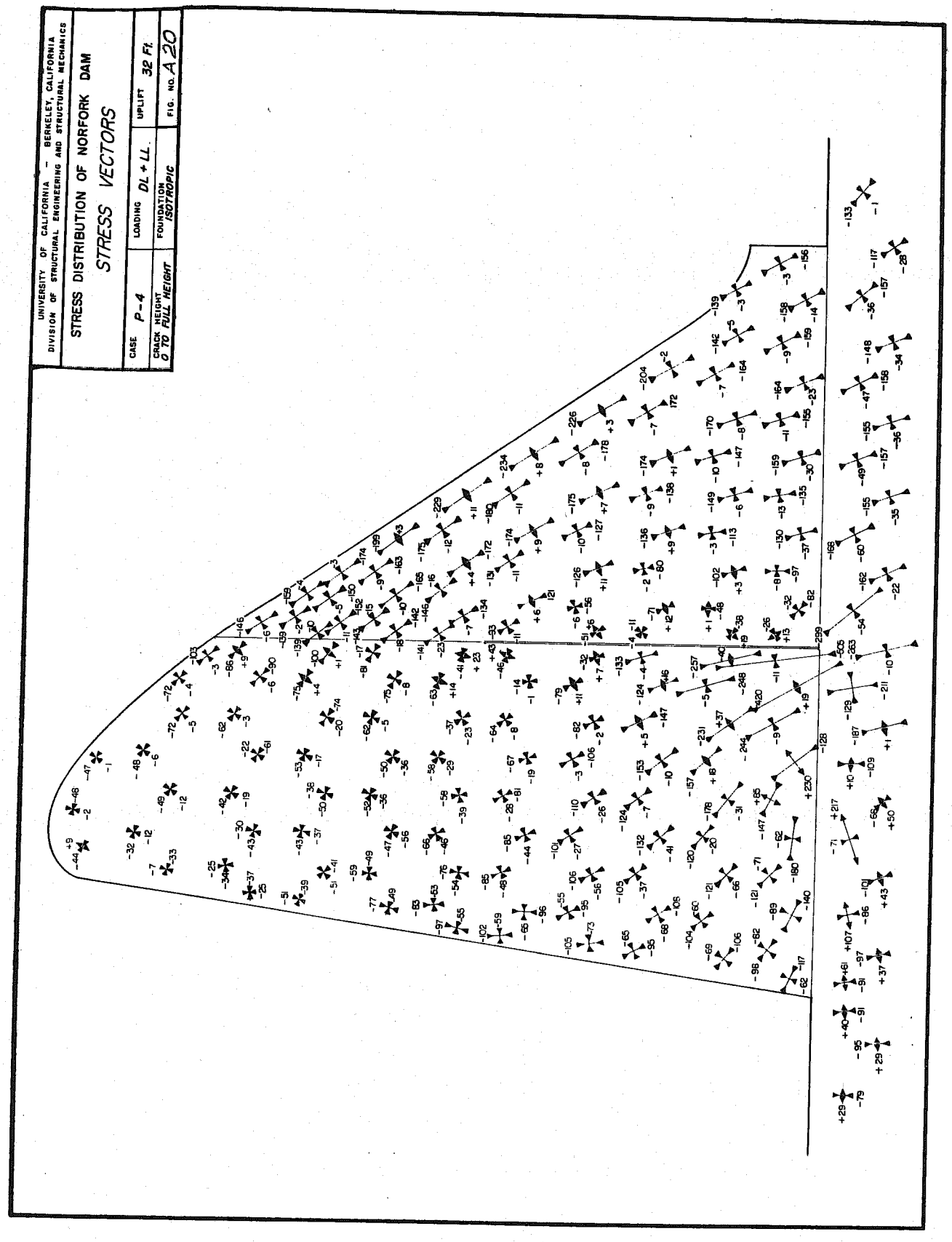
UNIVERSITY OF CALIFORNIA – BERKELEY, CALIFORNIA
DIVISION OF STRUCTURAL ENGINEERING AND STRUCTURAL MECHANICS
STRESS DISTRIBUTION OF NORFORK DAM
STRESS VECTORS
CASE P-4
LOADING DL + LL.
UPLIFT 32 Ft.
CRACK HEIGHT 0 TO FULL HEIGHT
FOUNDATION ISOTROPIC
FIG. NO. A 20

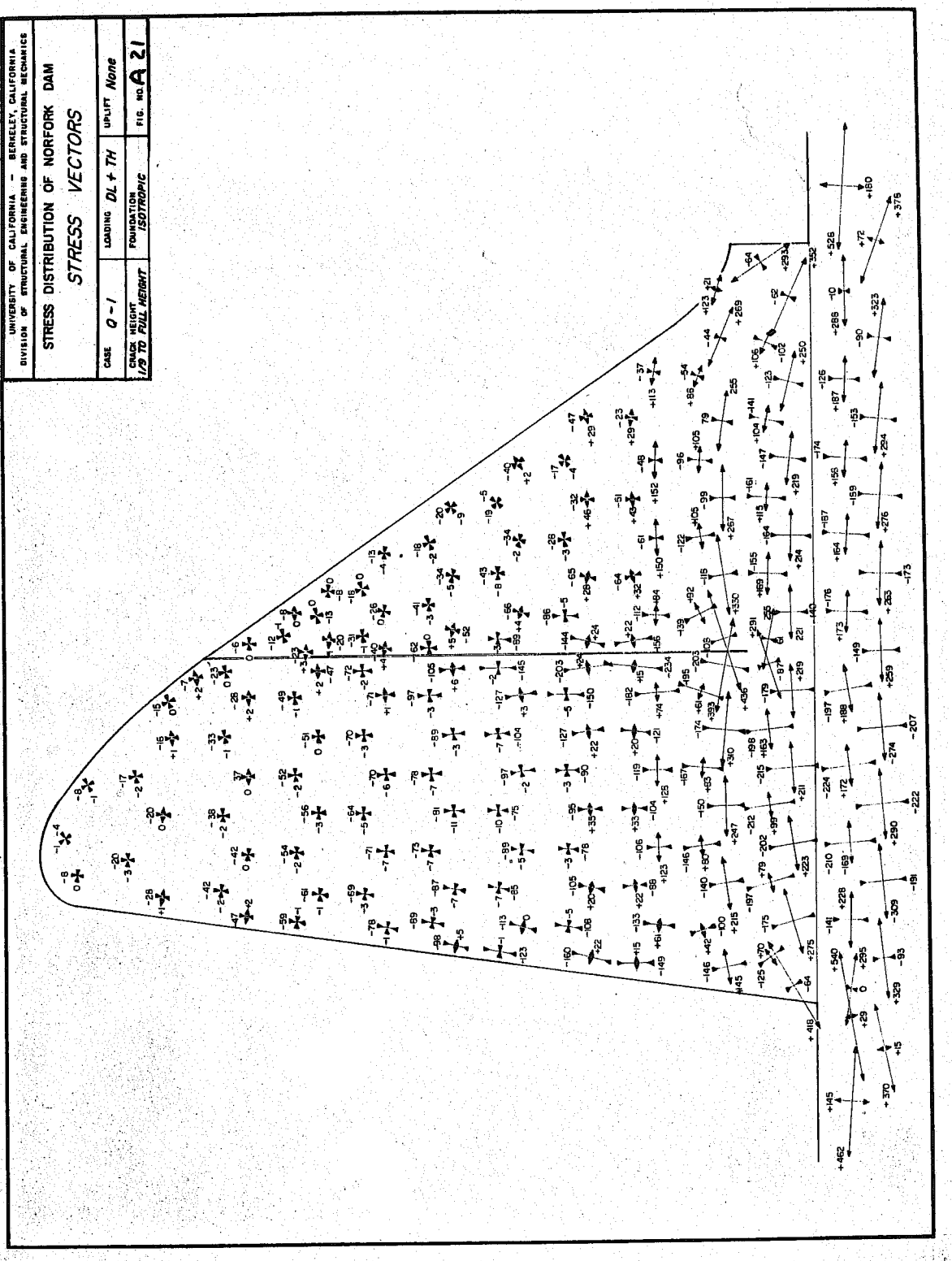
UNIVERSITY OF CALIFORNIA – BERKELEY, CALIFORNIA
DIVISION OF STRUCTURAL ENGINEERING AND STRUCTURAL MECHANICS
STRESS DISTRIBUTION OF NORFORK DAM
STRESS VECTORS
CASE 0-1
LOADING DL + TH
UPLIFT None
CRACK HEIGHT 1/9 TO FULL HEIGHT
FOUNDATION ISOTROPIC
FIG. NO. A 21

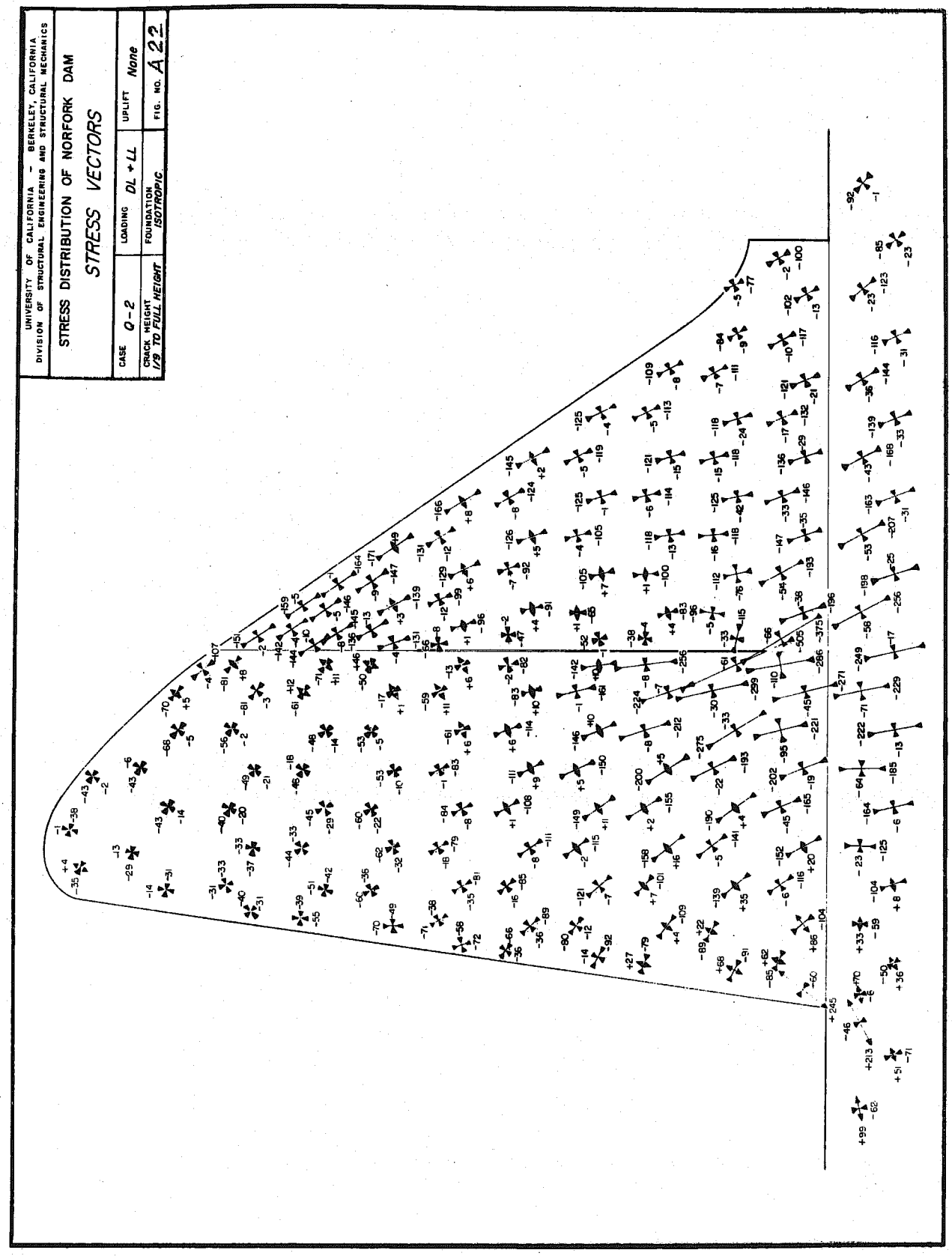
UNIVERSITY OF CALIFORNIA - BERKELEY, CALIFORNIA
DIVISION OF STRUCTURAL ENGINEERING AND STRUCTURAL MECHANICS
STRESS DISTRIBUTION OF NORFORK DAM
STRESS VECTORS
CASE Q-2
LOADING DL + LL
UPLIFT None
CRACK HEIGHT 1/9 TO FULL HEIGHT
FOUNDATION ISOTROPIC
FIG. NO. A 22

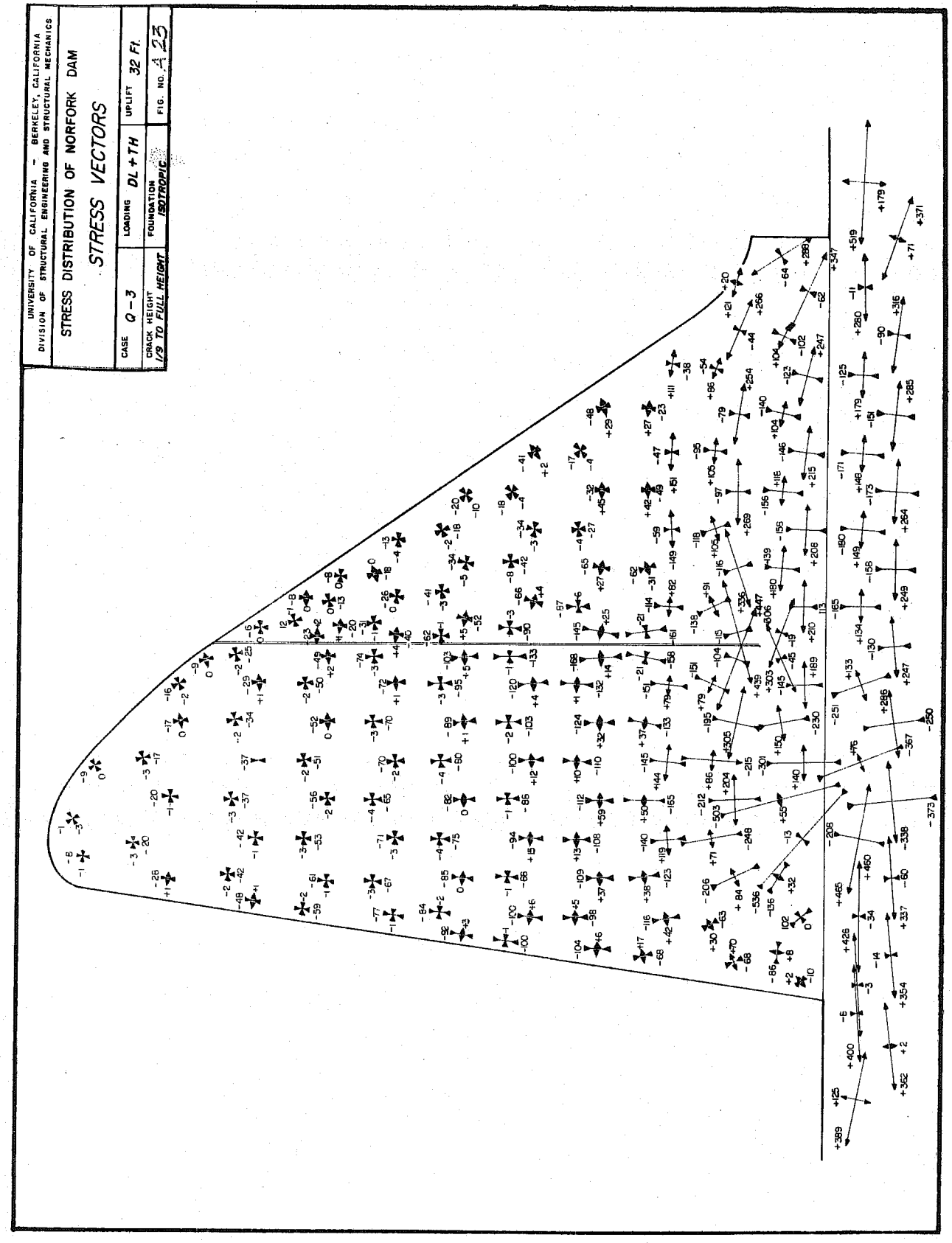
UNIVERSITY OF CALIFORNIA - BERKELEY, CALIFORNIA
DIVISION OF STRUCTURAL ENGINEERING AND STRUCTURAL MECHANICS
STRESS DISTRIBUTION OF NORFORK DAM
STRESS VECTORS
CASE O-3
LOADING DL+TH
UPLIFT 32 Ft.
CRACK HEIGHT 1/3 TO FULL HEIGHT
FOUNDATION ISOTROPIC
FIG. NO. A-23

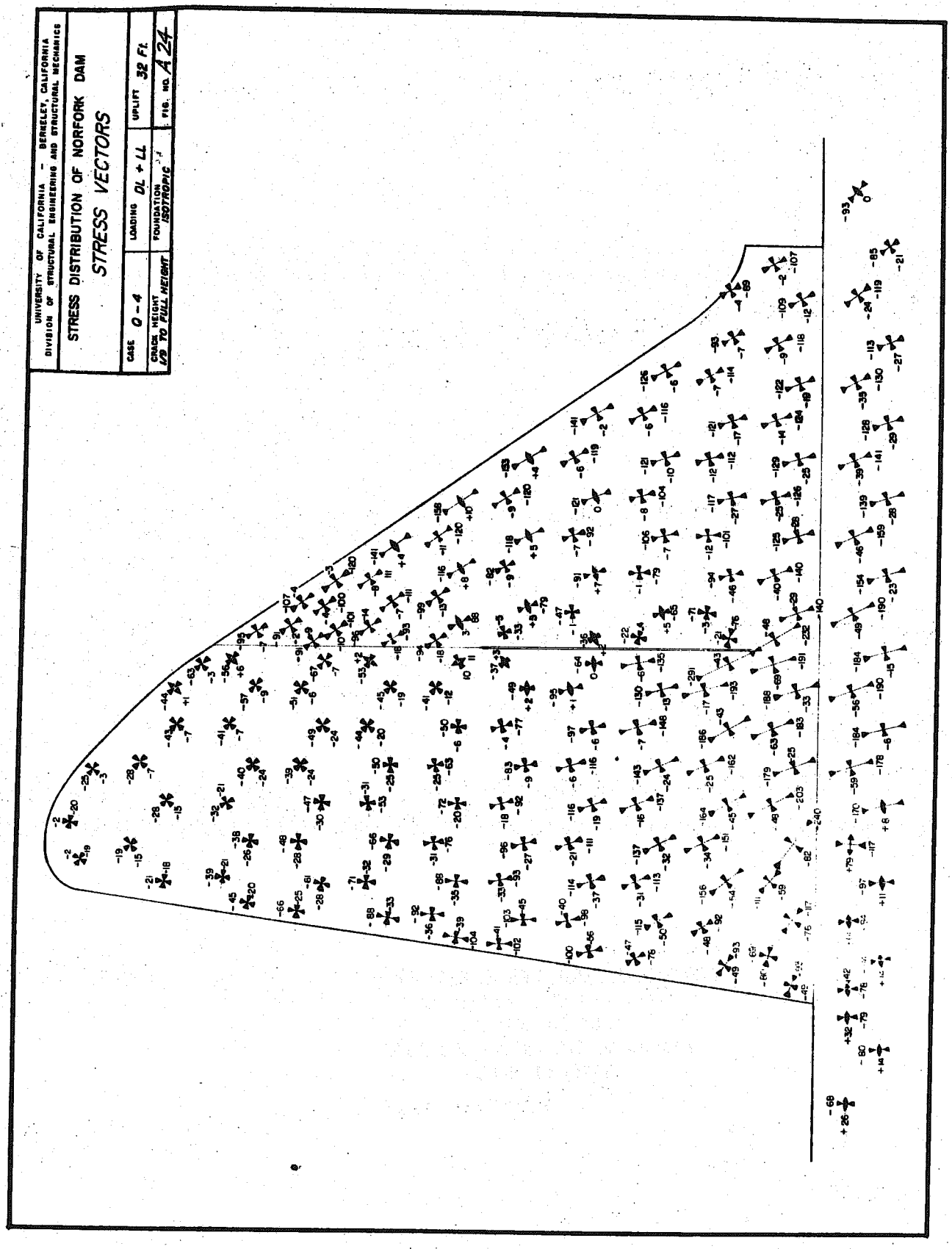
UNIVERSITY OF CALIFORNIA - BERKELEY, CALIFORNIA
DIVISION OF STRUCTURAL ENGINEERING AND STRUCTURAL MECHANICS
STRESS DISTRIBUTION OF NORFORK DAM
STRESS VECTORS
CASE 0-4
LOADING DL + LL
UPLIFT 32 Ft.
CRACK HEIGHT 1/2 TO FULL HEIGHT
FOUNDATION ISOTROPIC
FIG. NO. A 24